ACCESSIBILITY Open

OSLO METROPOLITAN UNIVERSITY
STORBYUNIVERSITETET

Master's Degree in
Structural Engineering and Building Technology
Department of Civil Engineering and Energy Technology

MASTER THESIS

THESIS TITLE Finite element model updating of the Stange railway overpass using operational modal analysis	DATE 08.06.2022 NUMBER OF PAGES 69
AUTHOR(S) Benedicte Tørre Nummestad Morten Aanvik	SUPERVISOR(S) Semih Gonen Emrah Erduran

IN COLLABORATION WITH BaneNOR, Oslomet	CONTACT PERSON

SUMMARY

This study determines and investigates the dynamic and modal parameters, responses, and properties of the easter Stange railway bridge, carrying track two with most of its traffic being northbound. It also studies the maximum accelerations of both the eastern bridge carrying track two, and the western bridge carrying track one. Vibration measurements were taken on both bridges, one bridge at the time, using a total of ten sensors which was installed on each of the two bridges with an equal but mirrored layout. The measurements were carried out over six days in February and March 2022. The data were uploaded in Matlab where flies containing half an hour to an hour was sorted and cropped into individual train passings. The anomalies where also removed. Using operational modal analysis and Covariance-driven Stochastic Subspace Identification the natural frequencies, damping ratios and mode shapes for each train passing where found. An initial model of the eastern bridge was created, with the dynamic analysis program CSiBridge, which produced initial modal responses to give an estimation of the model's credibility and accuracy. The model provided plausible results in the expected range of frequencies and with probable mode shapes. The model was updated with the results from the operational modal analysis to produce more accurate dynamic responses.

3 KEYWORDS
FEMU – Finite Element Model Updating
OMA – Operation Modal Analysis
Stange railway overpass

Foreword

This master thesis is written with the Department of Civil Engineering and Energy Technology at Oslo Metropolitan University within the field of Structural Engineering and Building Technology. This thesis is the final product of our Master of Science degree (MSc.) and counts a total of 30 ECTS credits. The thesis is written over a period of six months from January to June of 2022 and is a collaborative study between the students Benedicte Tørre Nummestad and Morten Aanvik, with Semih Gonen as our supervisor and mentor.

The Department of Civil Engineering and Energy Technology at Oslo Metropolitan University has constructed an attractive Master of Science program which offers highly relevant and interesting specialization studies within the field of structural engineering. The topic of dynamic behavior of constructions caught early our attention, and the interest of modal analysis came shortly after, as it is both exiting, rewarding and useful for the progression of our society. The NEAR-project and the research connected to it allowed us to learn new analytical computer programs together with advanced programming from scratch and from pre-built scripts.

The work put into this thesis has been both challenging and rewarding. With both authors experiencing passing of near family members near the deadline of the thesis, it became more challenging and tedious to complete the study, but with help from supervisors and hard effort, the work was completed on double within the extended deadline.

We would like to thank all who have helped with the thesis by providing help with extraordinary tasks, tips, solutions, support and general guidance, and a special consideration to Semih Gonen and Emrah Erduran of the Oslo Metropolitan University.

Abstract

The growing demand for public transportation and the need for trains at higher speeds highlights the importance of assessment and rehabilitation of train bridges. A challenge of rehabilitation is to restore or improve the structure without knowing the exact condition of the already existing bridge. This study determines and investigates the dynamic and modal parameters, responses, and properties of the easter Stange railway bridge, carrying track two with most of its traffic being northbound. The thesis also studies the maximum accelerations of both the eastern bridge carrying track two, and the western bridge carrying track one.

Vibration measurements were conducted to both bridges, one bridge at the time, using a total of ten sensors which was installed on each of the two bridges with an equal but mirrored layout. The measurements were carried out over six days in February and March 2022.

The data were uploaded in Matlab where flies containing from half an hour to an hour of data was sorted and cropped into individual train passings. The anomalies where also removed. Using operational modal analysis and Covariance-driven Stochastic Subspace Identification the natural frequencies, damping ratios and mode shapes for the train passings where found.

An initial model of the eastern bridge was created, with the dynamic analysis program CSiBridge, which produced initial modal responses to give an estimation of the model's credibility and accuracy. The model provided plausible results in the expected range of frequencies and with probable mode shapes. The model was updated with the results from the operational modal analysis to produce more accurate dynamic responses.

In addition, the maximum accelerations of each train passing were compared to the requirement of standard NS-EN 1990. The study succeeded to update the model and additionally concludes that all the maximum accelerations on track two are within the standards of NS-EN 1990, while 36% of the maximum accelerations on track one are not.

Table of contents

Table of figures

Table of tables

Table of equations

Abbreviations

FE	Finite Element
FEM	Finite Element Model
FEMU	Finite Element Model Updating
OMA	Operational Modal Analysis
SSI	Stochastic Subspace Identification
SSI-Cov	Covariance-driven Stochastic Subspace Identification

1 Introduction

Statistics show that the number of passengers on trains in Norway has increased by 28% from 2012 to 2019 [1]. The growing demand for public transportation and the need for trains at higher speeds highlights the importance of assessment and rehabilitation of train bridges. A challenge of rehabilitation is to restore or improve the structure without knowing the exact condition of the already existing bridge.

All bridges need maintenance, and when the wear and tear and decay of bridges leads to structurally critical levels, they will need rehabilitation. Because of this, it is of great interest to know the condition of the bridges such that harshly instances of decay can be discovered and corrected before it leads to severe problems [2]. It is also of interest to identify the current dynamic and static structural parameters of bridges which will undergo changes in loading due to new trains at new speeds.

The need for discovering decay of bridges rises with the climate change because it might decrease the expected life span of bridges by an unknow number of years. With the development of the Intercity triangle in Norway, which aims to reduce travel time between the cities of Skien, Halden, and Lillehammer, arises a need to know the structural capacity of the existing train bridges, and how the speed of the passing trains affects these bridges. During the mapping of these bridge's capacity, the attention was led to the Stange overpass.

The current model for analyzing the structural capacity and vibration levels of this bridge turned out to be extremely unprecise, to the extent of the model being completely useless, due to the modeling uncertainties. The inaccuracy of the finite element models can be alleviated by tuning the models with the experimentally measured data. This will lead to more reliable representation of the structural behavior and allow for dynamic parameters to be identified and analyzed. With a more accurate finite element model, it will be possible to predict and examine the actual dynamic behavior of the bridge in different scenarios without further investigations and data gathering. This can be a great advantage since future problems and issues might not be obvious to today's engineers [2].

1.1 Stange overpass

The Stange overpass consists of two separate train bridges crossing the county road FV222. The western bridge, which carries track number one, is the most trafficked since all regular train traffic passes on this track. The second bridge, to the east, carries track number two, and is used when meeting trains need to pass each other, and to relieve track number one when the traffic is very heavy. Both bridges were designed in 1999 and constructed in 2002 [3].

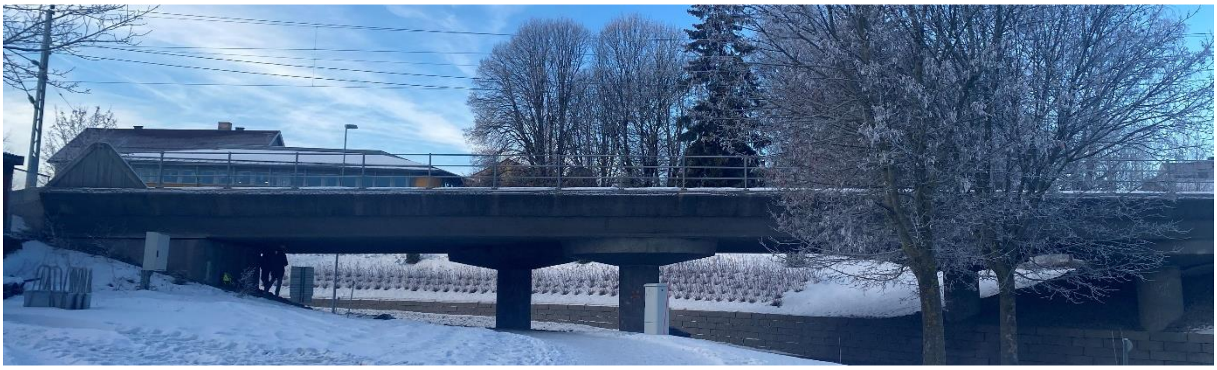

FIGURE 1: PICTURE OF THE EAST SIDE OF THE STANGE OVERPASS

1.2 Background

This chapter will go through the origin of the problem and the motivation for this study related to the bridges at Stange overpass.

1.2.1 Result from earlier analysis

The western bridge is concluded far from satisfying considering neither the safety nor the comfort criteria set forth by current standards by "*Rambøll*" and "*Sweco*" trough an assessment of the bridge for HSLM-A train load for speeds ranging from 30 km/h to 300 km/h. The comfort criteria according to standard NS-EN 1990 requires that maximum accelerations should not exceed 3.5 m/s^2, and the analysis results show that the maximum accelerations reach up to 35 m/s^2. The results from the assessment of the bridge showed that at speeds of as little as 30 km/h the train would exceed the maximum allowable acceleration (3,5 m/s^2) by three times, and for greater speeds of 100 km/h, the acceleration exceeded the allowable limit by as much as ten times. The calculation also showed that the bridge would collapse due to excessive shear forces. However, the bridge is still standing with no sign of damages to the structure, and there have been no reports from passengers or crew of conditions onboard the trains that might have come from accelerations of 10,0 m/s^2 [3]. A study conducted by Mathias Torp and Jacob Johnsen in 2021 [4] re-investigated the western bridge and build an updated finite element model and conducted a dynamic parameter analysis of the bridge, leaving great results with a much higher accuracy.

The result from the analysis also shows that maximum shear force in the bridge deck is two times higher than the capacity of the deck. This is indicating a danger to the safety of the bridge, but the most recent inspection report shows no visible damage. This indicates that the numbers from the analysis does not comply with the real situation of the bridge. There is therefore a need for a calibration of the finite element model of the Stange Overpass, since the best fitted model for calculating accelerations of the trains and vibrations and stresses on the bridge are completely useless [3].

1.2.2 NEAR

A collaborative research project called "*NEAR: Next Generation Finite Element Calibration Methods for Railway Bridges*" was started to gain an overview of the structural conditions and maintenance need for the train bridges in Bane NOR's disposal. The method for this is to create accurate finite element models for prediction of structural capacity and dynamic properties such as vibrational frequencies and mode shapes of the structures. The "NEAR-project" was also created to develop a finite element model to calculate the accelerations more accurately on the train and the vibration forces on the railway bridge in collaboration with Bane NOR. NEAR will use Stange railway overpass as a test for this project. The aim of the project is to first calibrate the measured vibrations in the bridge with the calculated vibrations from the finite element model, and when an accurately enough model is produced, it can be utilized on all bridges Bane NOR operates on. Their goal is to create a finite element calibration method that can accurately predict the maximum accelerations and forces caused by railway traffic [3].

This combination has shown to be the most important parameter to model and calibrate accurately to get a reliable result. The behavior of the soil varies with the loads it is exposed to and is therefore directly connected to the speed, axial load, axial position, and acceleration of the passing trains. This has not been properly included before and might be one of the reasons for the unprecise calculations. The "NEAR-project" aims to utilize the rapidly increasing sensor technology together with improvements in finite element modelling to generate more accurate and reliable models for railway bridge calculations and in the end having the availability to precisely determine the maximum allowable speed for passing trains [3].

1.2.3 Bane NOR

Bane NOR is a Norwegian state-owned enterprise responsible for infrastructure on the railways in Norway that was established in 2016. They are responsible for planning, development, management, operation and maintenance of the national railway network, traffic management and management and development of railway property. The purpose of Bane NOR is to provide accessible railway infrastructure and efficient and user-friendly services, including hub and freight terminal development. They have about 3400 employees and headquarters in Oslo [4], [5].

1.3 Experimental and operational modal analysis

Both experimental and operational modal analysis are great techniques for measuring and quantifying dynamic and modal properties of constructions. The two different techniques have similarities and differences and are applicable for different types of constructions. Both techniques will be briefly introduced in the two following subchapters.

1.3.1 Experimental modal analysis (EMA)

Experimental modal analysis is conducted onto structures or objects of a limited size and is done by inflicting a known amplitude of force or vibration in a known direction onto the object of analysis. The dynamic response of the object is then measured, and further modal analysis can be conducted to determine the objects dynamic and modal parameters. This technique is limited by the size of the force applied to the structure. If the force is not sufficiently large to induce an adequate amount of vibrations to be measured, the technique does not work. Therefore, is also the size of the object a direct limitation because if the object is too large, it will be difficult or ineffective to inflict the force necessary to get measurable vibrations in the object. Bridges are typically too large to be analyzed with EMA [6].

1.3.2 Operational modal analysis (OMA)

Operational modal analysis differs from experimental modal analysis because OMA only measures the vibrations, or output data, of the object without knowing the amplitude, duration, or direction of the force applied to the object to inflict said vibrations. The vibrations are measured as displacements or accelerations and analyzed to discover the object’s dynamic and modal parameters. This technique is beneficial for larger structures such as bridges, which are generally too large to be inflicted with sufficiently large known forces to return measurable vibrations [6].

1.4 Finite element method and FEMU

Approximations of a real solution are computed using the finite element method. To solve a problem, the finite element method breaks a complicated system into smaller, simpler elements called finite elements. Finite element updating was created to make a finite element model more comparable to a structure's actual behavior. Finite element model updating is used to correct errors and imperfections in the structure, such as damage to the structure, measurement or modeling errors, or changes in structural parameters over time [7], [8].

1.5 Purpose

The purpose of this thesis is split in two. The first purpose is to identify the dynamic and modal parameters of the eastern railway bridge at the Stange overpass, and to create an accurate finite element model of the eastern bridge that can be used for train speed verifications in later work.

The second purpose is to identify the maximum acceleration inflicted upon both the eastern and western bridge from regular train traffic to acquire better knowledge of todays' loading conditions.

This research will help with the overall speed verification of the intercity triangle on the south-eastern part of Norway, greatly improving traveling efficiency for the railway. It is also of interest to verify the approach and method for solving the general problem of identifying modal parameters for railway bridges with the help of operational modal analysis and finite element models.

1.6 Research question

The purpose and research question are highly connected, and their descriptions will overlap to an extent. The research question for this thesis is "*which modal parameters apply for the eastern railway bridge at Stange overpass and will an updated finite element model accurately represent the real dynamic behavior of the bridge?*".

1.7 Limitations

There are limitations to this thesis which can be divided into different categories. These categories will be described in the following subchapters, and are "*limitations of knowledge*", "*limitations of measurements*", "*limitations of the finite element model*", and "*limitations of boundary conditions precision*". The limitations impact on the final result will also be commented.

1.7.1 Limitation of knowledge

There is a limited amount of documentation for the bridges with a limited amount of details since both the drawings for the bridges, and the bridges themselves, was created more than 30 years ago, and the need of that time probably did not demand that level of details. This limitation of preliminary knowledge of the actual bridge hinders the accuracy of the constructed initial model and the ease of correlating the final model to the actual bridge. This should though not hinder the quality or accuracy of the final model.

1.7.2 Limitations of measurements

The two train bridges have different uses, where most of the traffic passes over the western bridge on track one. The second bridge is used only when there are delays or when trains need to pass another train along the single line railway. A result of this is that the vast majority of the train traffic is on the western bridge, and only a small amount of the traffic passes the eastern bridge. This restricted amount of measurements for the eastern bridge and can lower the accuracy of the data acquisition analysis and henceforth lower the accuracy of the final model, since it is to reflect the measured data.

1.7.3 Limitations of the finite element model

Both the initial and the final model has some simplifications done to them. The cross section of the bridge has a more advanced shape than the simplified rectangular deck with rectangular sides. The advanced geometry on the side of the bridge is however assumed to have little to no impact on the modal or dynamic parameters of the bridge, and is therefore not included in the design of the model

1.7.4 Limitations of boundary conditions precision

Boundary conditions contain many uncertainties and unknow parameters and are difficult to calculate correctly. This applies also to this project and simplifications of the boundary conditions and assumptions must be done during the construction of the model. Since the final updated model should resemble the real-life construction, this should not affect the final models' result too much, but it might prolong the time it takes to complete the updating.

1.8 Literature

Different literature was reviewed in preparation to this study. This to give insight in what has already been discovered, to get an overview of an effective approach to solve the problem, and to see if meaningful starting parameters existed, to reduce the time necessary for creating the initial model and later updating to the final model. A list of the preliminary literature read in preparation for this thesis, together with a short description of their content can be found in Table 1.

TABLE 1: PRELIMINARY LITERATURE REVIEW OVERVIEW

Title	**Author**	**Important learning outcome**
NEAR: Next Generation Finite Element Calibration Methods for Railway Bridges	Emrah Erduran	• Introduction to the problem with the current FEM. • Importance of solving the problem, and motivation to do so. • Interest for dynamic analysis and modal parametric analysis.
Modal identification and finite element model updating of railway bridges considering boundary conditions using artificial neural networks	Mohammadreza Salehi	• Explains the process of the modal identification and model updating of the Stange Overpass done in 2021.
The Finite Element Method (FEM)	Cosmol	• An introduction to the finite element method explaining how it works and what it is used for.

System Identification and Finite Element Model Updating of the Stange Railway Overpass	Jakob Braaten Johnsen and Mathias Torp	• Overview of Stange overpass, approach to building initial FEM. • Initial dynamic parameters.
Finite element modal analysis and vibration-waveforms in health inspection of old bridges	Salam Rahmatalla, Kyle Hudson, Ye Liu and Hee-Chang Eun	• The use of finite element modal analysis in combination with operational vibration-waveforms is discussed. • Gives insight on how OMA can be used on bridges.
Finite element modelling and updating of a lively footbridge: The complete process	Stana Živanović Aleksandar Pavic and Paul Reynolds	• Gives an example of FEMU on bridges.
Vibration-based structural health monitoring using output-only measurements under changing environment	A. Deraemaeker, E. Reynders, G. De Roeck and J.Kullaac	• Gives information on vibration-based structural health monitoring and the use of OMA.
Placement of sensors in operational modal analysis for truss bridges	N. Debnath, A. Dutta and S. K. Deb	• Discusses the importance of the placement of the sensors when doing OMA.
Subspace Algorithms in Modal Parameter Estimation for Operational Modal Analysis: Perspectives and Practices	S. Chauhan	• Gives information on OMA. • Explains the process of SSI and SSI-Cov.
Understanding Stochastic Subspace Identification	Rune Brincker and Palle Andersen	• Explains the different steps in the SSI techniques of importance for modal identification.

The reading of these reports, thesis, and studies provided a broad overview of the depth of the field of modal analysis from a theoretical point of view, together with inspiration on how to concretely solve the research question in this thesis.

2 Theory

This chapter will go through the theory upon which this thesis is build. This includes basic introductory descriptions of calculation methods, as well as more advanced modelling systems, data gathering and analyzing techniques, and brief introduction to the software utilized for solving the research question.

2.1 Finite element method

The finite element method is used to compute approximations of a real solution. The finite element method divides a complex system into smaller, simpler elements called finite elements in order to solve a problem. It uses numerical methods to solve partial differential equations. This is because these partial differential equations cannot be solved analytically for the majority of geometries and problems. Different methods of discretization are used to approximate the equations in most cases.

The method constructs a mesh of the object, which is a representation of a larger geometric domain by smaller discrete cells. Figure 2 shows an object with different types of mesh. The more and smaller elements the object is divided into, the more accurate, but also more complex the method becomes.

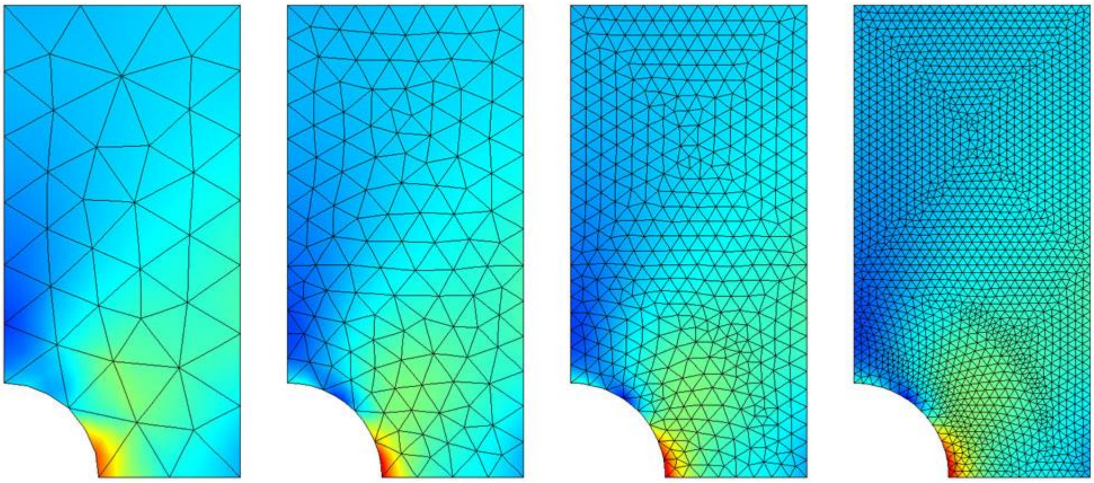

FIGURE 2: AN OBJECT WITH DIFFERENT TYPES OF MESH.

Structure analysis, heat transfer, fluid flow, mass transport, and electromagnetic potential are some of the most common problem areas of interest when it comes to the finite element method. Analyzing a phenomenon with the finite element method is called finite element analysis [7].

2.1.1 Finite element modeling and bridges

The finite element method can be used to do a numerical modal analysis of a healthy bridge to detect small areas of excessive stress or strain at natural frequencies. The benefits of the numerical model may be limited by new damage areas formed as a result of aging. However, if the changes in natural frequencies and mode shapes are not significant, a healthy bridge model may still provide helpful information about specific high-stress areas caused by excitation of some of the modes [8].

2.2 Finite element model updating

Finite element updating were developed to make a finite element model more similar to the real behavior of a structure. Finite element model updating is meant to fix shortcomings and flaws such as damages on the structure, mistakes in measurements or modeling, or the changes in structural properties that happen over a long period of time. Problems like this, when the initial structural model fails to accurately reflect the real-world responses of the structure, is a well-known challenge in model-based safety assessment approach [9].

The difference between the characteristics in finite element and experimentally estimated modal is often minimized using the finite element model updating process. This is accomplished by altering some finite element modeling parameters that have the potential to affect modal properties. The finite element model that is developed can then be used in additional analyses [10].

The process usually starts with manually tuning and later progresses to automatic model updating with the help of specialized software. Manual tuning requires making trial-and-error modifications to the model geometry and modeling parameters by using engineering reasoning. The goal is to get the numerical model as close to the experimental model as possible. Often, an analyst can improve the initial structural idealization, which is often connected to boundary conditions and non-structural aspects, during this procedure. Only a few essential settings are normally manageable manually during this process. By considering a larger number of uncertain parameters, automatic updating aims to improve the connection between numerical and experimental modal parameters. These parameters include all input values that defines the numerical model [10].

A model-based approach is one that is based on the mathematical description and computer simulation of a structure, such as a finite element model, with the first stage being the creation of an initial model based on design level data and documentation or preliminary study. There is also a non-model-based safety assessment approach, however, this is based on signal processing of data from in-situ and experimental studies. To identify damaging with this approach, dynamic flexibility measurements, matrix update methods, modal analysis, and wavelet transform techniques are used. Finite element model updating has become more important as the importance of accurate finite element models has grown. The use of vibration data from traffic loading is the most common and practical method since this data is easy to collect and analyze [11], [12].

2.2.1 Finite element model updating process

Finite element model updating is a procedure for determining the finite element model's uncertain physical properties. This is accomplished by experimenting with the results to create a finite element model that accurately represents the structure's observed behavior. The experimental data and results of in-situ testing are used as targets. The results of the finite element model are calibrated by changing the assumptions and parameters of the initial finite element model, resulting in a high level of similarity between the finite element model output and the existing counterpart [3], [13].

It is impossible to avoid mistakes in a finite element model, and these mistakes will also have an impact on the updated model. That is why it is critical to choose the right structural parameters to modify and update. Because the model updating process probably will lead some structural parameters to unrealistic values, using the right parameters has a significant advantage. The parameters with the least and most sensitivity to structural reactions can be determined via a sensitivity analysis [3].

2.2.2 Finite element model updating methods

The problem in finite element model updating can be approached by two different types of methods. These are either direct methods, also called "non-iterative techniques", or indirect methods, also called "iterative techniques".

The direct methods are better to use for less complexed models because it directly updates the mass and stiffness matrices of the structure. These can be used to update a model in just a single step. The simplicity of this method can make it both time and cost saving. However, these methods have the disadvantage of requiring precise measurements and a high-quality modal testing and analysis procedure [3].

For larger and more complex models, the indirect methods are the best to use. These methods update the physical properties, as material and geometric properties, behind the finite element model. During each iteration, they update the material properties and structural parameters. This helps to minimize the difference between experimental and finite element model responses, which is why they are more appropriate for larger and more complex models [3].

Though finite element modeling is a useful method, replicating the measured dynamic properties with high accuracy is difficult. It is necessary to update or calibrate a finite element model with regards to the measured actual response in order to enhance response prediction. Iterative model updating methods are particularly efficient since they apply modifications to the local physical parameters of the finite element method and produce physically interpretable updated results [14].

2.2.3 Challenges with finite element model updating

Finite element model updating is a widely used approach, although it cannot be used to update all finite element models of all structures. The initial finite element model must be prepared for it for it to have a functional automated updating of a finite element model. Therefore, it would be required to reduce discretization errors and to apply modeling approaches that can accurately represent all critical features of structural behavior and geometry. This implies that model geometry and other aspects should be carefully considered. Since the automatic model updating technique is incapable of correcting significant flaws in the geometry of the initial model, this is important. It can only correct mistakes produced by modeling parameter uncertainty in a geometrically properly defined model [10].

The differences between analytical and experimental modal responses should also be as small as possible while developing the finite element model for automated updating. This typically indicates natural frequencies and mode shapes. The automated updating process may encounter numerical difficulties or result in physically incorrect parameter changes if the differences are too vast. This is why manual tuning of the initial finite element model is advised first. As a result, the customized model should include significant initial parameters for formal updating [10].

2.3 Vibration-based health monitoring

Many scientific communities have spent the last few years discussing structural health monitoring issues. One of the issues is being able to identify, locate, and assess the extent of damage in a structure in order to determine the construction’s remaining life and maybe extend it. Global vibration-based strategies have been extensively developed over the years as an alternative to existing local inspection methods. All of the following are current and future trends in bridge monitoring:

- The use of vibration signals in the environment.
- Unknown excitation due to wind or traffic.
- The use of very wide arrays of sensors.

For remote monitoring applications, complete automation of the damage detection technique is required [15].

The main approach to detecting structural damage is to extract relevant features from measured data. The parameters are monitored in order to detect damage-related changes. All of the following complicate this problem:

- The "output-only" nature of the data.
- The extremely large amount of information to be processed, due to the large sensor arrays.
- The impact of the environment, which can cause changes in the monitored features of an order of magnitude equal to or greater than the damage to be detected, all complicate this problem [15].

Changes in modal data are used as an indicator to detect and identify damage in vibration-based damage identification. The inverse problem of predicting the location and severity of damage based on structural dynamic features before and after the damage has occurred is solved [15].

There are two basic categories of vibration-based damage identification techniques:
The first one is model-based, also known as parametric approach, and the second one is non-model-based, also known as non-parametric approach. The performance of parametric approaches is dependent on the quality of the model. This again is based on a model of the structure, some of whose parameters are updated using vibration data. Although non-parametric methods do not require a thorough model of the structure, the majority of them lack a strong theoretical and physical foundation. This considers the damage finding vector technique and the local flexibility method are exceptions [16].

The finite element model updating approach is a type of vibration-based damage detection technique that is parametric. The approach entails adjusting the unknown features of a finite element model so that the disparities between experimental modal data and finite element model predictions are as little as possible. The structural damage is indicated by a decrease in individual element stiffness, and the technique is carried out in two phases:

1. In the first phase the initial finite element model is tuned to the undamaged structure, which is used as a reference model.
2. In the second phase the reference finite element model is updated to produce a model that can reproduce the experimental modal data of the damaged condition.

The damage is represented by the correction factors of the latter process. Damage functions can be used to approximate the unknown damage pattern to reduce the number of unknown parameters [16].

2.4 Experimental and Operational Modal Analysis

The method of determining a structure's natural vibration properties is known as modal analysis. All complex vibrations that the structure might experience as a response to a certain excitation can be described as a combination of these natural vibration states if they are known. As a result, most of the vibration behavior of a structure may be predicted if the natural vibration states are known. The mode shape, natural frequency, and related damping determine a natural vibration state [17].

2.4.1 Experimental Modal Analysis

Vibration modes of a structure can be completely computed, for example, using finite element models, or developed from real measurement findings by fitting a mathematical model to them. The last method is called experimental modal analysis (EMA). Experimental modal analysis is a technique for describing the natural characteristics of a vibrating structure, such as frequency, damping, and mode shapes. Sensor technologies, data gathering, and a computer for monitoring and interpreting measurement data are all required in a standard experimental modal testing setup. Experimental modal analysis is applying known forces to the structure, such as shakers or impact hammers, and measuring the structure's reaction to these forces, generally with accelerometers. The structure is then characterized based on the known input forces and output responses [17] [18].

2.4.2 Operational Modal Analysis

Operational modal analysis (OMA), also called output-only system identification, is a modal identification method that includes both experimental testing and modal identification using a variety of system identification approaches. Operational modal analysis is also described as an output-only technique since it is based on output-only data. The finite element model is usually updated using output-only data, because forced vibration testing of large structures in operational settings is typically difficult and expensive. Even though operational modal analysis requires additional measures to obtain modal data, operational modal analysis is more suited to larger constructions like bridges. This is why operational modal analysis is gaining popularity for modal parameters, particularly for large structural systems under operational environment, when it comes to evaluation for the structural systems [19], [20], [16].

Because exact artificial excitation is difficult to implement, operational modal analysis only uses sensors. For a set of target modes, sensor placement cannot guarantee that the sensor placements will be able to represent good modal information such as modal frequency and modal damping. As a result, there is a lot of interest in identifying sensor locations with improved modal information for single or multiple target modes [20], [16].

Unmeasured ambient forces, such as wind or traffic loading, cause the measured response in operational modal analysis. Unmeasured ambient forces are modeled as stochastic quantities with unknown parameters but known behavior. Finite element model updating with operational modal analysis data has been used to successfully identify structural damage in a variety of structures, including concrete roadway bridges, historic masonry towers, and multi-story reinforced concrete building frames [16].

The primary limits of operational modal analysis are the finite element model's capacity to accurately represent the actual behavior of the structure and the ability to identify enough modal parameters. The sensitivity of structural stiffness regarding changes in modal parameters is higher for modes with a higher eigenfrequency when it is applied as a finite element updating parameter. As a result, precise identification of the higher modes is critical for model updating, particularly in damage detection applications [16].

2.4.2.1 Covariance-driven Stochastic Subspace identification method

A well-known operational modal analysis approach is stochastic subspace identification (SSI). This technique incorporates system identification theory, linear algebra, and statistics. The system matrix may be identified using matrix calculation, from which the modal parameters can be computed. It is based on state-space representation of a discrete linear time invariant system and can be described with the following formulas [21], [22]:

$$x_{k+1} = Ax_k + w_k$$

EQUATION 1

$$y_k = Cx_k + v_k$$

EQUATION 2

The factors in the formulars can be defined as following:

- x is the vector of state variables matrix,
- A is the state transition matrix,
- w is a process and measurement noise vector,
- y is the vector of measured responses,
- C is the output matrix,
- and v is another process and measurement noise vector.

The SSI method is regarded as one of the most advanced modal identification techniques. It can simultaneously determine natural frequencies, modal shapes, and damping ratios related to various modes of the system. It also eliminates some of the common drawbacks of frequency domain methods, such as inaccuracy for identifying closely spaced modes and inadequate frequency domain resolution [21].

One of the most popular variants of this algorithm is the covariance-driven is stochastic subspace identification (SSI-Cov). This approach uses covariance functions to operate. The method consists of two basic steps:

1) Singular value decomposition is used to derive the system matrix from the output vector's covariance matrix.
2) From the system matrix, determine the modal parameters of the analyzed system.

In order to use SSI-Cov, raw output time histories must first be used to estimate covariance functions. This is because SSI-Cov makes use of these covariance functions to estimate modal parameters [21], [22].

The process begins with The Hankel matrix being constructed from the output data. The Hankel matrix will then be used to get the Toeplitz matrix with projection procedures. This matrix has the information to find matrix A form equation 1 and matrix C from equation 2. The Toeplitz matrix can also drastically decrease the number of analytical data while preserving the signal's original information. Lastly, singular value decomposition manipulation may be used to identify the system matrix, and eigenvalue decomposition is used to identify the structure's modal parameters. This process is illustrated in Figure 3 [21].

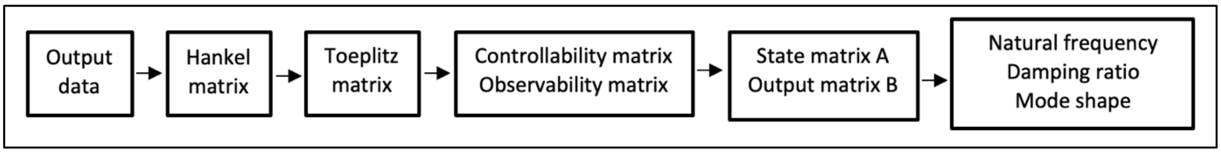

FIGURE 3: SSI-COV PROCESS.

2.5 Vibrations and earlier finite element models

Vibrations relevant for this thesis is divided into two groups, namely forced vibrations and free vibrations. Both will be briefly described in the following sub-chapters as they have different properties and ways to be utilized in the field of modal parametric research.

2.5.1 Forced vibrations

Forced vibrations depend on the properties and attributes of applied loading. For the Stange overpass, this will be the passing trains. Their weight, number of axels, axel distance and distance between the pairs of axels, together with the trains speed and acceleration. The measurement of acceleration, displacement, and strain from the forced vibrations returns the actual conditions the bridge is subjected to, but since all the loading parameters are unknown is it difficult to accurately predict the bridges actual dynamic parameters from this data. These vibrations are therefore less relevant for the updating of the finite element model of the bridge. They are however relevant for determining the actual loading and vibrations the bridge is subjected to [3].

2.5.2 Free vibrations

Free vibrations and the damping of these, are only dependent on the material properties and physical attributes of the bridge, hereunder stiffness, mass, and damping ratio. The measured free vibrations of the bridge can be used to calculate the bridge's natural frequencies, mode shapes, and damping ratio which will be used in the finite element model updating [3].

2.5.3 Assumptions for earlier finite element models

As stated previously in this thesis have there been a finite element model constructed of the Stange Overpass, which returned unusable results. This has most likely come from the assumption that the end of the bridge is resting on soil which acts as a support for the bridge. This has however been investigated by geo-technicians to be a wrongful assumption as the soils is most likely compressed to the state of having no actual support for the overlaying bridge. This again results in the ends of the bridge acting like cantilevers with an unknown amount of support from the connection to the rest of the railway and from whatever unknown supports are left in the soil and other contact areas of the underside of the bridge [3].

2.6 CSiBridge as a design- and analysis program

CSiBridge is a reputable program from the company "*Computers and Structures incorporated*", founded in 1975. The program used in this thesis, CSiBridge, is a semi-parametric modeling program that can create simple beam structures, surface area shell models and volumetric shell element models. It uses a mathematical finite element model method to calculate the static and dynamic properties of the construction, after meshing surfaces and volumes and assigning them materialistic properties and attributes. The dynamic property of the construction is calculated using an engine that can support 64-bit solvers with eigen value analysis and Ritz analysis which is a suitable technique for concrete and steel bridges. The parametric modelling feature of the program allows for swift and effective changes and updates to the model which helps when making an updated model based on experimental measurements [23], [24], [25].

2.7 Equipment for data gathering

This chapter will describe the equipment used for data gathering at the Stange overpass. It will briefly describe all equipment and highlight details relevant for this thesis.

2.7.1 Sensors

The sensors used for the data acquisition is the PCB 393A03 from the company "PCB Piezotronics Inc." They are seismic ceramic shear accelerometers with a 1 V/g, ±5% variation, measuring in frequencies from 0,5 up 2000 Hz from the two-pin top connector [26]. An installed sensor on a steel plate in a preliminary installation test can be seen in Figure 4.

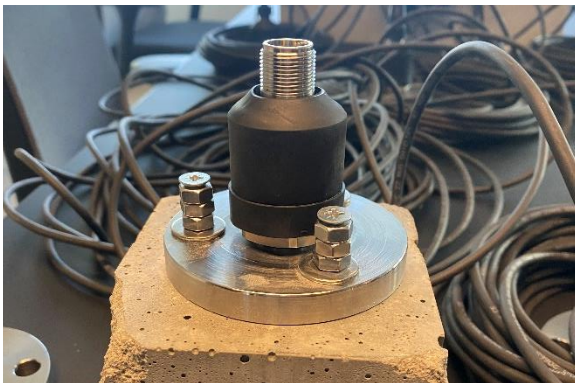

FIGURE 4: INSTALLED PLATE WITH ATTACHED SENSOR ON A TRIAL CONCRETE CUBE IN PREPARATION FOR THE REAL-LIFE INSTALLATION

2.7.2 Steel plates

Steel plates were custom ordered for the project to have bases for attachment of the sensors. They are disc shaped with a thickness of 10 mm and with a diameter of 80 mm. They have three holes around the center of the disc, with diameters of 8 mm, allowing them to be installed onto surfaces with screws or bolts. They are also equipped with screw treads, allowing the sensors to be firmly attached to the plates and assuring all vibrations inflicted upon the plates are transferred to the sensors. One of the installed plates on the western bridge can be seen in Figure 5.

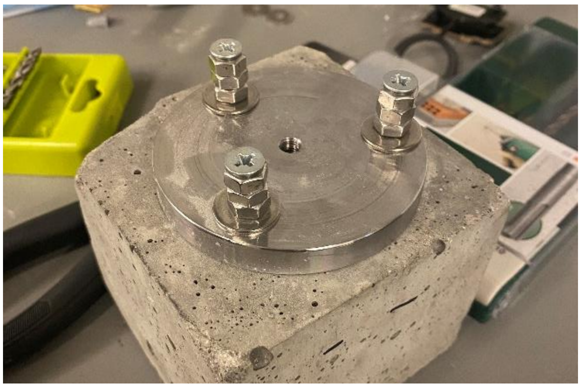

FIGURE 5: INSTALLED STEEL PLATE WITH THREE SCREWS ON A TRIAL CONCRETE CUBE

2.7.3 Control unit

The control unit used for the data gathering is a "*Gantner Q station XT*" unit with connection to the "*Bloxx*" system used by the same provider. The control unit has capacity to process data of speeds up to 100 KHz and writer speed up to 48 Mbps. It can handle data input with six digits and has the option of connecting directly to Matlab for effective data processing in site [27]. The control unit can be seen as the far-right steel box in Figure 6.

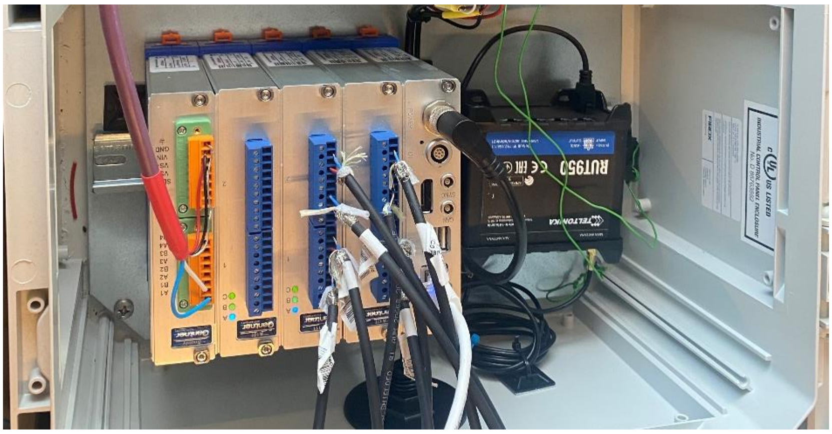

FIGURE 6: CONTROL UNIT AND DATA RECEIVING COMPONENTS INSIDE A PROTECTIVE CABINET

2.7.4 Battery

The battery powering the measurements (Figure 7) is an Eco flow Max battery with a capacity of 2016Wh, and a weight of approximately 21 kg [28]. The battery has capacity to allow continues measurements for almost 18 hours with 8 sensors.

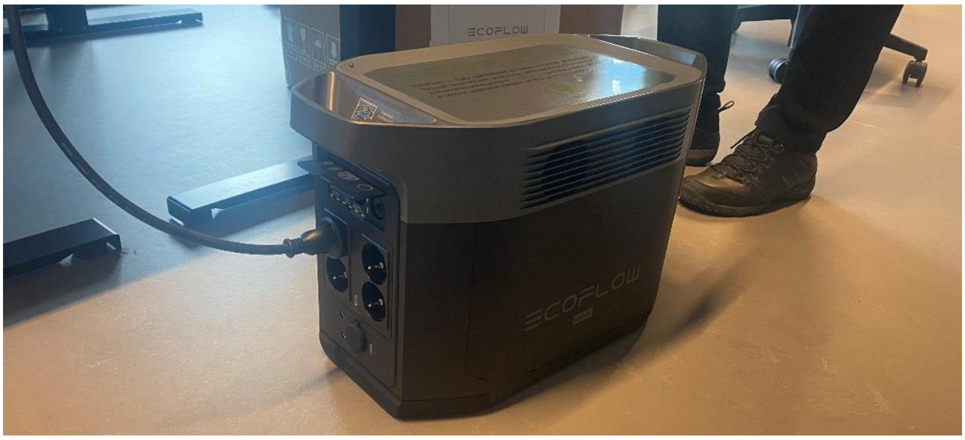

FIGURE 7: BATTERY USED FOR POWERING THE DATA GATHERING ON SITE

2.8 Matlab

Matlab is a mathematical programming program from the company "Mathworks", which has been used and developed since 1984 and has per 2020 more than 4 million users worldwide [29]. While it was initially developed to calculate matrix operations it is today wieldy used as a general calculation program which can analyze data, make algorithms and scripts, and be used for modelling. This makes the program suitable for data processing and modal parameter identification since it allows for advanced data processing. There is also developed toolboxes for Matlab which add features such as the possibility to do symbolic calculations, signal processing, mapping, and system identification [29]. The relevant toolboxes for this thesis is further explained in the following subchapters.

2.8.1 Signal processing Toolbox

The Signal Processing Toolbox allows for signal data to be analyzed, pre-processed, and further processed. It makes the process of extracting features from uniformly and nonuniformly sampled signals easier with the built-in functions. The toolbox also includes functions that helps filtering signal data and create power spectrums for time- and frequency domain signal data [30].

2.8.2 Mapping Toolbox

The mapping toolbox is mainly used for transforming and processing geodata and creating maps from raster and vector data. It also has built-in functions for extracting field data from signal data, and tools for trimming, interpolation and resampling and processing transformation data [31].

2.8.3 System Identification Toolbox

The System Identification Toolbox helps with the construction of mathematical models of dynamic systems from measured data. It has built functions to help dynamic system modelling which is not easily modelled from specifications alone. It supports time-domain and frequency-domain data for identification of transfer functions and process models amongst other. The toolbox provides identification techniques such subspace system identification and can estimate parameters for user-defined models with grey-box system identifications [32].

3 Method

This chapter will describe the scientific approach and method used for this thesis. There will also be a brief description of the initial preparations and initial literature studies conducted in preparation to produce this thesis.

In preparation for solving the proposed research question in this study, some preliminary examinations were conducted. They consisted of a visual inspection of the bridge together with the preparation of the sensor layout, and a brief literature study to get a better overview of what research has already been done to this topic and this bridge specifically.

The assumed best method for solving the research question presented in this thesis is the quantitative method, applied through a specific case study.

To fulfill the purpose of this study and to fully answer the research question, a series of steps must be followed in succeeding or parallel order. The first objectives are to acquire acceleration data measured from the bridge and to create the initial final element model. The next steps are to do a modal analysis on both the initial model and the acquired data. The results from the data will return the actual dynamic response of the bridge within the quantified error margins. The modal analysis of the initial model will create an overview of corresponding mode shapes and frequencies, which in turn will be used when the model is updated, to assure that the correct modal parameters are matched for the final model. The last step is a loop that continues until a satisfactory result is achieved. This loop consists of altering and updating the FE model before conducting a modal parameter analysis, and lastly evaluating the results to measure the difference between the updated model and the assumed correct dynamic behavior of the bridge earlier found from the acquired data analysis.

The flowchart below (Figure 8) shows the arrangement of operations performed for solving the research question.

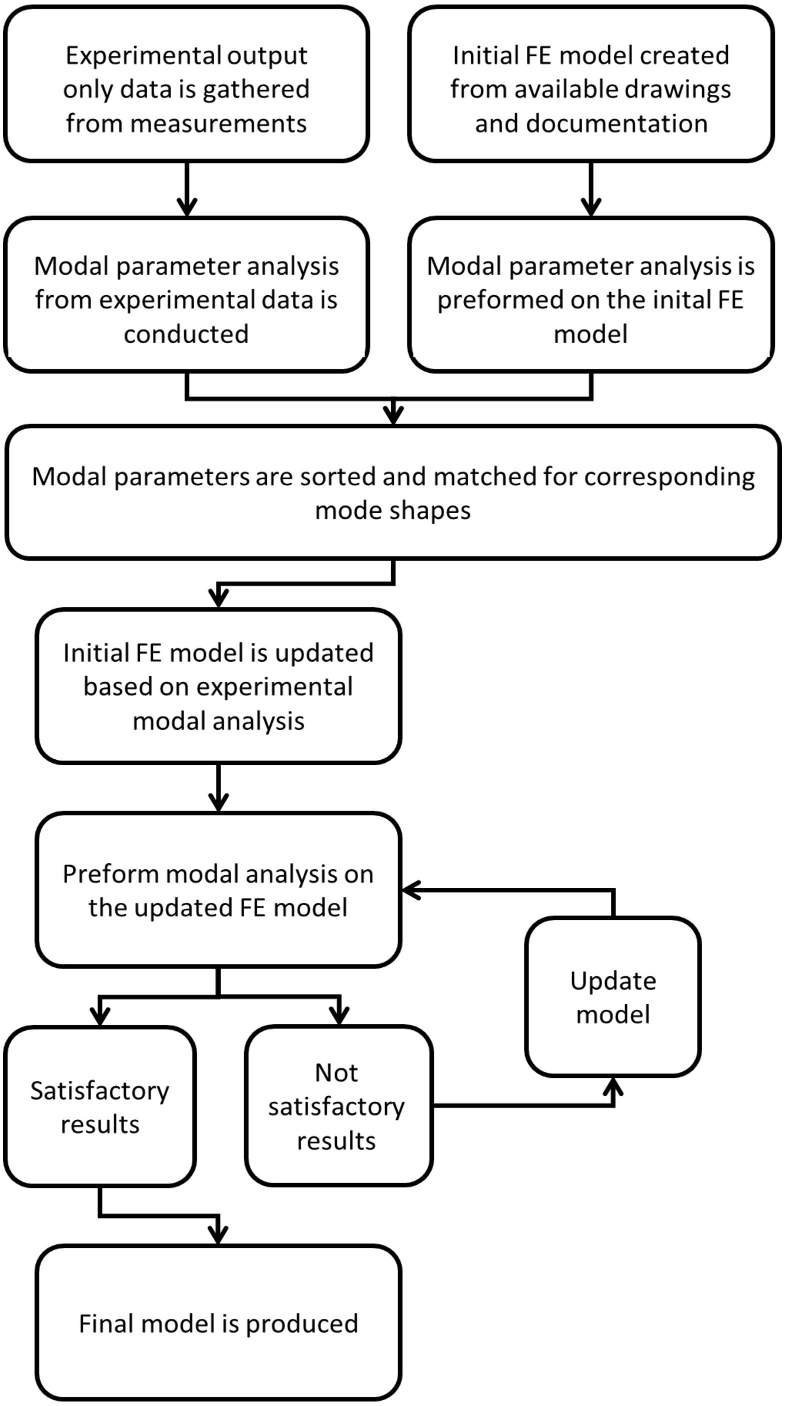
Experimental output only data is gathered from measurements
Initial FE model created from available drawings and documentation
Modal parameter analysis from experimental data is conducted
Modal parameter analysis is preformed on the inital FE model
Modal parameters are sorted and matched for corresponding mode shapes
Initial FE model is updated based on experimental modal analysis
Preform modal analysis on the updated FE model
Update model
Satisfactory results
Not satisfactory results
Final model is produced

FIGURE 8: FLOWCHART DESCRIBING THE GENERAL WORKFLOW OF THE THESIS

The chosen updating process for this case is the direct updating process executed by manual tuning of structural parameters. General knowledge and intuitive prediction of the bridge's response to altering of structural properties has been acquired through studying the geometry, structural parameters, and conducting research studies of the bridge in advance to the creation of the model. Since the bridge is a fairly simple structure there is no need for overcomplicated and advanced time-consuming iterative updating processes and therefore is the direct updating method with manual tuning chosen.

4 Sensor setup and installation

This chapter will present a description of the sensor setup an installation on the bridge prior to the data gathering preformed in two instances in February and March 2022.

4.1 Sensor setup

A total of ten sensors was installed on each of the two bridges with an equal but mirrored layout, due to the bridges same identical but mirrored design. The sensors were placed from a preliminary expectation of where the bridges mode shape would have the most displacement and hence return clearer data. Figure 9 shows the layout of the sensors on the eastern bridge, where data was gathered on the twenty-third to twenty-fifth of February 2022. Figure 10 shows the layout of the sensor on the western bridge, where data was acquired on the second to fourth of March 2022. All locations were measured and marked with paint before the installation of the measuring equipment started.

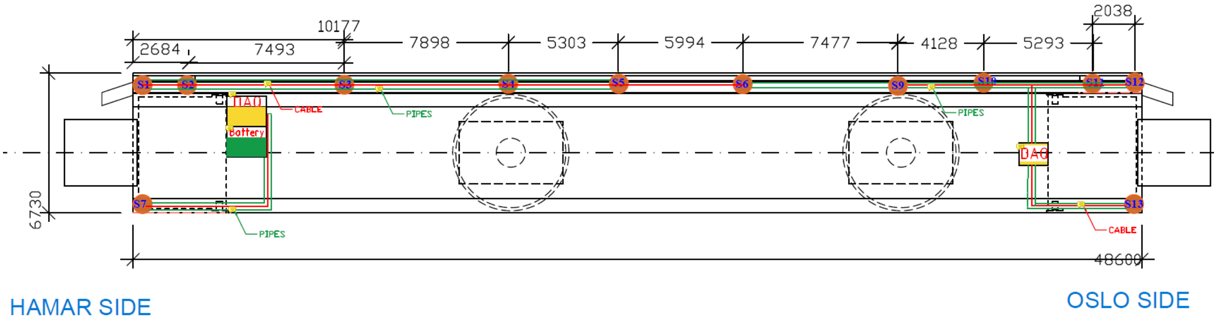

FIGURE 9: SENSOR LAYOUT FOR THE EASTERN BRIDGE.

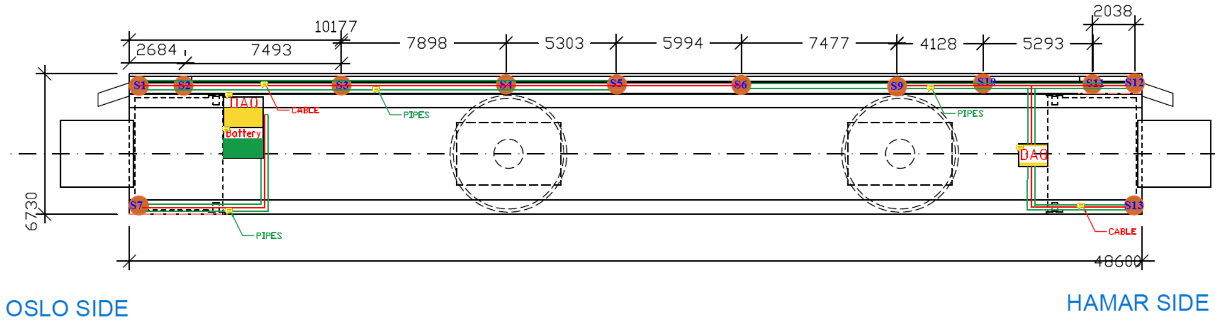

FIGURE 10: SENSOR LAYOUT FOR THE WESTERN BRIDGE

4.1.1 Sensor installation

The sensors were installed to the bridge on metal discs which was firmly and properly fastened to the surface of the concrete cover on the bridge. The location of the discs was marked with paint, and where the concrete was covered with ice, this was removed. The concrete was briefly sanded to have a smoother surface for the discs to have a steady contact with the concrete surface. The discs were attached by three bolts with a series of nuts to adjust the effective length of the bolts according to the drilling depth. A fully installed steel disc on the sanded concrete surface can be seen in Figure 11.

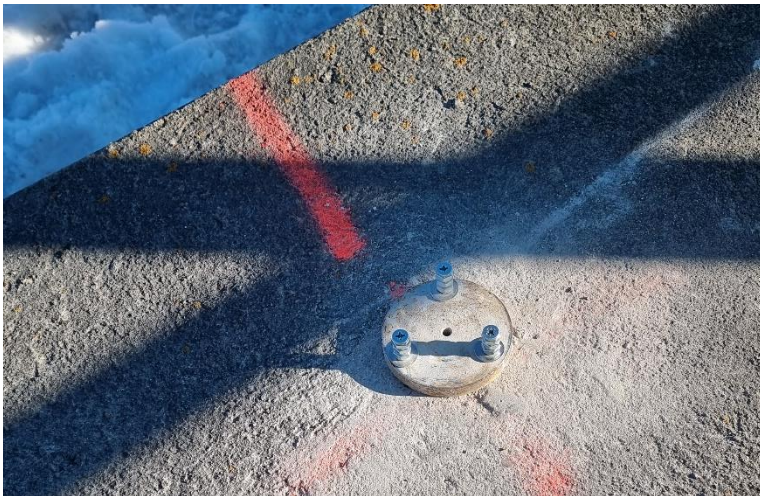

FIGURE 11: FULLY INSTALLED STEEL DISC ON THE WESTERN BRIDGE

The initial drilling depth of the holes was 25 mm and with a width of 8 mm. However, due to varying drilling skills of the drill operator and structural inconsistencies in the concrete surface and cover, some of the holes were up to 10 mm deeper, up to a total depth of 35 mm. The adjusting bolt length mechanism assured that all discs were firmly attached for all sensors even with this variation.

4.1.2 Control unit and battery

The last step is to connect the sensors and the battery to the control unit. This is done after all discs and sensors are installed, and after all the cable management is complete. The cables were carefully gathered and attached to the railing of the bridge to prevent them from moving and to ensure they would cause as little disruption as possible to the signals from the sensor. After the measuring was started, the control unit and battery were securely fastened to the railing of the bridge with straps to make sure nothing would be in danger of moving during the measurements. The battery was covered with a ventilated plastic cover to ensure that it would not overheat nor get wet from snow or rain. Figure 12 shows the fully secured and locked protective cabinet with the control unit inside which was set up for data gathering on the twenty-third of February 2022.

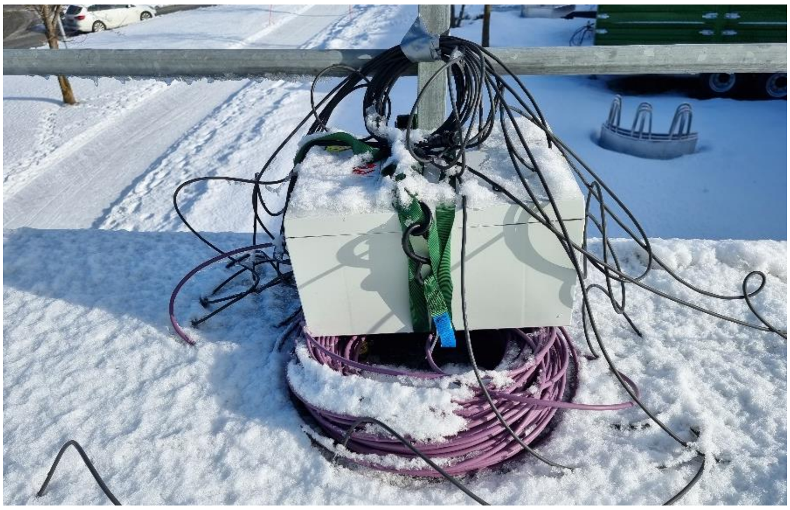

FIGURE 12: LOCKED AND SECURED PROTECTIVE CABINET WITH CONTROL UNIT

5 Extracting data with Matlab

The method for extracting sensor data using Matlab will be covered in this chapter. After all of the measurements were completed, the data was converted to txt-flies so that it could be easier to work with in Matlab. All the data was distributed into four folders depending on which days they were recorded. Three of the folders contained data from the recordings of track two on the eastern bridge:

- 2022.02.23-24
- 2022.02.24-25
- 2022.03.02-03

The last folder contained the data from the recordings of track one on the western bridge:

- 2022.03.03-04

Each txt-file in the folder contained 30 to 60 minutes of data. The initial step was to crop these files into smaller files containing the train passings, that each have 2 minutes of data. The next step was to remove the anomalies in the train passings that contained anomalies. After following these two steps, a stabilization diagram and mode shapes could be made of each train passing. This process will be explained in detail in the next subchapters, as well as the process for checking the maximum accelerations.

5.1 Cropping data

To crop the data into smaller files of 2 minutes of data containing the train passings, the code in appendix A was used. The code will be examined in this subchapter. The wanted folder with the data from each day was chosen with the code in Figure 13.

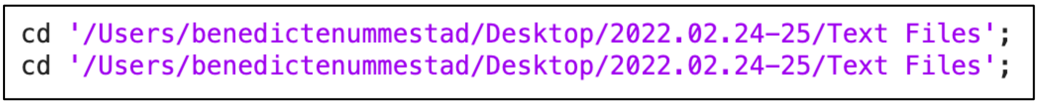

```
cd '/Users/benedictenummestad/Desktop/2022.02.24-25/Text Files';
cd '/Users/benedictenummestad/Desktop/2022.02.24-25/Text Files';
```

FIGURE 13: CODE USED TO CHOOSE THE WANTED FOLDER.

The next step in the code is shown in Figure 14.

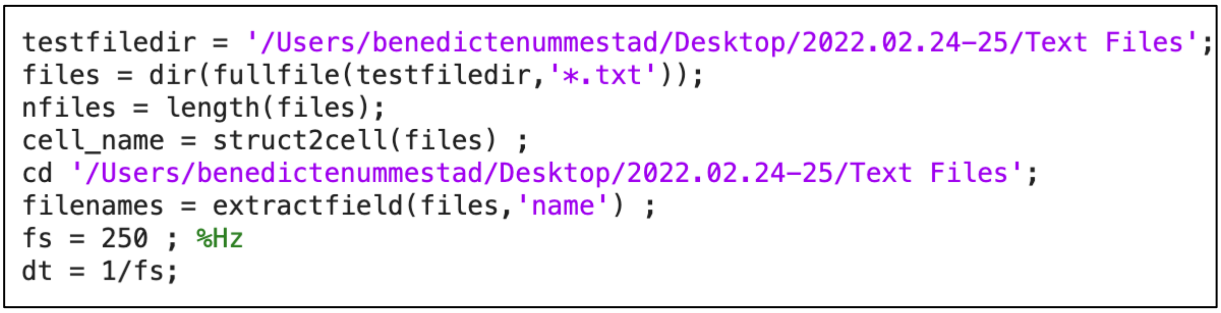

```
testfiledir = '/Users/benedictenummestad/Desktop/2022.02.24-25/Text Files';
files = dir(fullfile(testfiledir,'*.txt'));
nfiles = length(files);
cell_name = struct2cell(files) ;
cd '/Users/benedictenummestad/Desktop/2022.02.24-25/Text Files';
filenames = extractfield(files,'name') ;
fs = 250 ; %Hz
dt = 1/fs;
```

FIGURE 14: CODE USED TO DETERMINE "TESTFILEDIR", "FILES", "NFILES", "CELL_NAME", "FILENAMES", "FS" AND "DT".

This code is used for the following:

- "testfiledir" determents where the files are retrieved from,
- "files" creates a struct with all the files,
- "nfiles" decides the number of files in the chosen folder,
- "cell_name" creates a table with the information of the files,
- "filenames" lists all the names of the files,
- "fs" is how many parts each second is divided into,
- and "dt" is the formula used to create the time vector later in the code.

The file that is going to be used from the chosen folder, is chosen with "i" from the code in Figure 15.

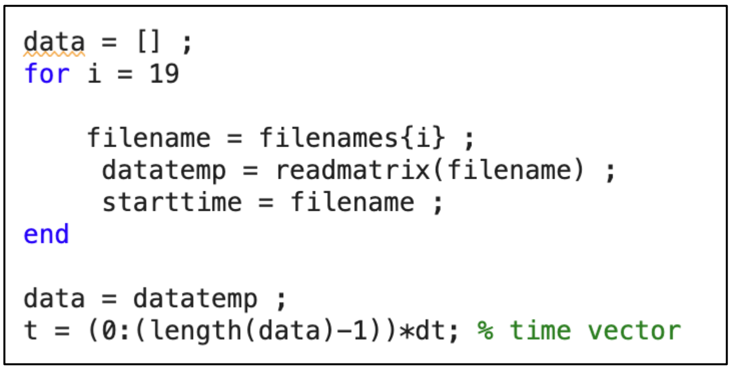

```
data = [] ;
for i = 19

    filename = filenames{i} ;
     datatemp = readmatrix(filename) ;
     starttime = filename ;
end

data = datatemp ;
t = (0:(length(data)-1))*dt; % time vector
```

FIGURE 15: CODE USED TO DETERMINE "I", "FILENAME", "DATATEMP", "STARTTIME", "DATA", "DATATEMP" AND "T".

This code is used for the following:

- “filename” shows the filename of the chosen file,
- “datatemp” reads the matrix in the file,
- “starttime” defines where the measurement starts,
- “data” shows the matrix made with “datatemp”,
- and “t” defines the time vector.

The outlay of the figure was decided with the code in Figure 16.

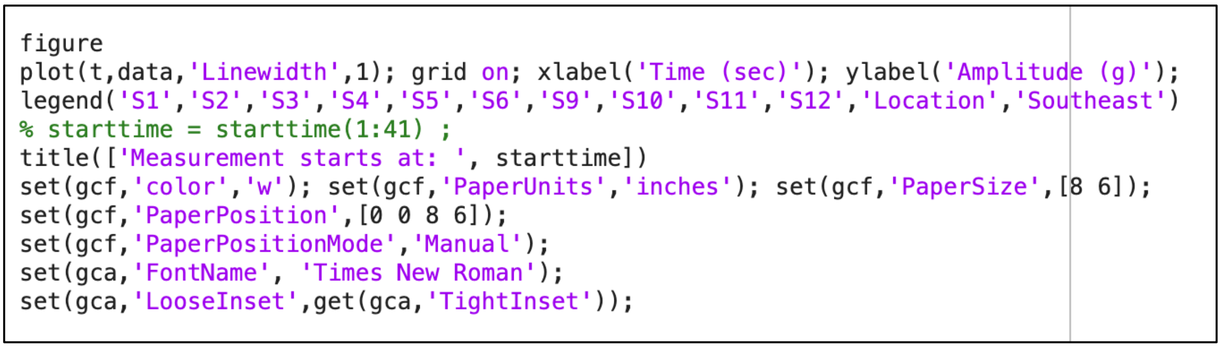

```
figure
plot(t,data,'Linewidth',1); grid on; xlabel('Time (sec)'); ylabel('Amplitude (g)');
legend('S1','S2','S3','S4','S5','S6','S9','S10','S11','S12','Location','Southeast')
% starttime = starttime(1:41) ;
title(['Measurement starts at: ', starttime])
set(gcf,'color','w'); set(gcf,'PaperUnits','inches'); set(gcf,'PaperSize',[8 6]);
set(gcf,'PaperPosition',[0 0 8 6]);
set(gcf,'PaperPositionMode','Manual');
set(gca,'FontName', 'Times New Roman');
set(gca,'LooseInset',get(gca,'TightInset'));
```

FIGURE 16: CODE USED TO DETERMINE THE OUTLAY OF THE FIGURE.

After running this code, Matlab will show the figure of the vibrations from the chosen train passing, which mostly is either half an hour or an hour. Figure 17 shows an example.

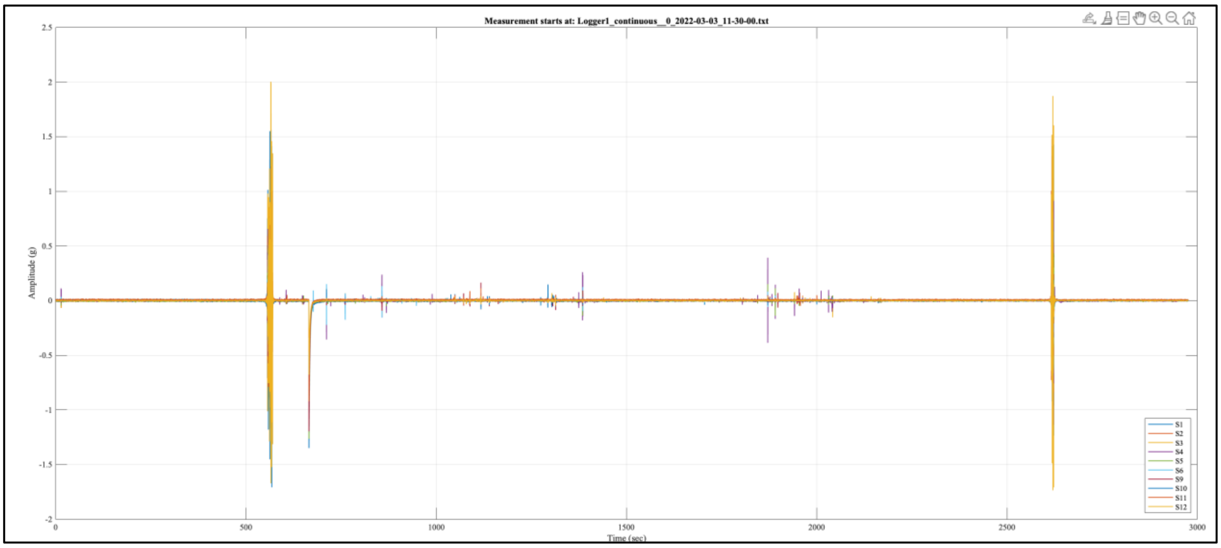

FIGURE 17: EXAMPLE OF A FIGURE OF TRAIN PASSING DATA.

This is then needed to be cropped into one or several parts, depending on the number of crossings that can be seen in the figure. The cropped data should have the length of 120 seconds and should contain the train passing. The code used for this is shown in Figure 18.

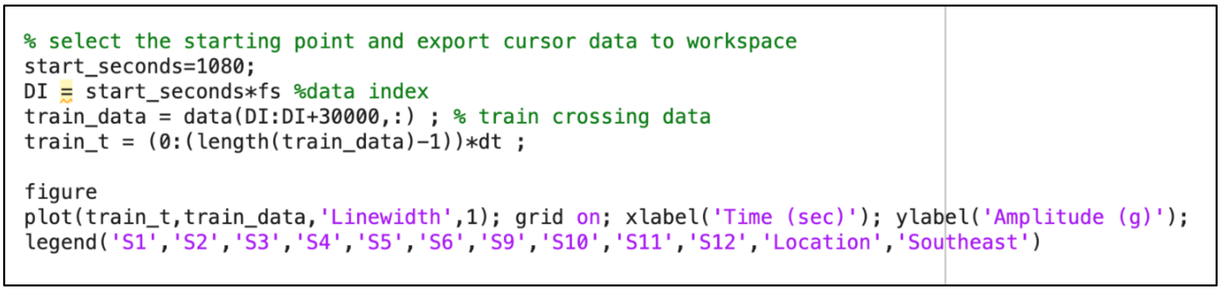

```
% select the starting point and export cursor data to workspace
start_seconds=1080;
DI = start_seconds*fs %data index
train_data = data(DI:DI+30000,:) ; % train crossing data
train_t = (0:(length(train_data)-1))*dt ;

figure
plot(train_t,train_data,'Linewidth',1); grid on; xlabel('Time (sec)'); ylabel('Amplitude (g)');
legend('S1','S2','S3','S4','S5','S6','S9','S10','S11','S12','Location','Southeast')
```

FIGURE 18: CODE USED TO CROP THE DATA.

The wanted starting point, usually 0-60 seconds before the train passing, is written as “start_seconds”. “DI” multiplies this with “fs”, and “train_data” decides the starting point and ending point. Figure 19 shows an example of a figure shown after using this code.

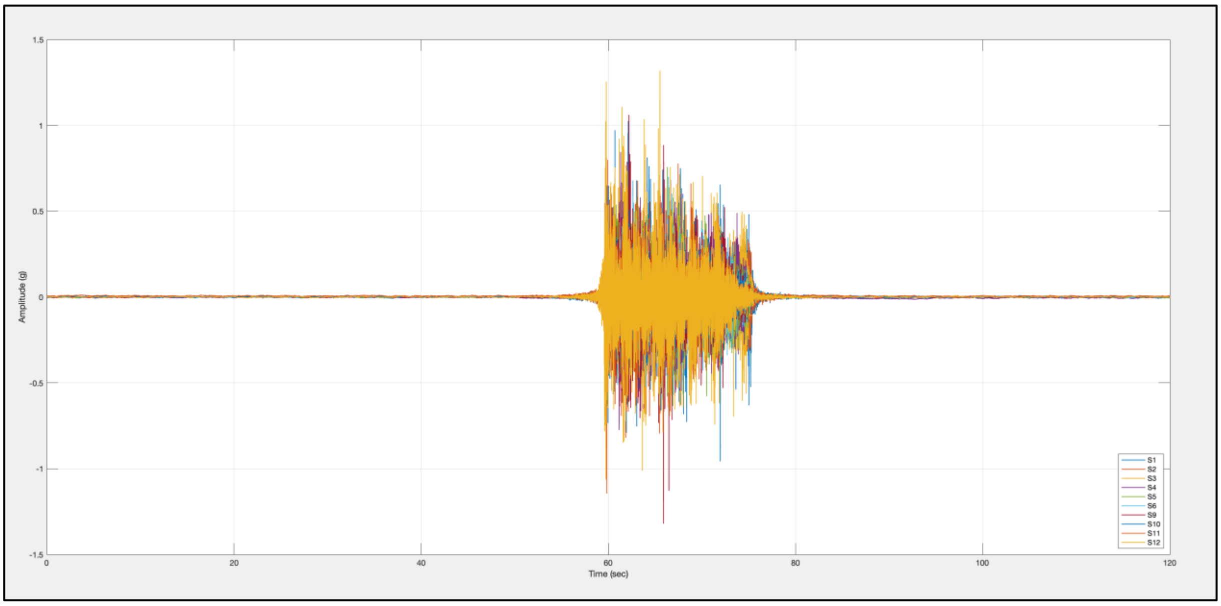

FIGURE 19: EXAMPLE OF TRAIN DATA CROPPED INTO 120 SECONDS.

This cropped data is then saved as a txt-file with the code shown in Figure 20.

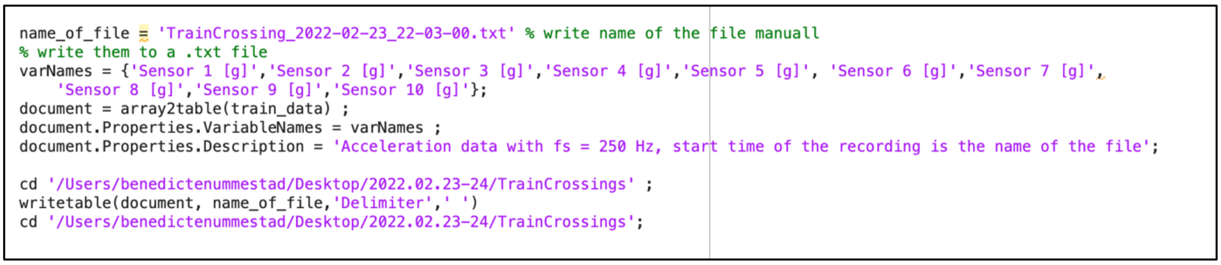

```
name_of_file = 'TrainCrossing_2022-02-23_22-03-00.txt' % write name of the file manuall
% write them to a .txt file
varNames = {'Sensor 1 [g]','Sensor 2 [g]','Sensor 3 [g]','Sensor 4 [g]','Sensor 5 [g]', 'Sensor 6 [g]','Sensor 7 [g]',
    'Sensor 8 [g]','Sensor 9 [g]','Sensor 10 [g]'};
document = array2table(train_data) ;
document.Properties.VariableNames = varNames ;
document.Properties.Description = 'Acceleration data with fs = 250 Hz, start time of the recording is the name of the file';

cd '/Users/benedictenummestad/Desktop/2022.02.23-24/TrainCrossings' ;
writetable(document, name_of_file,'Delimiter',' ')
cd '/Users/benedictenummestad/Desktop/2022.02.23-24/TrainCrossings';
```

FIGURE 20: CODE USED TO SAVE THE CROPPED DATA INTO A TXT-FILE.

5.2 Removing anomalies

Some of the data contained anomalies within the train passings, which needed to be removed for the data to be useable. Figure 21 shows an example of how a train passing with an anomaly could look like.

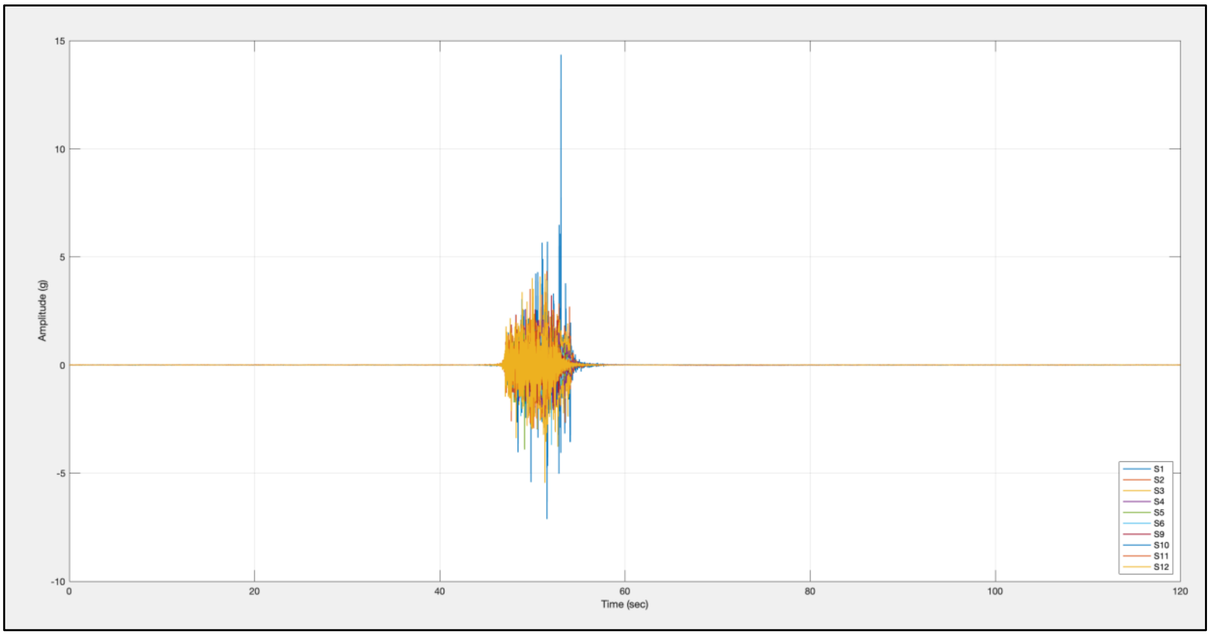

FIGURE 21: EXAMPLE OF HOW A TRAIN PASSING WITH AN ANOMALY COULD LOOK LIKE.

To remove the anomalies, the code in appendix B was used. This subchapter will analyze the code in this appendix.

First, the code shown in Figure 22 is utilized. This is the same code used at the beginning of appendix A, and it is explained in the previous subchapter.

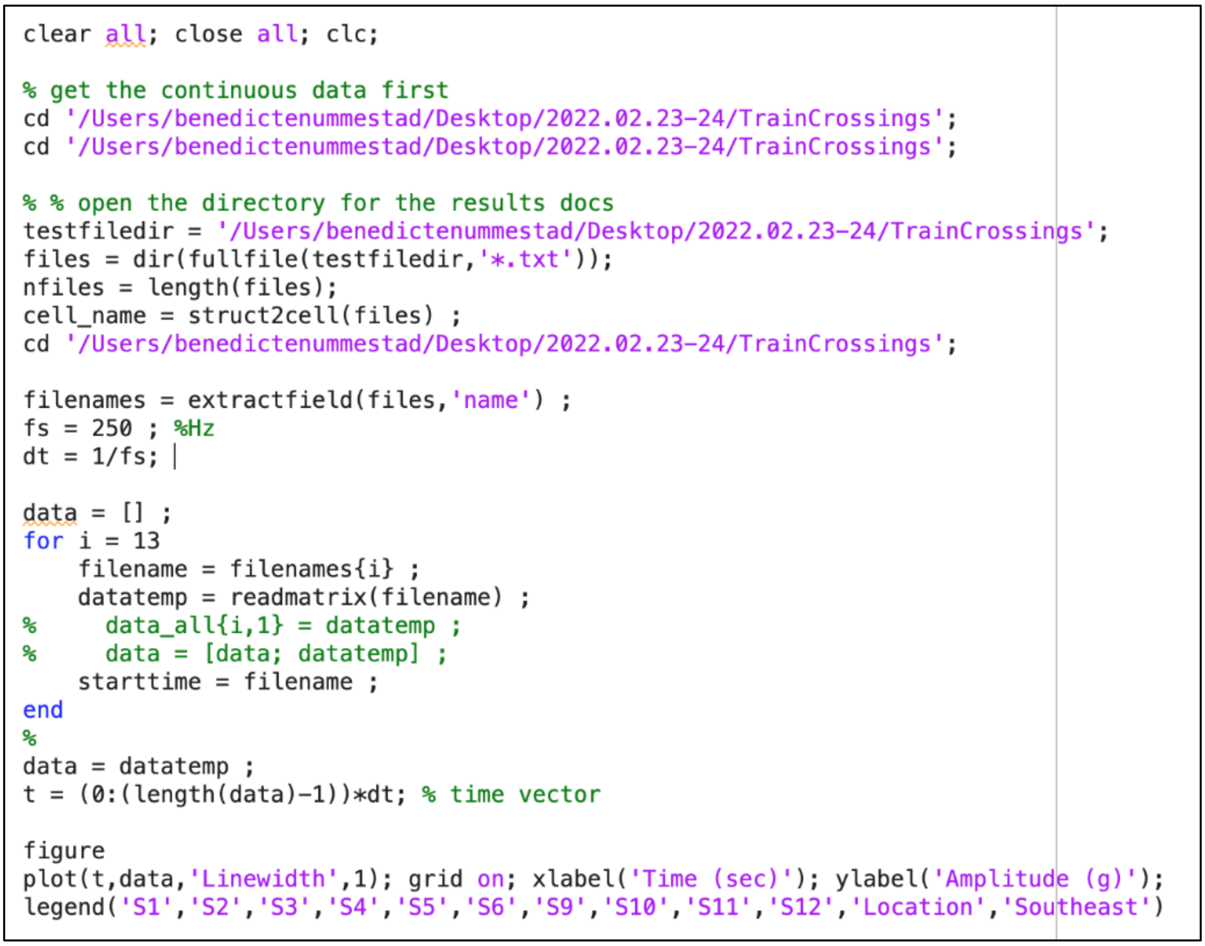

```
clear all; close all; clc;

% get the continuous data first
cd '/Users/benedictenummestad/Desktop/2022.02.23-24/TrainCrossings';
cd '/Users/benedictenummestad/Desktop/2022.02.23-24/TrainCrossings';

% % open the directory for the results docs
testfiledir = '/Users/benedictenummestad/Desktop/2022.02.23-24/TrainCrossings';
files = dir(fullfile(testfiledir,'*.txt'));
nfiles = length(files);
cell_name = struct2cell(files) ;
cd '/Users/benedictenummestad/Desktop/2022.02.23-24/TrainCrossings';

filenames = extractfield(files,'name') ;
fs = 250 ; %Hz
dt = 1/fs; 

data = [] ;
for i = 13
    filename = filenames{i} ;
    datatemp = readmatrix(filename) ;
%     data_all{i,1} = datatemp ;
%     data = [data; datatemp] ;
    starttime = filename ;
end
%
data = datatemp ;
t = (0:(length(data)-1))*dt; % time vector

figure
plot(t,data,'Linewidth',1); grid on; xlabel('Time (sec)'); ylabel('Amplitude (g)');
legend('S1','S2','S3','S4','S5','S6','S9','S10','S11','S12','Location','Southeast')
```

FIGURE 22: CODE USED FOR PURPOSES EXPLAINED IN PREVIOUS SUBCHAPTER.

When the figure is shown, the “Data Tips” function is used to mark the anomaly, and “Export Cursor Data to Workspace…” is chosen. This will save the chosen point as “cursor_info”. To check if the chosen point really is an anomaly, the code in Figure 23 is utilized.

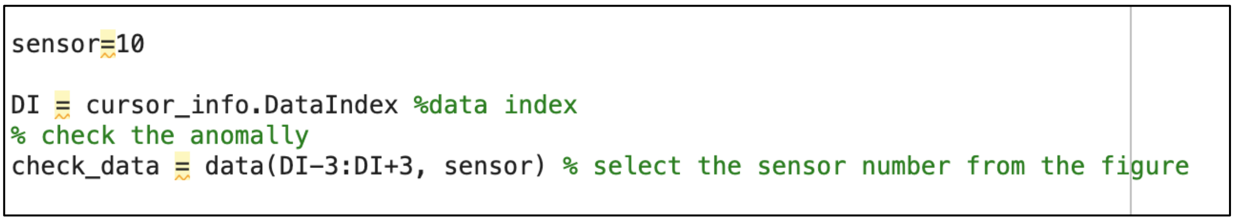

```
sensor=10

DI = cursor_info.DataIndex %data index
% check the anomally
check_data = data(DI-3:DI+3, sensor) % select the sensor number from the figure
```

FIGURE 23: CODE USED TO CHECK IF THE CHOSEN POINT IS AN ANOMALY.

After “sensor=” the sensor number of the sensor with the anomaly is written. When the code is run, the value of the chosen point is shown, as well as the value of the three points before and after the chosen point. If the value of the chosen point differs significantly from the values of the points before and after, it can be concluded that the chosen point is an anomaly.

The code in Figure 24 is used to delete the anomaly. This will delete the 1/250 second where the chosen point was set. After running the code, a figure of how the train passing looks like now will be shown. If there are more than one anomaly in the train crossing, the figure shown can be used to choose a new point to check another anomaly. Another point is chosen with the “Data tips” function and the process using the code from Figure 23 and Figure 24 is then be repeated.

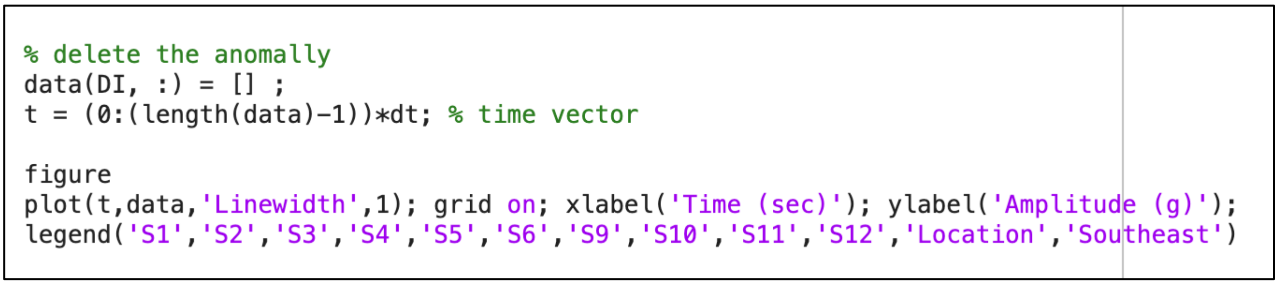

```
% delete the anomally
data(DI, :) = [] ;
t = (0:(length(data)-1))*dt; % time vector

figure
plot(t,data,'Linewidth',1); grid on; xlabel('Time (sec)'); ylabel('Amplitude (g)');
legend('S1','S2','S3','S4','S5','S6','S9','S10','S11','S12','Location','Southeast')
```

FIGURE 24: CODE USED TO DELETE ANOMALY.

When all the anomalies are deleted, the code in Figure 20 is used to save the fixed data as a txt-file.

5.3 SSI-Cov

After the data is cropped and the anomalies are removed, the data is ready for the operational modal analysis (OMA) using the covariance-driven stochastic subspace identification (SSI-Cov) method. To do this the code in appendix C is used. The first part of the code, shown in Figure 25, is used and described in chapter 5.1.

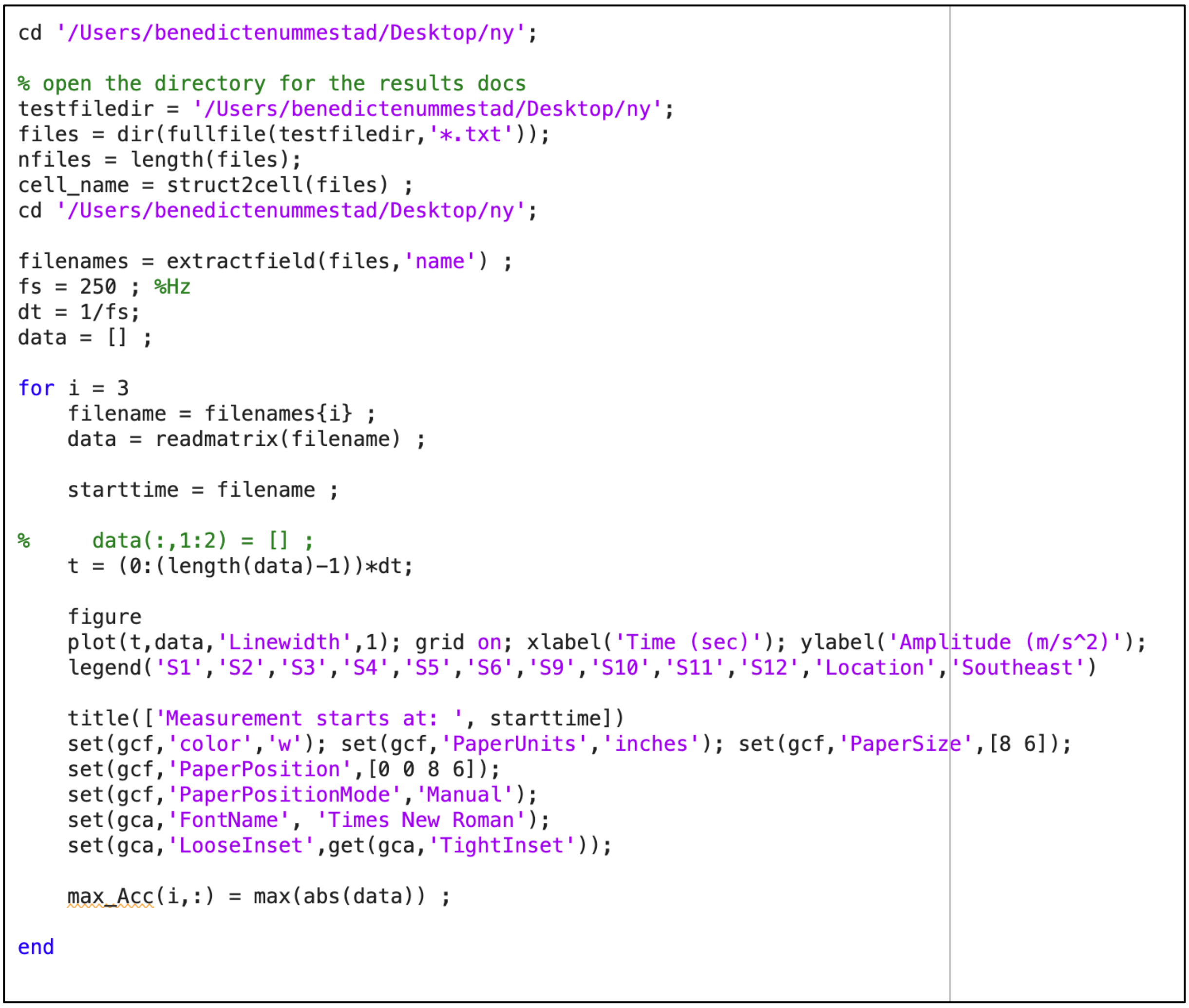

```
cd '/Users/benedictenummestad/Desktop/ny';

% open the directory for the results docs
testfiledir = '/Users/benedictenummestad/Desktop/ny';
files = dir(fullfile(testfiledir,'*.txt'));
nfiles = length(files);
cell_name = struct2cell(files) ;
cd '/Users/benedictenummestad/Desktop/ny';

filenames = extractfield(files,'name') ;
fs = 250 ; %Hz
dt = 1/fs;
data = [] ;

for i = 3
    filename = filenames{i} ;
    data = readmatrix(filename) ;

    starttime = filename ;

%     data(:,1:2) = [] ;
    t = (0:(length(data)-1))*dt;

    figure
    plot(t,data,'Linewidth',1); grid on; xlabel('Time (sec)'); ylabel('Amplitude (m/s^2)');
    legend('S1','S2','S3','S4','S5','S6','S9','S10','S11','S12','Location','Southeast')

    title(['Measurement starts at: ', starttime])
    set(gcf,'color','w'); set(gcf,'PaperUnits','inches'); set(gcf,'PaperSize',[8 6]);
    set(gcf,'PaperPosition',[0 0 8 6]);
    set(gcf,'PaperPositionMode','Manual');
    set(gca,'FontName', 'Times New Roman');
    set(gca,'LooseInset',get(gca,'TightInset'));

    max_Acc(i,:) = max(abs(data)) ;

end
```

FIGURE 25: CODE WITH PURPOSES EXPLAINED EARLIER IN THIS CHAPTER.

When the figure is shown after running this code, the “Data Tips” function is used to mark the anomaly, and “Export Cursor Data to Workspace…” is used to choose a starting point. This is usually around one second before the vibrations are significantly lower. When a starting point is chosen, the next part of the code, shown in Figure 26, can be run.

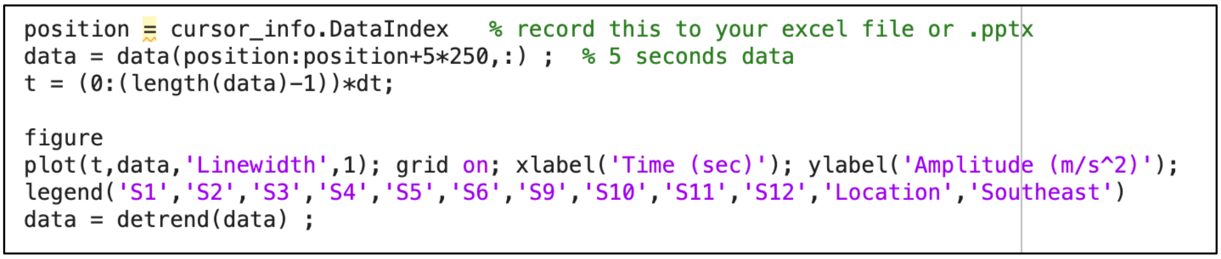

```
position = cursor_info.DataIndex   % record this to your excel file or .pptx
data = data(position:position+5*250,:) ;  % 5 seconds data
t = (0:(length(data)-1))*dt;

figure
plot(t,data,'Linewidth',1); grid on; xlabel('Time (sec)'); ylabel('Amplitude (m/s^2)');
legend('S1','S2','S3','S4','S5','S6','S9','S10','S11','S12','Location','Southeast')
data = detrend(data) ;
```

FIGURE 26: CODE USED TO CROP THE DATA INTO 5 SECONDS AFTER THE CHOSEN STARTING POINT TO CAPTURE THE FREE VIBRATIONS.

This code crops the data into 5 seconds after the chosen starting point to capture the free vibrations. This will also show a figure of the cropped data. An example of how the cropped data of the free vibrations can look like is shown in Figure 27.

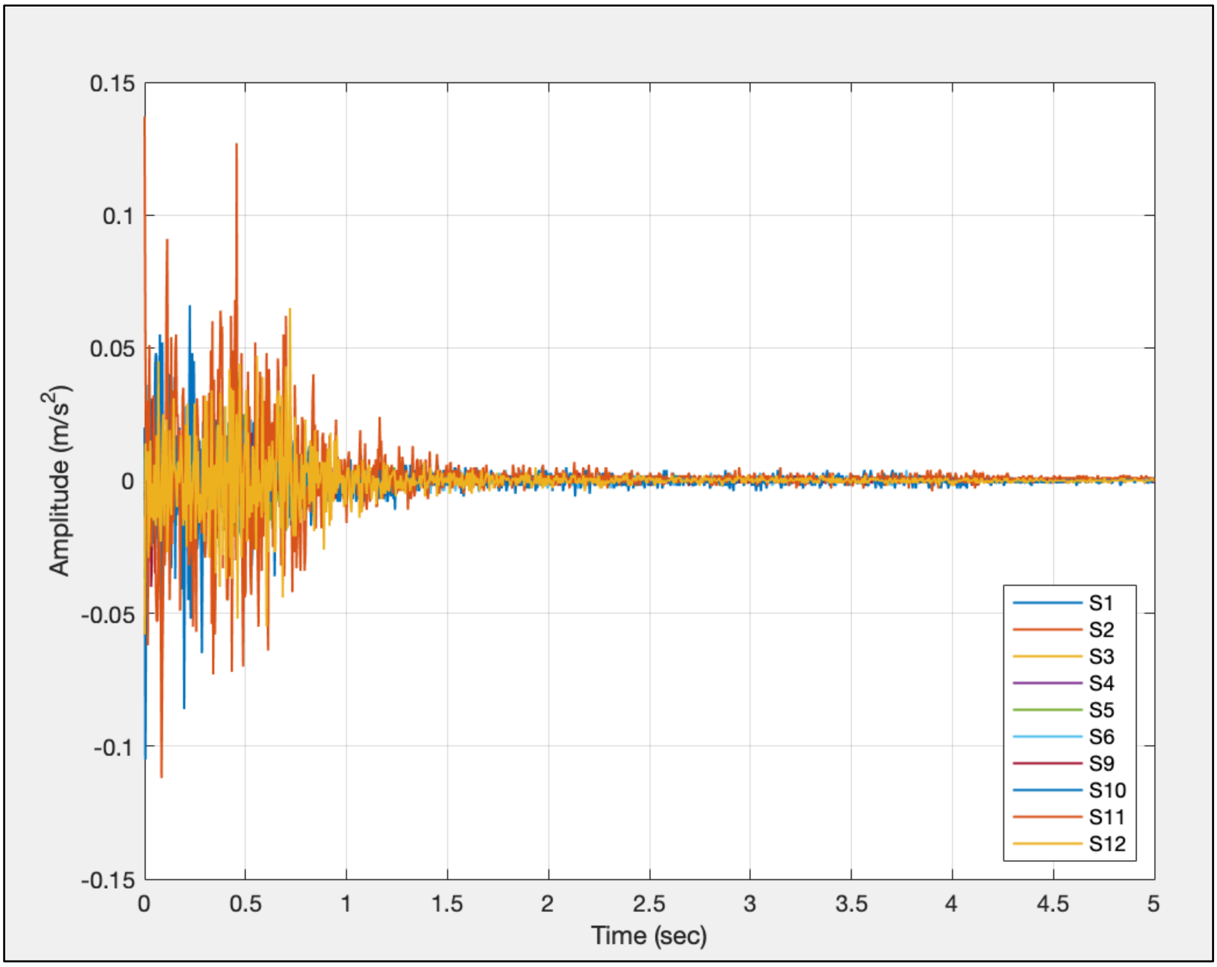

FIGURE 27: EXAMPLE OF HOW THE CROPPED DATA OF THE FREE VIBRATIONS CAN LOOK LIKE.

When the free vibrations are captured, the system identification can be run. To create a stabilization diagram, the code in Figure 28 is utilized.

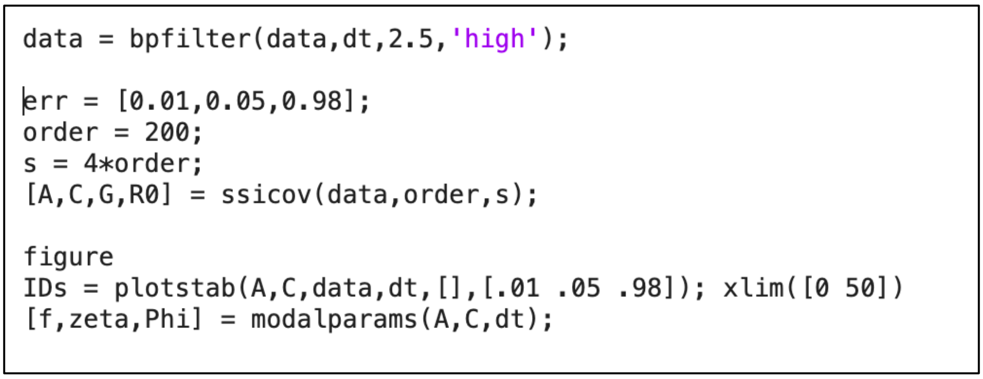

```
data = bpfilter(data,dt,2.5,'high');

err = [0.01,0.05,0.98];
order = 200;
s = 4*order;
[A,C,G,R0] = ssicov(data,order,s);

figure
IDs = plotstab(A,C,data,dt,[],[.01 .05 .98]); xlim([0 50])
[f,zeta,Phi] = modalparams(A,C,dt);
```

FIGURE 28: COD USED TO CREATE A STABILIZATION DIAGRAM.

“err” choses 1% error in frequency, 5% error in damping, and 98% confidence in mode shape vectors. “order” choses the order of the stabilization diagram, which here is set to 200. The higher the order is set, the longer the process takes, but it will also give the possibility to choose from more orders later when finding the mode shapes.

To run the figure part of the code, the “*plotslab”*-function in appendix D is needed. After running the code in Figure 28, which usually takes a few minutes depending on the chosen order, a stabilization diagram will be shown. An example of a stabilization diagram is shown in Figure 29. This is the stabilization diagram to the free vibrations in Figure 29.

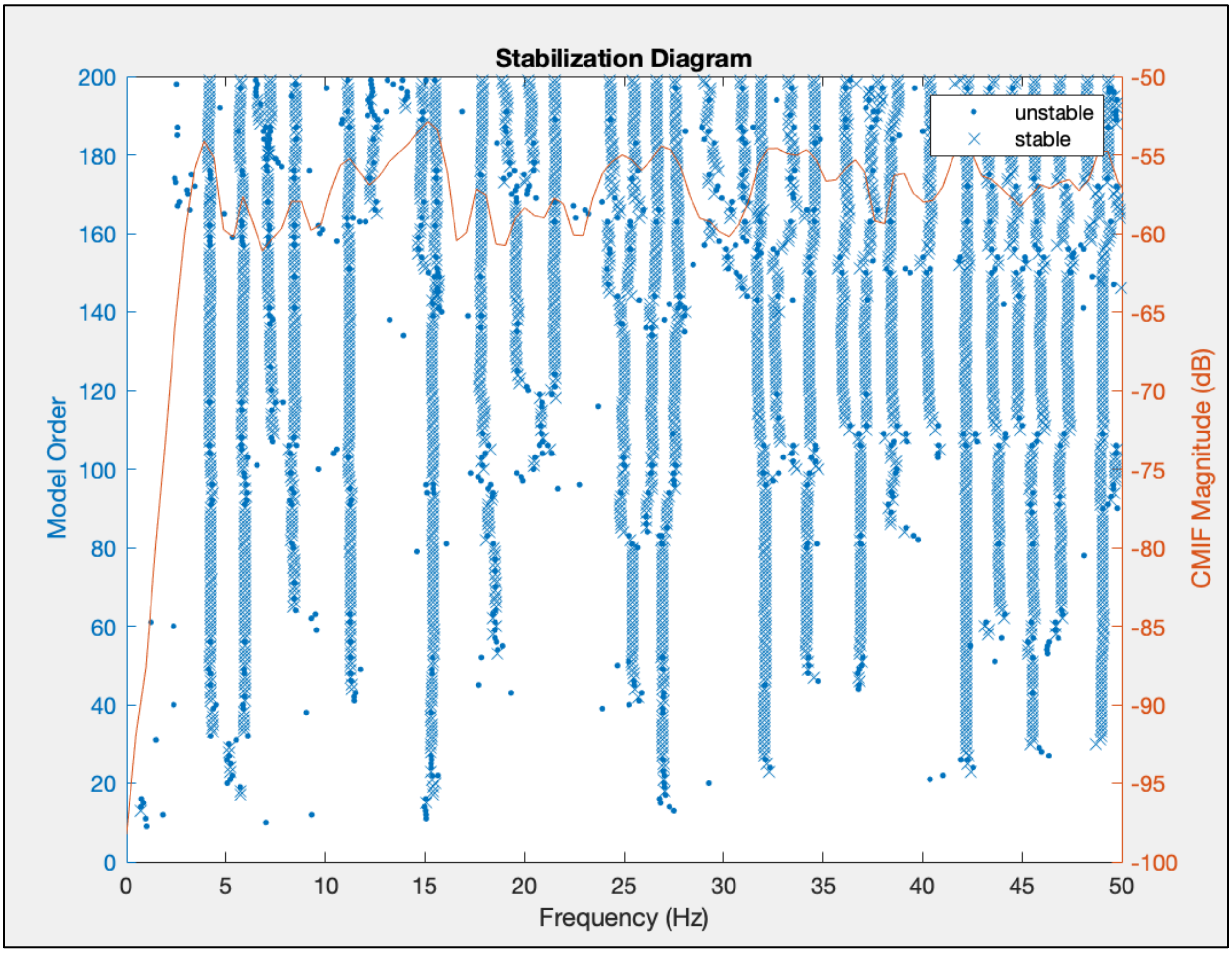

FIGURE 29: EXAMPLE OF A STABILIZATION DIAGRAM.

Looking at the stabilization diagram, an order can be selected. The higher the chosen order is, usually the more mode shapes will be shown. The next part of the code is used to determine the mode shapes and damping ratios and is shown in Figure 30.

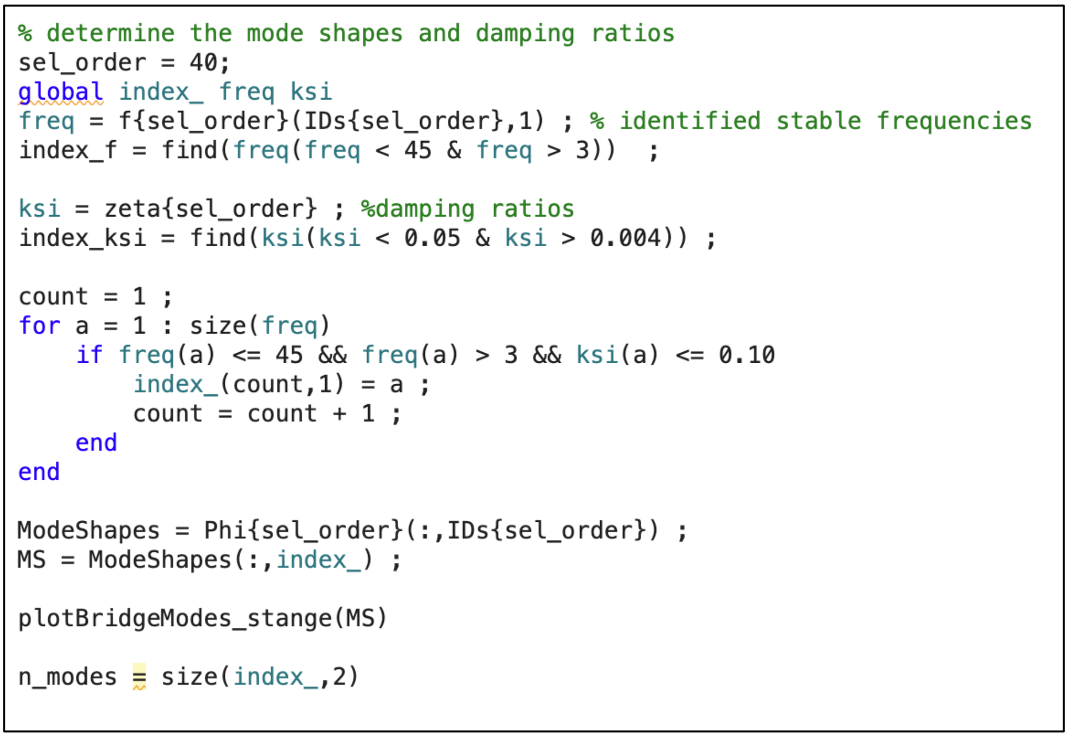

```
% determine the mode shapes and damping ratios
sel_order = 40;
global index_ freq ksi
freq = f{sel_order}(IDs{sel_order},1) ; % identified stable frequencies
index_f = find(freq(freq < 45 & freq > 3))  ;

ksi = zeta{sel_order} ; %damping ratios
index_ksi = find(ksi(ksi < 0.05 & ksi > 0.004)) ;

count = 1 ;
for a = 1 : size(freq)
    if freq(a) <= 45 && freq(a) > 3 && ksi(a) <= 0.10
        index_(count,1) = a ;
        count = count + 1 ;
    end
end

ModeShapes = Phi{sel_order}(:,IDs{sel_order}) ;
MS = ModeShapes(:,index_) ;

plotBridgeModes_stange(MS)

n_modes = size(index_,2)
```

FIGURE 30: CODE IS USED TO DETERMINE THE MODE SHAPES AND DAMPING RATIOS.

Behind “sel_order” the selected order is written. For example, selecting order 50 for the stabilization diagram in figure xxx will show the six mode shapes in Figure 31.

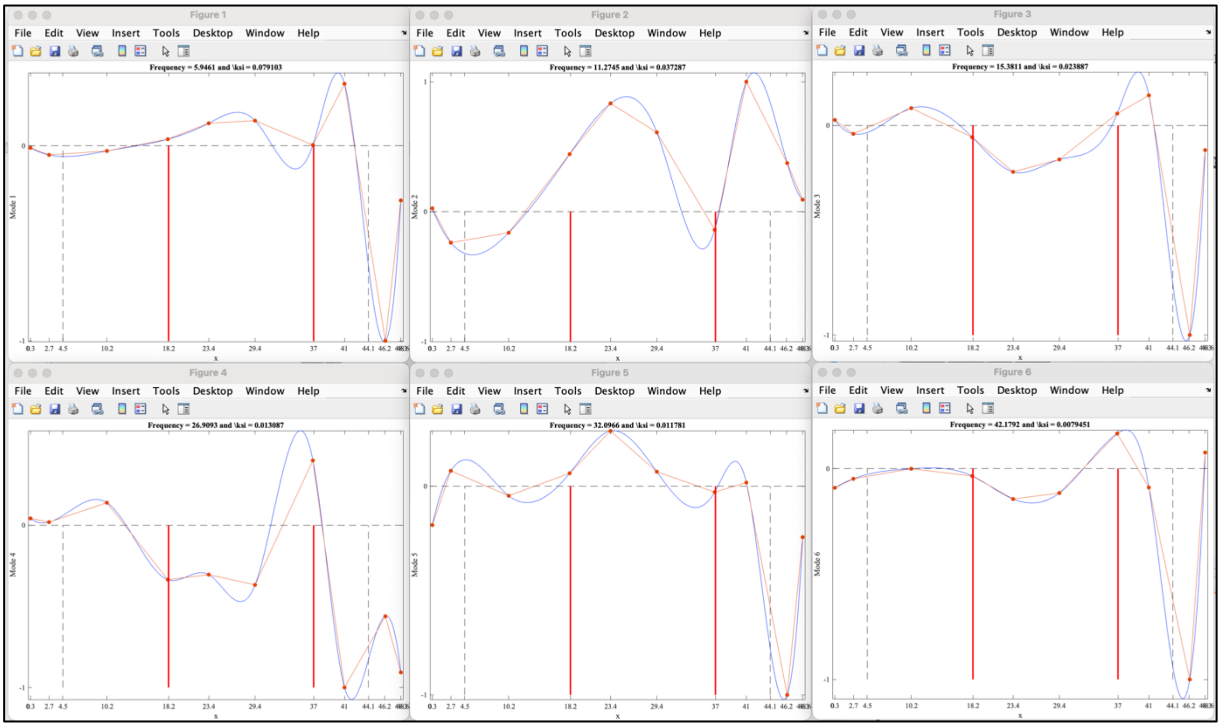
Figure 1
File Edit View Insert Tools Desktop Window Help
Frequency = 5.9461 and \ksi = 0.079103
Figure 2
Frequency = 11.2745 and \ksi = 0.037287
Figure 3
Frequency = 15.3811 and \ksi = 0.023887
Figure 4
Frequency = 26.9093 and \ksi = 0.013087
Figure 5
Frequency = 32.0966 and \ksi = 0.011781
Figure 6
Frequency = 42.1792 and \ksi = 0.0079451
Mode 1
Mode 2
Mode 3
Mode 4
Mode 5
Mode 6
0.3 2.7 4.5 10.2 18.2 23.4 29.4 37 41 44.1 46.2 48
x

FIGURE 31: EXAMPLES OF MODE SHAPES.

Here it is important to try out different selected orders to get a satisfactory result. It can also be helpful to run the SSI-COV on different periods of time of the free vibrations by setting the starting point chosen a different place. The chosen starting point should still be 0 to 2 seconds before the vibrations are reduced significantly. For this thesis, the goal was to find mode shapes resembling the ones in Figure 32.

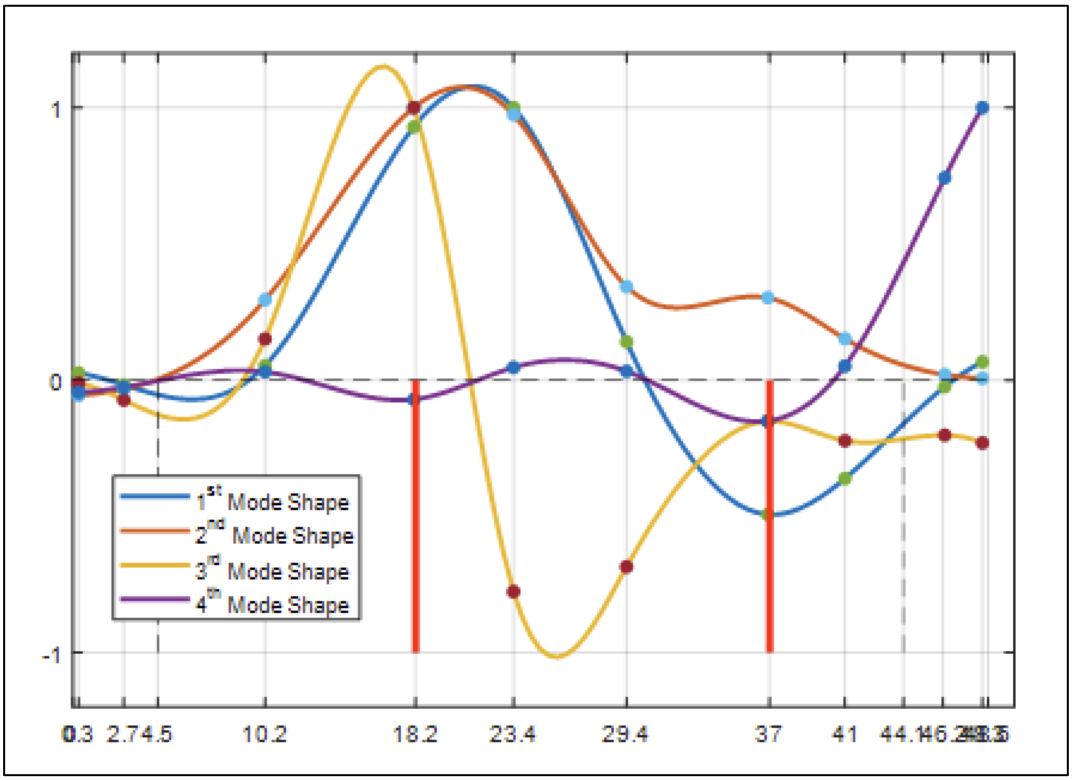

FIGURE 32: WHAT THE MODE SHAPES TO BE FOUND SHOULD LOOK LIKE.

The mode shapes should the found around following frequencies:

- 1st mode shape around 10Hz,
- 2nd mode shape around 15Hz,
- 3rd mode shape around 25Hz,
- And 4th mode shape around 33Hz.

There had to be found at least 5 resembling mode shapes for each of these mode shapes. To find one or more resembling mode shape within a train passing, multiple time periods of free vibrations and selected orders was tested. Appendix E, F and G shows the resembling modes shapes found and used as well as the chosen period of time for the free vibrations, the created stabilization diagram for this period of time and the selected order for the stabilization diagram. The mode shapes for the train passings occurring 2022.02.23-24 are in appendix E, the mode shapes for 2022.02.24-25 are in appendix F, and the mode shapes for 2022.03.02-03 are in appendix G.

The y-values from each mode shape were converted into real numbers with the code in appendix H. This is also shown in Figure 33.

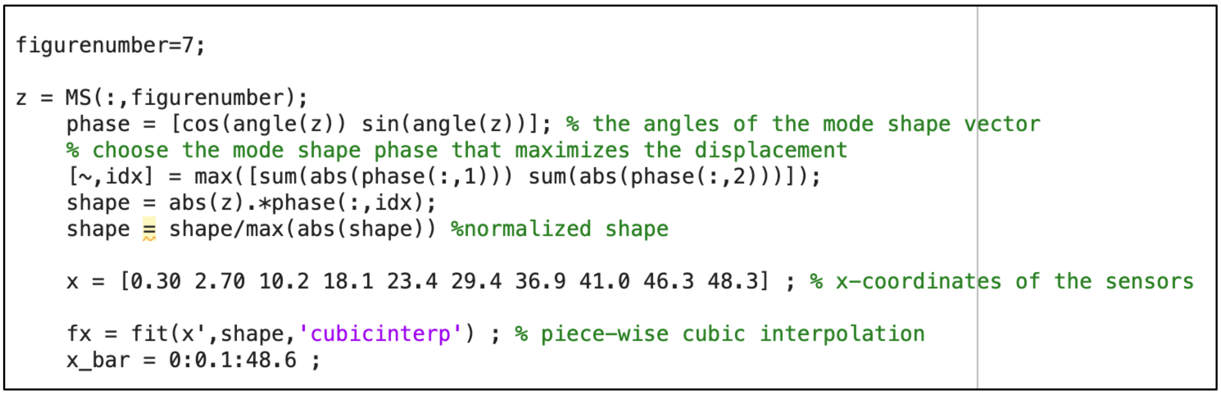

```
figurenumber=7;

z = MS(:,figurenumber);
    phase = [cos(angle(z)) sin(angle(z))]; % the angles of the mode shape vector
    % choose the mode shape phase that maximizes the displacement
    [~,idx] = max([sum(abs(phase(:,1))) sum(abs(phase(:,2)))]);
    shape = abs(z).*phase(:,idx);
    shape = shape/max(abs(shape)) %normalized shape

    x = [0.30 2.70 10.2 18.1 23.4 29.4 36.9 41.0 46.3 48.3] ; % x-coordinates of the sensors

    fx = fit(x',shape,'cubicinterp') ; % piece-wise cubic interpolation
    x_bar = 0:0.1:48.6 ;
```

FIGURE 33: CODE USED TO CONVERT ALL THE Y-VALUES FROM EACH MODE SHAPE INTO REAL NUMBERS.

The figure number if the wanted mode shape is written behind “figurenumber”, and when the code is run the y-values of sensor 1 to 10 is shown in the command window. These values are then copied into the excel sheet shown in appendix I. Table 2 shows an example where mode the 1st, 2nd and 3rd mode shape are found, and their y-values are copied into excel.

TABLE 2: AN EXAMPLE WHERE MODE THE 1ST, 2ND AND 3RD MODE SHAPE IS FOUND AND THEIR Y-VALUES ARE COPIED INTO EXCEL.

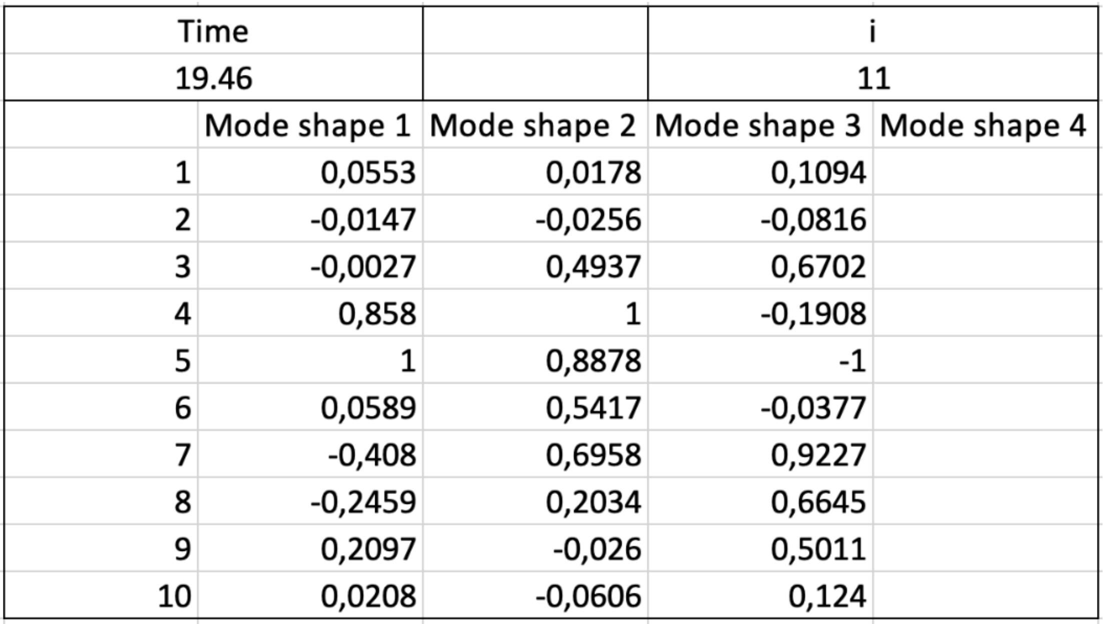

Time			i	
19.46			11	
	Mode shape 1	Mode shape 2	Mode shape 3	Mode shape 4
1	0,0553	0,0178	0,1094	
2	-0,0147	-0,0256	-0,0816	
3	-0,0027	0,4937	0,6702	
4	0,858	1	-0,1908	
5	1	0,8878	-1	
6	0,0589	0,5417	-0,0377	
7	-0,408	0,6958	0,9227	
8	-0,2459	0,2034	0,6645	
9	0,2097	-0,026	0,5011	
10	0,0208	-0,0606	0,124	

After all the needed mode shapes were found and their y-values was copied into excel, excel was used to calculate a matrix containing the average y-value of each sensor on each mode shape. This matrix is shown in Table 3

TABLE 3: CALCULATED MATRIX CONTAINING THE AVERAGE Y-VALUE OF EACH SENSOR ON EACH MODE SHAPE.

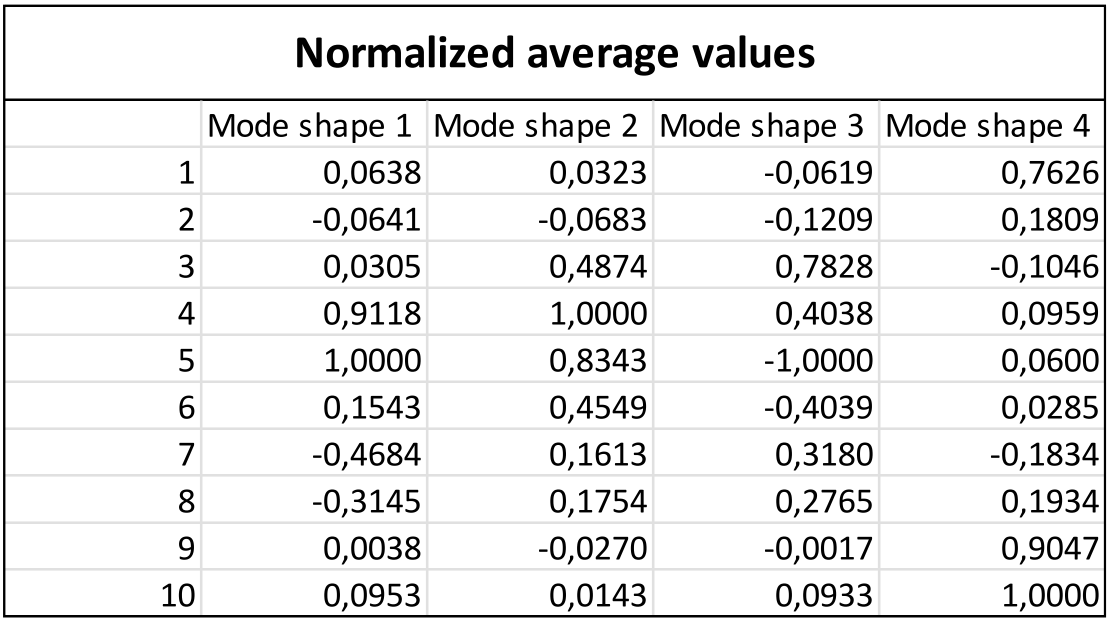

Normalized average values				
	Mode shape 1	Mode shape 2	Mode shape 3	Mode shape 4
1	0,0638	0,0323	-0,0619	0,7626
2	-0,0641	-0,0683	-0,1209	0,1809
3	0,0305	0,4874	0,7828	-0,1046
4	0,9118	1,0000	0,4038	0,0959
5	1,0000	0,8343	-1,0000	0,0600
6	0,1543	0,4549	-0,4039	0,0285
7	-0,4684	0,1613	0,3180	-0,1834
8	-0,3145	0,1754	0,2765	0,1934
9	0,0038	-0,0270	-0,0017	0,9047
10	0,0953	0,0143	0,0933	1,0000

The average mode shapes were then plotted using the code I appendix J which is also shown in Figure 34.

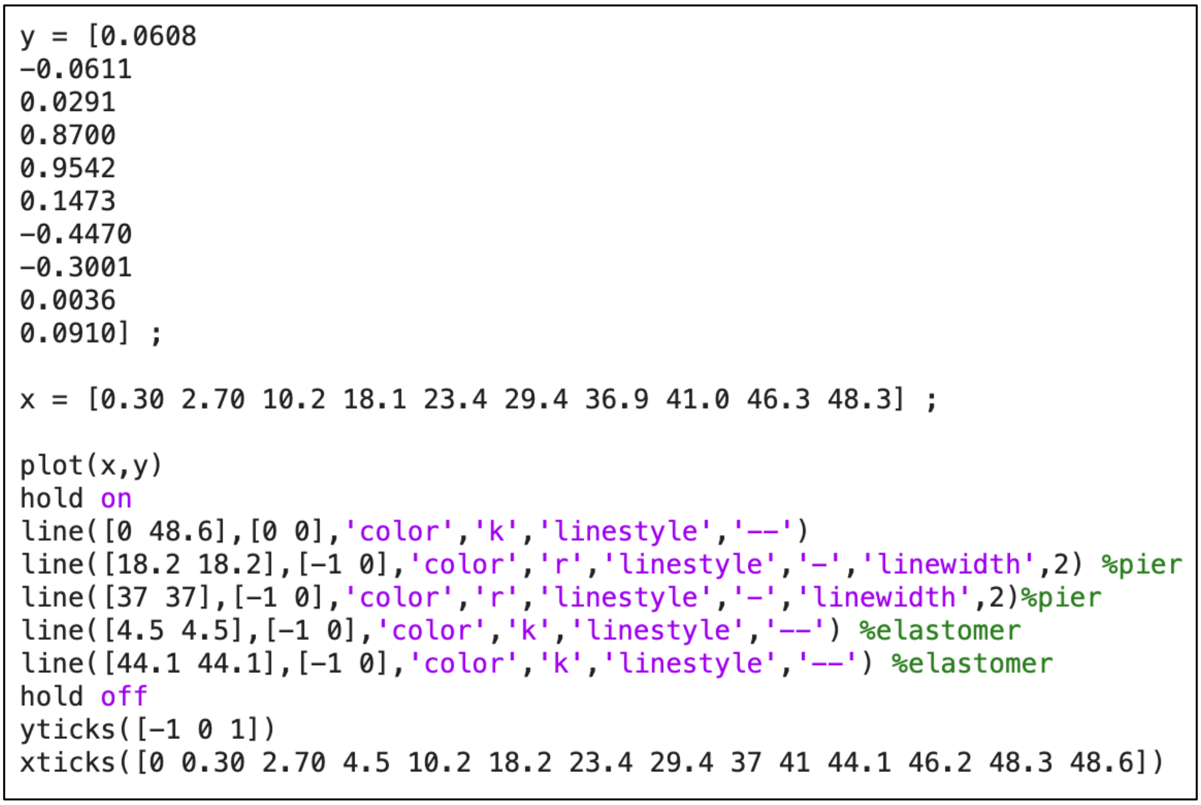

```
y = [0.0608
-0.0611
0.0291
0.8700
0.9542
0.1473
-0.4470
-0.3001
0.0036
0.0910] ;

x = [0.30 2.70 10.2 18.1 23.4 29.4 36.9 41.0 46.3 48.3] ;

plot(x,y)
hold on
line([0 48.6],[0 0],'color','k','linestyle','--')
line([18.2 18.2],[-1 0],'color','r','linestyle','-','linewidth',2) %pier
line([37 37],[-1 0],'color','r','linestyle','-','linewidth',2)%pier
line([4.5 4.5],[-1 0],'color','k','linestyle','--') %elastomer
line([44.1 44.1],[-1 0],'color','k','linestyle','--') %elastomer
hold off
yticks([-1 0 1])
xticks([0 0.30 2.70 4.5 10.2 18.2 23.4 29.4 37 41 44.1 46.2 48.3 48.6])
```

FIGURE 34: CODE USED TO PLOT THE AVERAGE MODE SHAPES.

The x-values are already known, and the y-values are copied from the matrix in excel containing the average y-values. This was done for each mode shape. Figure 35 shows the four mode shapes with the 1st mode shape on top left, 2nd mode shape on top right, 3rd mode shape on bottom left and 4th mode shape on bottom right.

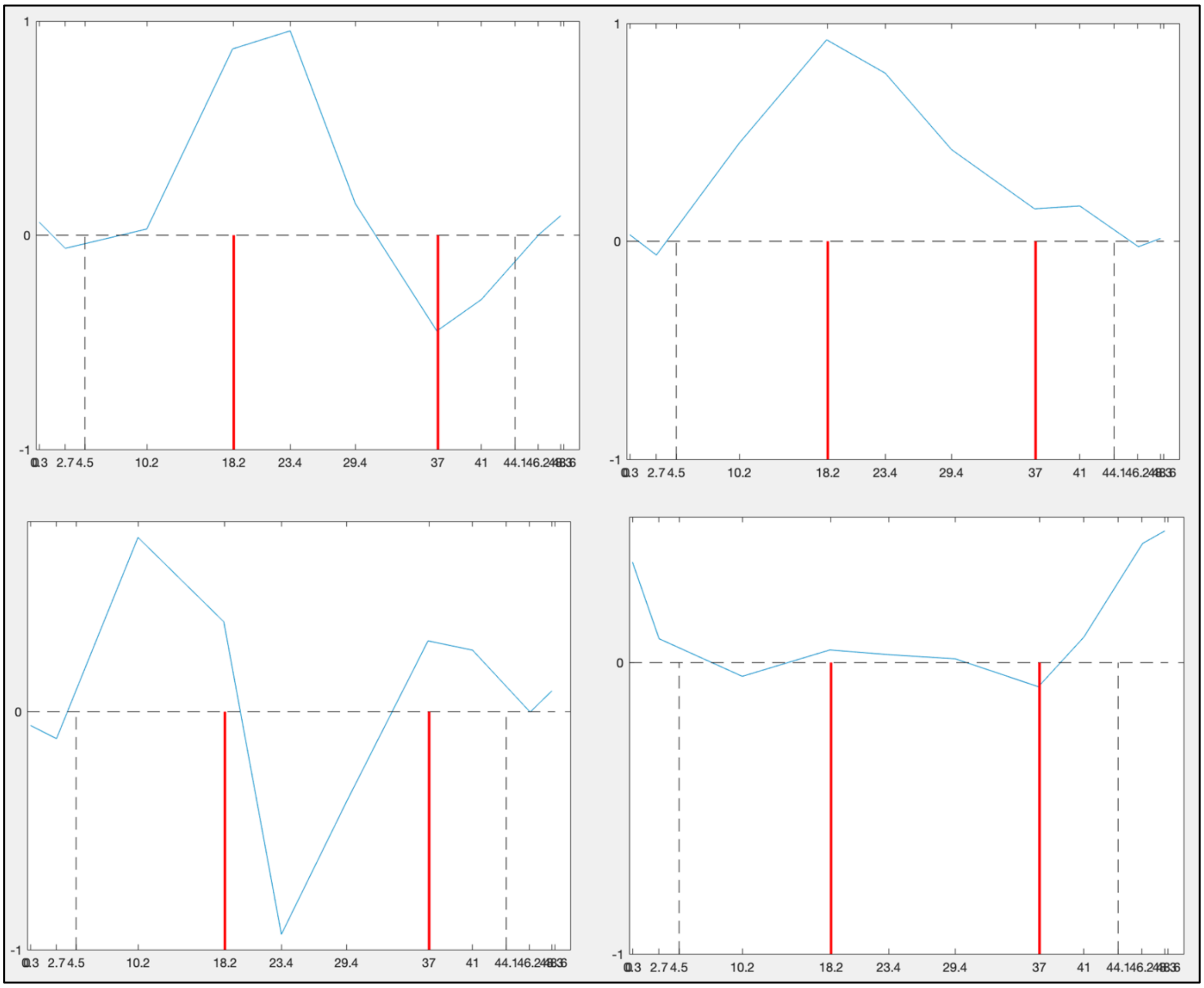

FIGURE 35: THE FOUR MODE SHAPES WITH THE 1ST MODE SHAPE ON TOP LEFT, 2ND MODE SHAPE ON TOP RIGHT, 3RD MODE SHAPE ON BOTTOM LEFT AND 4TH MODE SHAPE ON BOTTOM RIGHT.

This data can now be used to update the model. The process to update the model will be shown and explained in the next chapter.

5.4 Checking maximum accelerations

To check the maximum accelerations a excel file was made with the following information on each train passing:

- Scheduled train passing
- Actual train passing
- From-To
- Train code
- Txt-file number
- Acceleration above 3.5 m/s^2

“Scheduled train passing” tells the time when the train was supposed to pass. This was found with the “route plan” to Bane NOR for each day which can be found for the relevant days in appendix K. Some of the measured train passings could not be found on the route plan and is therefore noted with “not found”. Where it was hard to tell if the measured train passing belonged to one or another time, both times were noted.

“Actual train passing” tells the time of the actual train passing. The more time that differs between scheduled train passing and actual train passing, the more possible is it that the train passing data belongs to another train.

“From-To” tells if the train was going from Hamar to Oslo (H-O), or from Oslo to Hamar (O-H). “Train code” shows what type of train that passed. Both of these were also found in the route plan.

“Txt-file number” tells in which txt-file the train passing can be found, in the txt-folder for each day. “Acceleration above 3.5 m/s^2” tells if the accelerations measured exceeds 3.5 m/s^2 or not. This is because 3.5 m/s^2 is the maximum acceleration allowed for a railway bridge deck according to standard NS-EN 1990, which can be read about in chapter 1.2.1.

The excel file can be found in appendix L. The first 6 train passing from 2022.02.23-24 were excluded from this file due to the fact that they were unstable.

5.4.1 Results for maximum accelerations

Looking at the results for track 2, none of the 30 train passings exceeds 3.5 m/s^2 which means all the train passings on the eastern bridge are within the limitations of NS-EN 1990. However, studying the results for track 1 it can be seen that 22 out of the 61 train passings has accelerations exceeding 3.5 m/s^2. This means that 36% of the measured train passings can point to the fact that the western bridge is not within the limitations of NS-EN 1990.

6 Model – findings – results

This chapter will describe the initial and final model utilized in this thesis and which choices, assumptions, limitations, parametric choices and values, and calculation methods used. The model is built as a surface shell element model with a continues bridge deck, resting on top of bearings on the abutments, and on top of the pir caps on the columns. The bridge is fixed to the pier caps, and has individual spring resistances in X-, Y,- and Z-direction in the bearings, together with free rotation in all three dimensions. The abutments and columns are fixed to ground level, preventing movement and rotation in any spatial directions. This is assumed to give the most realistic representation of the actual bridge, and a more precise representation than the simplified beam model alternative

6.1 Initial model

Both the initial and final, upgraded model are built with the same initial steps, but with the final model being more advanced and with a dynamic behavior as similar as possible to the real situation. The initial model was constructed from available drawings from the Revit model and the Autocad model provided from the faculty, and the most central element of the model will be described further in this chapter. A figure showing a 3D-view of the initial model can be shown in Figure 36.

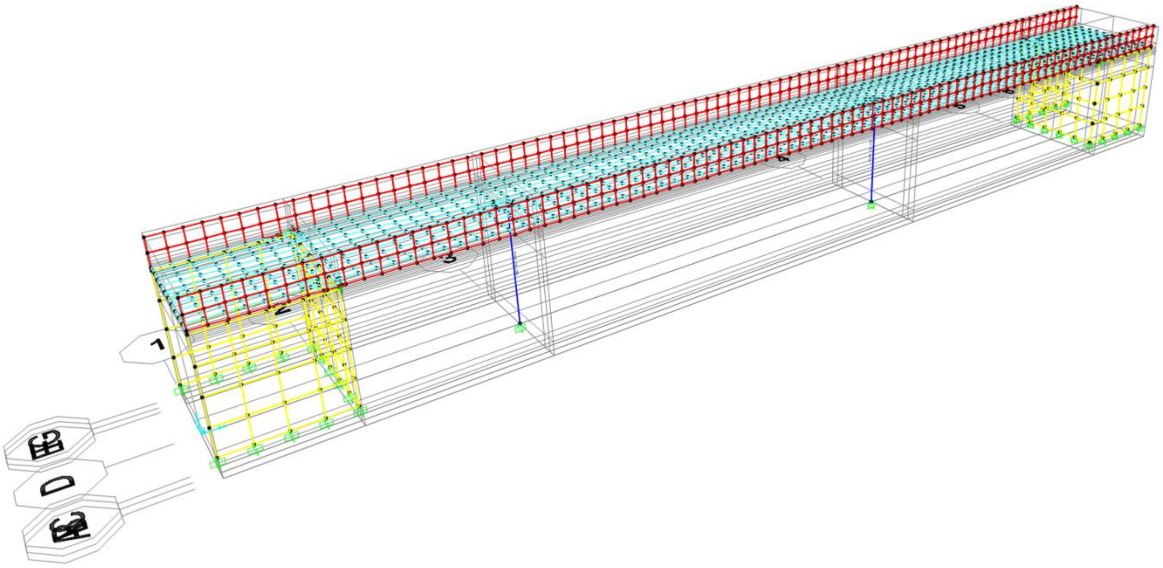

FIGURE 36: 3D-VIEW OF INITIAL MODEL

6.1.1 Element and material overview

With the knowledge that the model would be constructed with surface shell elements, a carefully planned three-dimensional grid was created for a swifter construction of the model. Surface area sections was created for different distinct parts for the bridge, namely bridge sides, bridge deck, abutments, bearings, columns, and pier caps and given assigned different materialistic qualities and parametric values based on available information of the bridge. Table 4 shows the different elements of the bridge, their location, color in 3D-model, element type, material quality and calculational thickness.

TABLE 4: ELEMENT DESCRIPTION AND PROPERTIES

Name	Location	3D-model color	Element type	Quality	Calculational thickness [m]
Deck bottom	Entire horizontal part of the bridge deck	Teal	Area	C35/45	0,5
Deck sides	Both vertical sides of the bridge deck	Red	Area	C35/45	0,7
Pier caps	Underside of bridge deck	Blue	Frame	C35/45	
Columns	Underside of Pier caps	Blue	Frame	C35/45	[1,4 -5,6]
Abutments	Underside of bridge deck	yellow	Area	C35/45	0,4
Bearings	Between abutments and underside of bridge deck	Black	Frame	[-]	[-]

Table 5 shows the two materials utilized in the initial model. The concrete is a standard C35/45 concrete and the material used for the bearings are based on findings from previous studies conducted by Johnsen & Torp [19].

TABLE 5: CONCRETE AND CUSTOM MATERIAL USED FOR BEARINGS IN INITIAL MODEL

Propertiy and value		Bearings	
C35/45		Custom	
E-modulus:	36000000	E-modulus:	185900
Poisson (U)	0,2	Poisson (U)	0,3
Shear modulus	15000000	Shear modulus	71500
Mass pr unit volume	2,5987	Mass pr unite volume	7,849

6.1.2 Bridge components

The initial model was constructed by creating the shell elements through the centerlines of the objects and assigning them a thickness for the software to calculate upon. The different elements were assigned different areal section groups such that it would be possible to swiftly make changes to the individual elements of the model.

The columns are designed as frame elements as they have a simpler geometric form, and since CSiBridge allows for circular sections with adjusting diameters. This allowed for the pier caps to be constructed with the exact same form as the bridges. Figure 38 shows the column created in CSiBridge for the initial model, and Figure 38 shows the actual column on site.

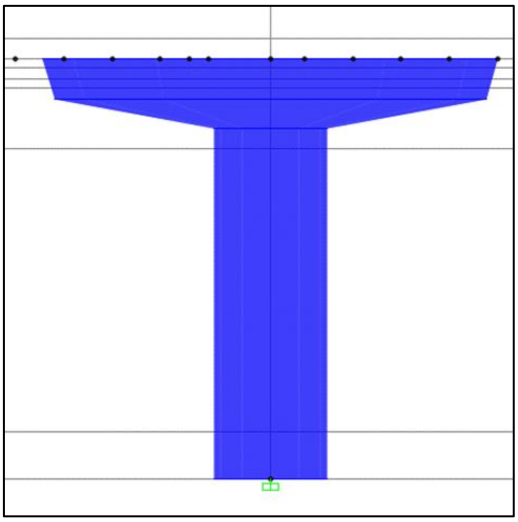

FIGURE 38: CROSS SECTION OF COLUMN WITH PIER CAP FROM INITIAL MODEL

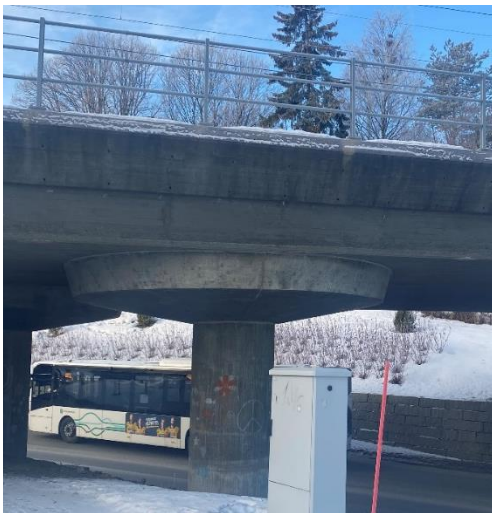

FIGURE 38: SOUTH COLUMN OF BRIDGE TWO OF THE STANGE OVERPASS

6.1.3 Connectivity of nodes and meshing

After the outline of the shell elements were created, the model was meshed automatically with a dividing function included in CSiBridge. The deck was divided into 820 mesh elements, each side into 162 mesh elements, and the abutments into 48 elements each, to a total of 1264 mesh elements. This is deemed to be an adequate amount of mesh element for an analysis of this magnitude and precision. The top point of the columns and the bearing points needed to be manually attached to the bridge deck meshing and was done by creating custom defined surface poly-shapes. The same procedure was done to points added corresponding to the sensors layout so that it would be easier to analyze the results. Both these operations added an extra 67 mesh element, to a new total of 1331 mesh elements. The four bearings were each attached to the top, inner corner of both abutments, and veridically extended and connected to the underside of the bridge deck. They were designed to freely rotate with no moment capacity in both ends, and with a vertical stiffness of $1{,}63 \cdot 10^6$ kN/m as a starting value, which has been suggested from Johnsen & Torp as a probable value [19]. The translational stiffness in global X- and Y-direction was set to 1500 kN/m as an initial value.

6.1.4 Boundary conditions

The boundary conditions were defined as fixed, with no translation or rotation in all spatial directions, for all bottom points, of both abutments and both columns. The ends of the bridge has no restraints in the initial model which is an intentional decision to see how the simplified model will behave.

6.2 Initial results

The initial model was run with modal calculation analysis, and the results are presented in this chapter. CSiBridge returns mode shapes for transverse shapes, torsional shapes, and vertical shapes. This thesis is focused on the vertical mode shapes, and therefore will only these mode shapes be addressed and presented. The mode shapes are exported from CSiBridge to Excel as displacement data along the centerline of the bridge deck and normalized individually before being plotted versus the length of the bridge. The locations of the columns and bridge centerline are added to the plots to give a better visualization of the shapes. Note that the size of the columns is not in scale to the length of the bridge and only serves as a visual location marker.

The mode shapes’ frequency is consistently ascending for each mode shape, and the periods are consistently descending, indicating that the mode shape calculations are correct, and the model is working properly. While analyzing the model, it was discovered that the second and third mode shapes were very similar with a cantilever behavior on either the right side, or the left side. This is the same phenomena that were observed for the modal analysis from the measured data. For simplicity was only one of these shapes chosen for further analysis and discussion, which is the third vertical mode shape, while the second vertical mode shape is then neglected. Since the model also produces horizontal and translational mode shapes, are the vertical mode shapes re-numbered for them to be compared more easily. The first five vertical mode shapes from CSiBridge are mode shape number 5, 6, 9, 10 and 12, where mode shape 6 is neglected and mode shape 9 is kept for analysis. The mode shapes are renumbered to mode shape 1, 2, 3, and 4 for easier comparison with the same mode shapes from the data acquisition. It is also observed from comparison of the two modal analyses that the third and fourth mode shape of the model and the measured data is interchanged, most likely due to inaccuracies or differences in the model from the real bridge. These two mode shapes are swapped for the initial model results to make the comparison easier and clearer for the reader.

6.2.1 Mode Shape 1

Mode Shape 1 is the first vertical mode shape from the modal analysis. The period is T = 0,12758 and the period is f = 7,83812. The mode shape is shown in Figure 39.

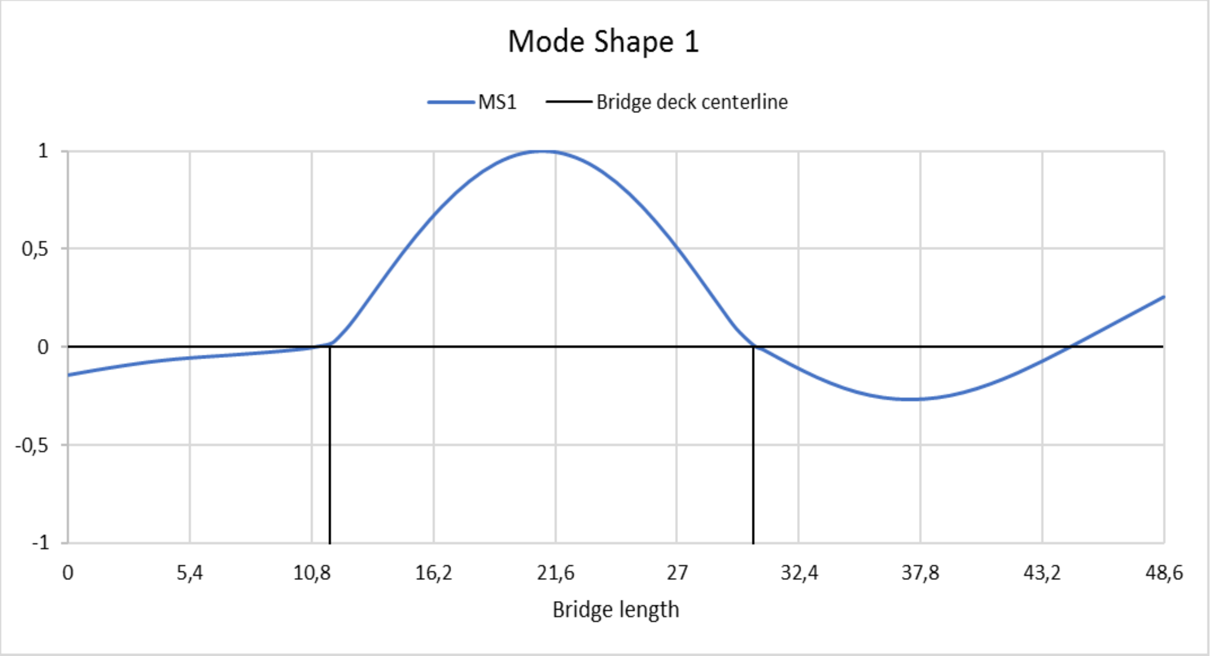

FIGURE 39: MODE SHAPE 1 FROM THE INITIAL MODEL

Mode shape 1 breaks at the columns and has a slight damping at the bearing point at 4,5 and a cross point at the bearing at 44,1 meters. Both the period and the frequency are plausible for this construction and for this shape.

6.2.2 Mode Shape 2

Mode Shape 2 is the third vertical mode shape from the modal analysis. The period is T = 0,06948 and the period is f = 14,39299. The mode shape is shown in Figure 40.

Mode shape 2 has a flatter shape, with a cantilever behavior on the left side and a sine function shape in the mid span. The curve of mode shape 2 also straightens at the column at 30,4 meters. Both the period and the frequency are plausible for this construction and for this shape.

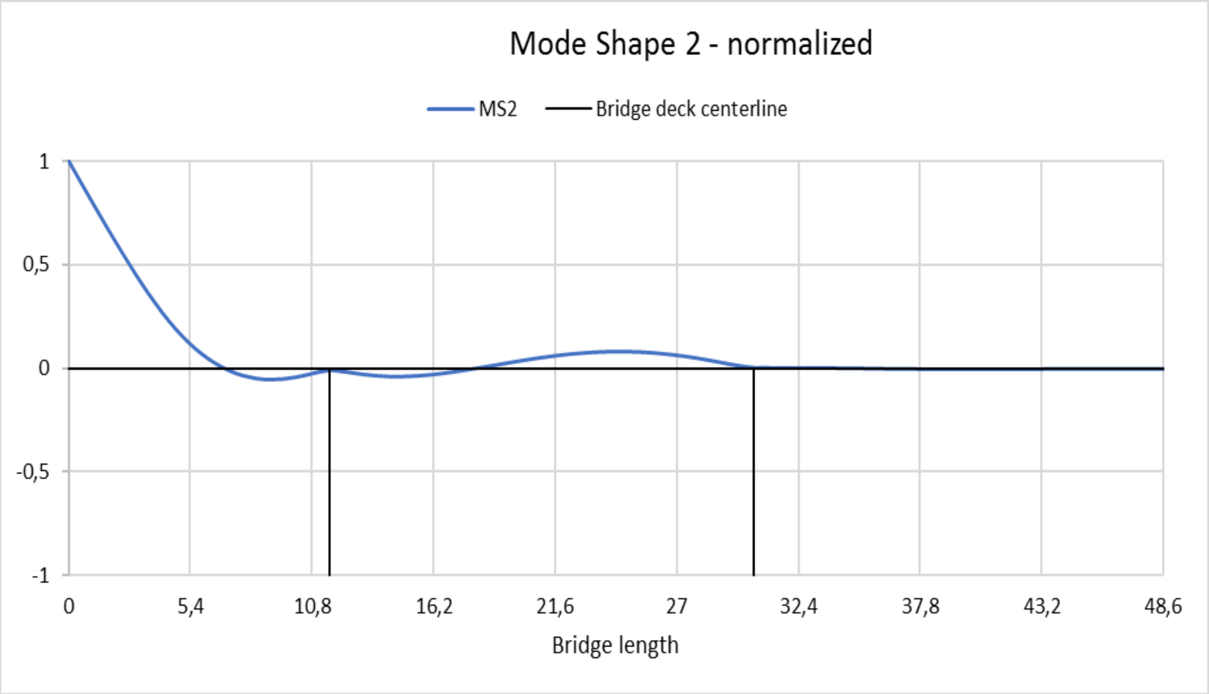

FIGURE 40: MODE SHAPE 2 FROM THE INITIAL MODEL

6.2.3 Mode Shape 3

Mode Shape 3 is the fourth vertical mode shape from the modal analysis. The period is T = 0,05077 and the period is f = 19,69775. The mode shape is shown in Figure 41.

Mode shape 3 is the most complex of the four three vertical mode shapes but behaves in many ways as the previous two. It has an almost perfect sin function shape between the columns and straightens at the bearing points at 4,5 and 44,1 meters. Both the period and the frequency are plausible for this construction and for this shape.

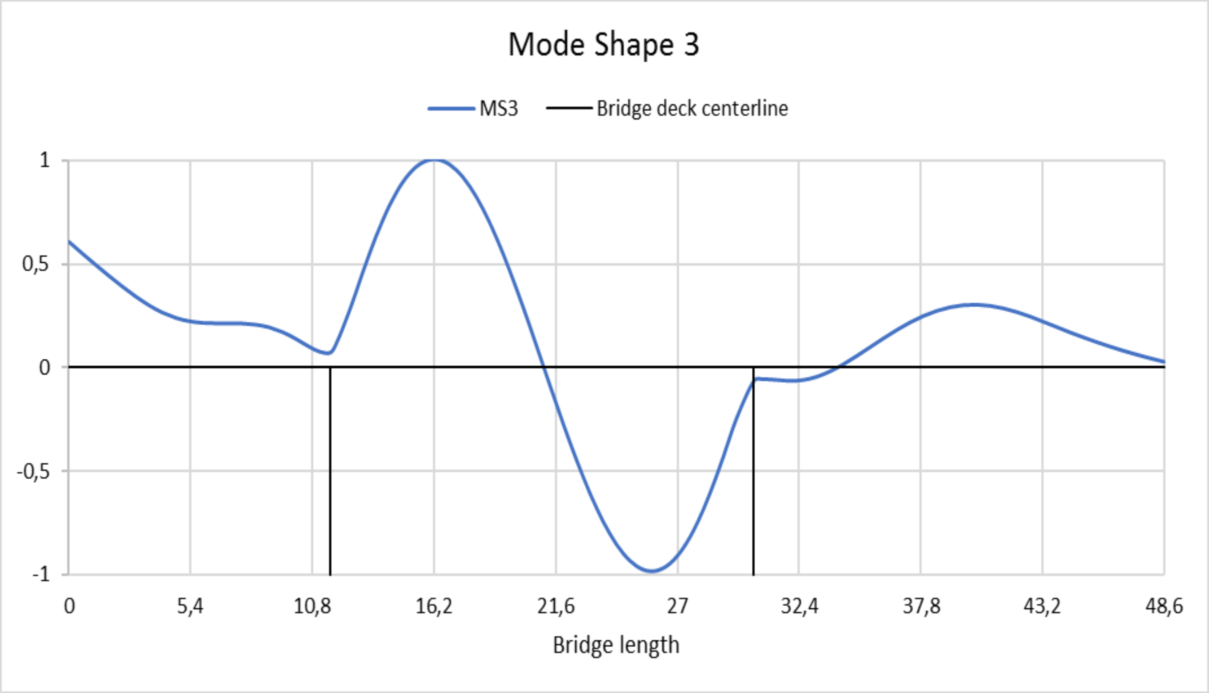

FIGURE 41: MODE SHAPE 3 FROM THE INITIAL MODEL

6.2.4 Mode Shape 4

Mode Shape 4 is the third vertical mode shape from the modal analysis. The period is T = 0,06142 and the period is f = 16,28054. The mode shape is shown in Figure 42. As described for mode shape 2 is mode shape 4 similar in concept, but with the cantilever behavior on the right side, and no crossing of the natural line. The displacement curve is somewhat more extreme than for mode shape 2, which might be due to the longer cantilever part of the right side of the bridge. The curve of mode shape 4 straightens from the second bearing point at

44,1 meters. Both the period and the frequency are plausible for this construction and for this shape.

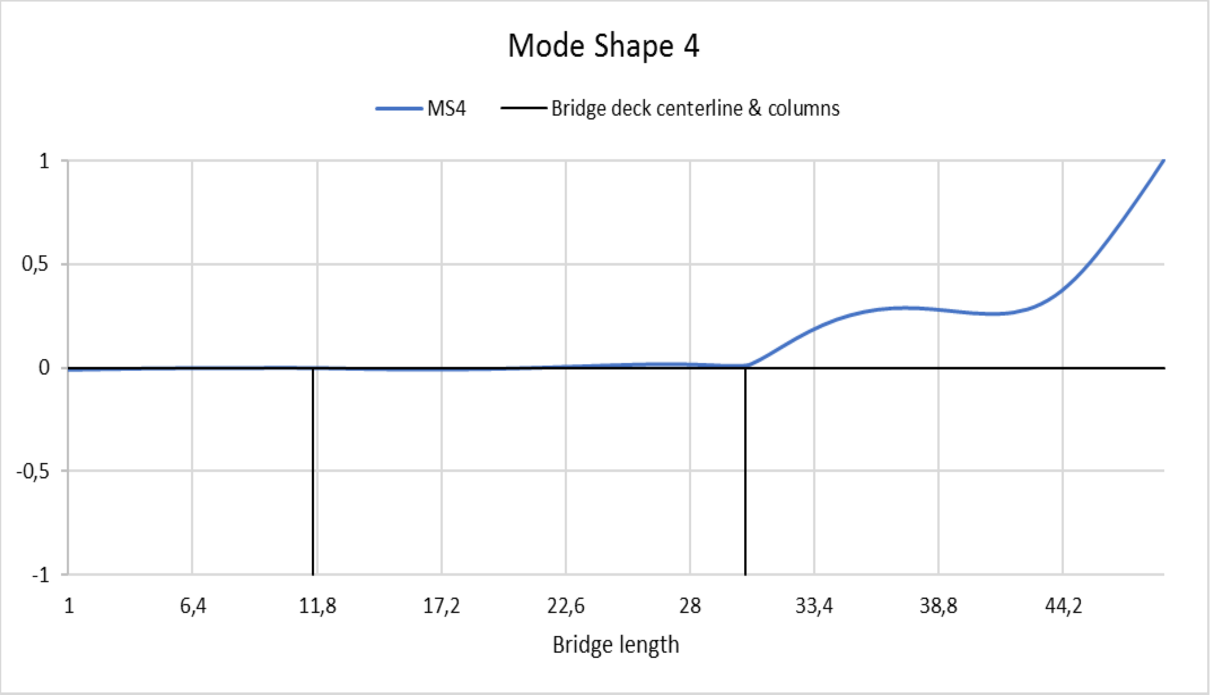

FIGURE 42: MODE SHAPE 4 FROM THE INITIAL MODEL

6.2.5 Comparing initial model to acquired data

This chapter will summarize and compere the initial model's mode shapes and frequencies to the ones found from the Matlab analysis of the measured data from site. Figure 43 shows all initial model's mode shapes and Figure 44 shows all mode shapes from the Matlab analysis of the data acquisition. Figure 44 also shows the placement of the sensors used for the data gathering.

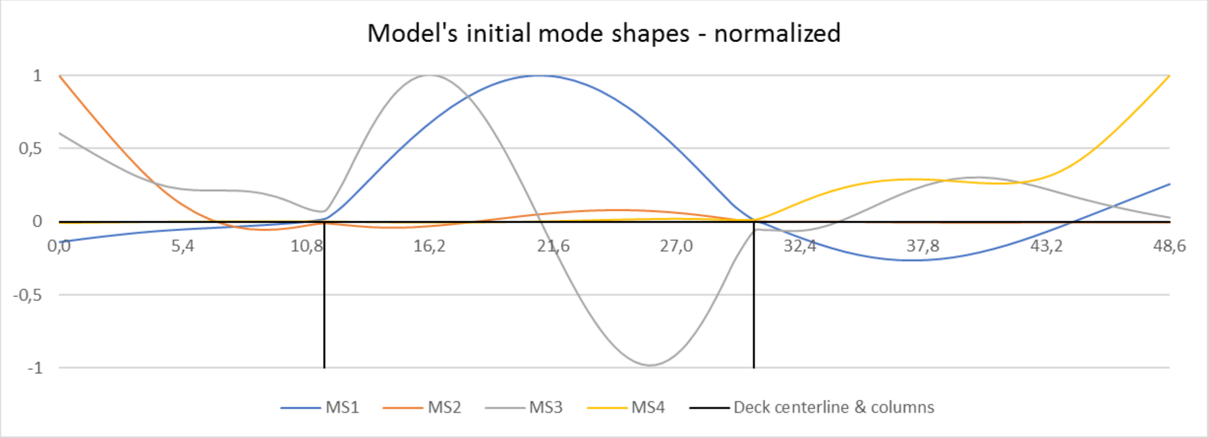

FIGURE 43: ALL INITIAL MODE SHAPES FROM INITIAL MODEL

The first and the third mode shapes are spotted as the most equal ones with the most similar shapes, while mode shape two and four differs more from the Matlab analyzed ones. The initial model preforms calculations under more idealistically conditions and the results reflects this with the mode shapes being more symmetrical and having clearer change in behavior near restraints in the bearings and columns. All mode shapes from the Matlab analysis also have different behavior at the connection at the ends of the bridge. This is assumed to be more realistic as is reflects the real-life boundary conditions better than for the initial model, which has no restraints at the end of the bridge. Even though mode shape one and three are the most similar, they have some differences. The bell of mode shape one is skewed to the right for the Matlab analyzed mode shape, and mode shape three is skewed to the left.

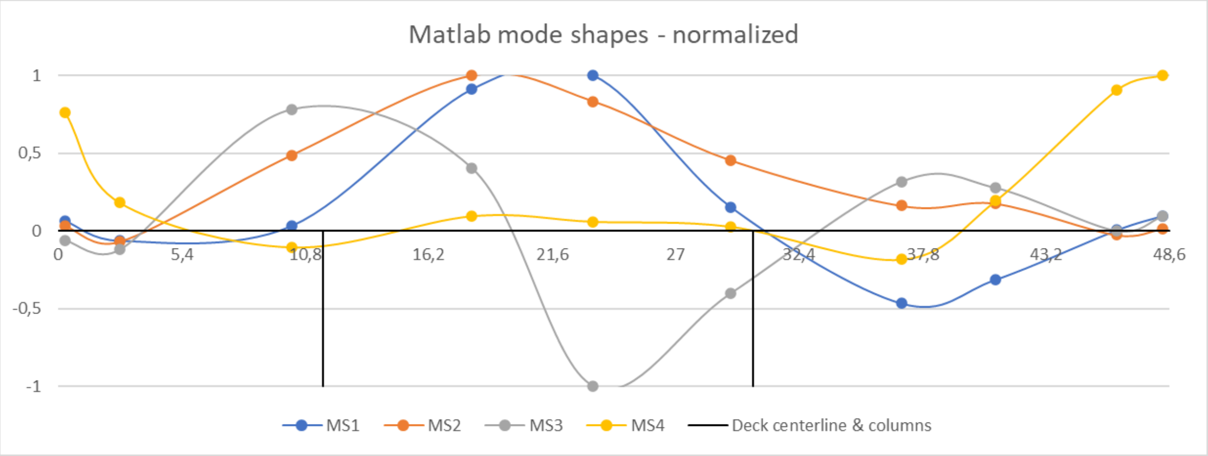

FIGURE 44: ALL MODE SHAPES FROM DATA ACQUISITION

6.3 Updating the model

This chapter will explain the changes done to the initial model so that it would resemble the real-life structure more and have a better correlation of mode shapes. The model was updated with a direct updating method of manual tuning. It was done by identifying the key dynamic parameters of the bridge and their extremal points and manually iterating through a range of values withing these points. Other aspects of the model were also investigated but revealed to have little to no impact on the dynamic behavior of the bridge for within their natural range of variation. The quality of the concrete was tested for an upper and lower extremal point without impacting the overall behavior and was therefore left untouched in the final model as there were no suspicion of it having degraded or improved significantly.

The main elements identified to impact the model dynamic response was the bearings' material and properties, and the ends of the cantilevering part of the bridge. These elements and which changes has been done to the model will be further described in the following sub-chapters.

The last change that was done to the final model was to change the mode shape identification line from the center of the bridge to a line near the eastern end of the bridge, at the same location as where the sensors were installed. This lead to a much greater correlation between the updated model's mode shapes and the Matlab analyzed mode shapes.

6.3.1 Bearings

The bearings were identified as one of the key dynamic parameters. The vertical stiffness greatly impacted the theoretical approximation of the mode shapes, whereas higher stiffnesses returned more symmetrical and theoretically mode shapes, and lower stiffnesses returned mode shapes more similar to the Matlab analyzed mode shapes. The upper level of the tested range for the bearings' stiffness was $2{,}5 \cdot 10^6$ kN/m and the lowest tested value was $0,5 \cdot 10^6$ kN/m. The final value for the model is $1,09 \cdot 10^6$ kN/m with an assumed error margin of $0,2 \cdot 10^6$ kN/m of within no observable changes was observed to the mode shapes.

Another change that was done to the bearings was that its mechanical functionally of having spring properties for both compression and tension was changed to compression only. This is assumed to resemble the real-life situation closer, as the in-situ observation of the bearings indicated no tensional limitations.

6.3.2 Connectivity at cantilevering ends

The initial model had free cantilevering ends on both sides of the bridge. This is a rather theoretical approximation to the construction, as the bridge is connected to the rest of the railway. The type of connection and its properties however are unknown and has to be identified through the finite model updating process. Both rotational stiffness and linear vertical stiffness was added to the ends of the bridge to simulate the boundary condition to the surrounding railway. The lower and upper range levels for both springs was respectively 3000 kN/m and 250.000 kN/m with uneven incremental increasing and decreasing according to the modal analysis in between tuning. The first updating was done symmetrically with equal spring values at both ends, and asymmetrical values was tested later, with ratios varying from 5:1 up to 1:10. The final values ended at 150.000 kN/m at the southern connection and 75.000 kN/m at the northern connection, both in the vertical direction and with no rotational stiffness. It is also assumed that the cantilevering parts of the bridge rests on a semi-elastic material that prevents the cantilever from bending too much downwards, which however, was not added to the model as it was deemed too time consuming to implement towards the completion of the thesis.

Since the eastern bridge has no supporting plate under the cantilevering parts of the bridge, like the western bridge has, the spring supports was only added to the corners of the connecting part, which is in contact with the underlaying abutment as it is assumed to be the most realistic condition.

6.3.3 Final model

The final model’s mode shapes occurred in the same order as the ones from the Matlab analysis and needed no rearrangement other than being re-numbered from 5, 7, 10, and 14 to 1, 2, 3, and 4. The final models mode shapes can be observed in Figure 45 and the Matlab analyzed mode shapes in Figure 46 for easier comparison.

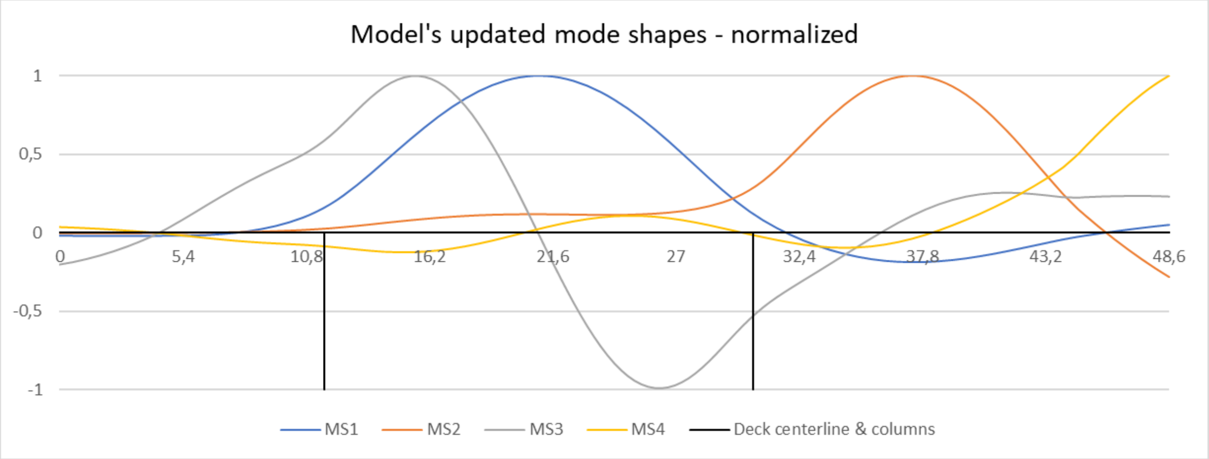

FIGURE 45: FINAL UPDATED MODEL'S MODE NORMALIZED MODE SHAPES

It is observed that mode shape 1 is the closest in shape, and mode shape 3 and 4 are similar to each other, but with more noticeable differences to the overall shape and especially near the left side on the figure. Mode shape 2 has the least corresponding shape of the four

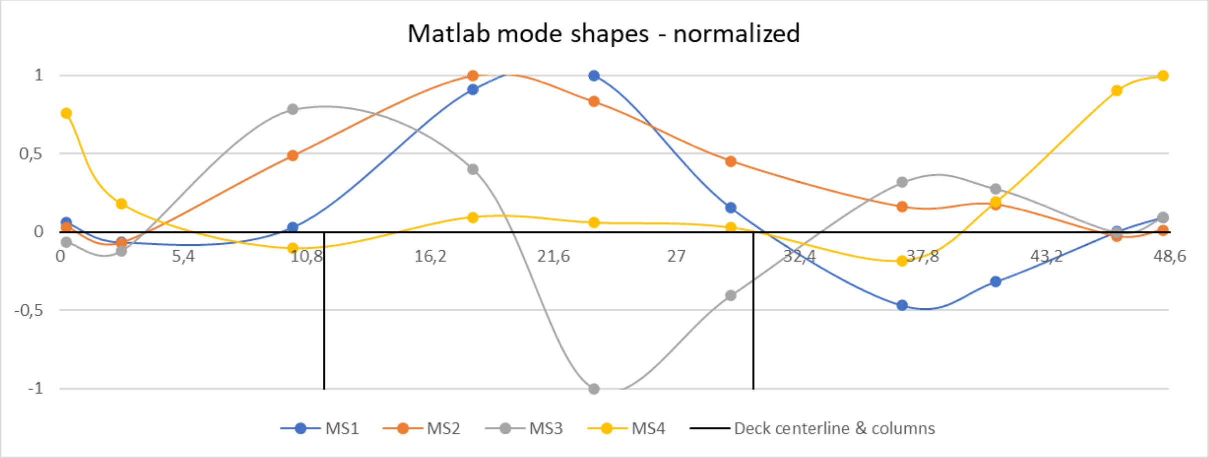

FIGURE 46: ACTUAL MODE SHAPES FROM MATLAB ANALYZED DATA ACQUISITION

identified mode shapes. All changes that were made to the model is summarized in Table 6. The final model's mode shape corresponding frequencies are shown in Table 7.

TABLE 6: SUMMARY OF CHANGES CONDUCTED TO THE FINAL UPDATED MODEL

Bearing	**Initial model**	**Final model**	
Compressional stiffness	Yes	yes	
Tensional stiffness	Yes	No	
Stiffness	$1{,}69 \cdot 10^6$ kN/m	$1{,}09 \cdot 10^6$ kN/m	
Cantilever connections	Both ends	Southern end	Northern end
Vertical stiffness	0 kN/m	$0{,}15 \cdot 10^6$ kN/m	$0{,}075 \cdot 10^6$ kN/m
Mode shape measured at	Centerline	Sensor line	

The frequencies correspond well with the Matlab analyzed frequencies, indicating that the model is working properly and further updating and tuning can be done without changing the fundamental construction of the model.

TABLE 7: MODE SHAPES FREQUENCIES

Mode shape			
1	2	3	4
7,90877	10,76804	19,42103	21,1018

7 Discussion and conclusion

Our research question is "*which modal parameters apply for the eastern railway bridge at Stange Overpass, and will an updated finite element model accurately represent the real dynamic behavior of the bridge?*".

When extracting the data with Matlab, it is important to consider the uncertainties of the process. When finding the train passings, it can be difficult to determine if the vibrations are from a train passing or something else, and if the measurements are stable. These uncertainties may have caused some stable train passings to not occur in the study, or some of the stable ones not being included. It can also be challenging to determine if some of the vibrations are anomalies or not. Therefore, some of removed data that was considered anomalies may have been real vibrations, which could have affected the results of maximum acceleration.

The SSI-Cov method is a process where the results differ with the chosen time period of free vibrations and the selected order. Changing the time period or the selected order just a little can result in more or fewer mode shapes, as well as very different mode shapes, frequencies and damping ratios. This could therefore have affected the values in the mode shape that was found. However, since five or more similar mode shapes were found of each of the four represented mode shapes, the average mode shape probably would not differ a lot.

The final updated finite element method is a great improvement from the earlier finite element method created for the bridge by "*Rambøll*" and "*Sweco*". The mode shapes have a fair resemblance to the mode shapes found from the Matlab analysis and the corresponding frequencies are within the probable range for this construction. The model could be more accurate, had more experimenting and tuning been conducted, preferably together with a sensitivity analysis and a Modal Assurance Criterion analysis for a more quantitative description of the model's accuracy.

The model shows that the bearing stiffness is at approximately $1{,}09 \cdot 10^6$ kN/m with compressive spring-behavior only, and that the vertical spring stiffness of the support on the northern side of the bridge probably is smaller than the spring stiffness of the support on the southern side, where their approximate values are near 0,15 · 10^6 kN/m and 0,075 · 10^6 kN/m. The frequency of the first four mode vertical mode shapes is calculated with the final model to be 7,90877 Hz, 10,76804 Hz, 19,42103Hz, and 21,10180 Hz. The thesis concludes that the findings from the final finite element model are fairly accurate, but the dynamic parameters should be further investigated and the model followingly updated to achieve an even better and more precise result.

When it comes to maximum accelerations it can be concluded that none of the train passings on track 2 exceeds 3.5 m/s^2 which means all the train passings on the eastern bridge are within the limitations of NS-EN 1990. Also, 22 out of the 61 train passings on track 1 has accelerations exceeding 3.5 m/s^2. This means that 36% of the measured train passings can point to the fact that the western bridge is not within the limitations of NS-EN 1990.

8 Future work

While thesis has successfully identified the modal and dynamic parameters of the eastern bridge at the Stange overpass and conducted thoroughly data acquisition of the western bridge and build an updated finite element model of the eastern bridge, more research can still be conducted to better assure the quality and reliability of the findings presented.

A continues power source could let the researcher conduct continuous measurements and data acquisition for a longer time, and therefore gather more data to better identify the modal parameters. This could help more precisely describing the modal parameters of both bridges.

The final updated finite element model could be further upgraded by investigating the boundary conditions of the abutments, columns, and bearings and implementing the findings in the model. A correlation test such as the Modal Assurance Criterion test could be conducted during the updating of the model to quantitively describe the accuracy of the finite element model.

And lastly, the sensor installation and data acquisition should be conducted during the spring, summer, or early autumn, and not during the winter months, as snow, ice, and freezing temperatures can be a large source of error due to added snow weight to the bridges and other difficulties with sensor installation and data acquisition that follow these climate conditions.

References

[1] Statistiak setralbyrå, «Jernbanetransport,» [Internett]. Available: https://www.ssb.no/statbank/table/10484/.

[2] E. Emrah, *Applied Structural Dynamics - Current and Future Research,* 2021.

[3] E. Erduran, «NEAR: Next Generation Finite Element Calibration Methods for Railway Bridges,» Dept. of Civil Eng. and Energy Tech., Oslo Metropolitan University, Oslo, 2020.

[4] Bane NOR, «Om Bane NOR,» 12 06 2018. [Internett]. Available: https://www.banenor.no/Om-oss/Om_Bane-NOR/.

[5] Bane NOR, «Årsrapport,» 2019. [Internett]. Available: https://arsrapport.banenor.no/uploads/documents/arsrapport.pdf.

[6] Siemens Digital Industries Software, «What is OMA? Operational Modal Analysis,» Siemens Digital Industries Software, 10 7 2020. [Internett]. Available: https://community.sw.siemens.com/s/article/OMG-What-is-OMA-Operating-Modal-Analysis. [Funnet 20 5 2022].

[7] Comsol, «The Finite Element Method (FEM),» 15. March 2016. [Internett]. Available: https://www.comsol.com/multiphysics/finite-element-method.

[8] S. Rahmatalla, K. Hudson, Y. Liu og H.-C. Eun, «Finite element modal analysis and vibration-waveforms in health inspection of old bridges,» Januray 2014.

[9] M. Sanayeia, A. Khaloob, M. Gulc og F. N. Catbas, «Automated finite element model updating of a scale bridge model using measured static and modal test data,» 2015. [Internett]. Available: https://www.researchgate.net/publication/282795309_Automated_finite_element_model_updating_of_a_scale_bridge_model_using_measured_static_and_modal_test_data.

[10] S. Živanović, A. Pavic og P. Reynolds, «Finite element modelling and updating of a lively footbridge: The complete process,» pp. 126-145, 20 March 2007.

[11] C. R. Farrar og K. Worden, «An introduction to structural health monitoring,» 2006.

[12] S. Saadat, M. N. Noori, G. D. Buckner, T. Furukawa og Y. Suzuki, «Structural health monitoring and damage detection using an intelligent parameter varying (IPV) technique,» 2004.

[13] S. Sehgal og H. Kumar, «Structural Dynamic Model Updating Techniques: A State of the Art Review,» Archives of Computational Methods in Engineering, 2016.

[14] P. O. Faheem Butta, «Seismic response trends evaluation and finite element model calibration of an instrumented RC building considering soil–structure interaction and non-structural components,» pp. 111-123, 15 April 2014.

[15] A. Deraemaeker, E. Reynders, G. D. Roeck og J. Kullaac, «Vibration-based structural health monitoring using output-only measurements under changing environment,» pp. 34-56, January 2008.

[16] E. Reynders, A. Teughels og G. D. Roeck, «Finite element model updating and structural damage identification using OMAX data,» pp. 1306-1323, July 2010.

[17] Polytec, «Modal analysis,» [Internett]. Available: https://www.polytec.com/int/vibrometry/modal-analysis.

[18] S. Chauhan, «Parameter Estimation and Signal Processing Techniques for Operational Modal Analysis,» University of Cincinnati, 2008.

[19] J. B. Johnsen og M. Torp, «System Identification and Finite Element Model Updating of the Stange Railway Overpass,» Oslo, 2021.

[20] N. Debnath, A. Dutta og S. K. Deb, «Placement of sensors in operational modal analysis for truss bridges,» pp. 196-216, August 2012.

[21] Z. Li, J. Fu, Q. Liang, H. Mao og Y. He, «Modal identification of civil structures via covariance-driven stochastic subspace method,» 2019.

[22] S. Chauhan, «Subspace Algorithms in Modal Parameter Estimation for Operational Modal Analysis: Perspectives and Practices».

[23] Computers and Structures, Inc., «About,» Computers and Structures, Inc, 2021. [Internett]. Available: https://www.csiamerica.com/about. [Funnet 9 5 2022].

[24] Computers and Structures, Inc., «CSiBridge Bridge analysis, design and rating,» Computers and Structures, Inc., 2021. [Internett]. Available: https://www.csiamerica.com/products/csibridge. [Funnet 9 5 2022].

[25] Computers and Structures, Inc., «CSi Knowledge base Home,» Computers and Structures, Inc., 15 6 2021. [Internett]. Available: https://wiki.csiamerica.com/display/csibridge/Home. [Funnet 9 5 2022].

[26] PCB Piezotronics, Inc., «Model : 393A03 | Accelerometer, ICP®, Seismic,» PCB Piezotronics, Inc., 2022. [Internett]. Available: https://www.pcb.com/products?model=393a03. [Funnet 16 5 2022].

[27] Gantner Instruments Inc., «Q.station XT,» [Internett]. Available: https://shop.elkome.com/en/mwdownloads/download/link/id/3586/. [Funnet 5 6 2022].

[28] EcoFlow US, «EcoFlow DELTA Max Portable Power Station,» EcoFlow US, 2022. [Internett]. Available: https://us.ecoflow.com/products/delta-max-portable-power-station?variant=39435795988553. [Funnet 18 5 2022].

[29] Wikipedia, «Matlab,» Wikipedia, 28 4 2022. [Internett]. Available: https://en.wikipedia.org/wiki/MATLAB. [Funnet 10 5 2022].

[30] The MathWorks, Inc., «Signal Processing Toolbox,» The MathWorks, Inc., 2022. [Internett]. Available: https://se.mathworks.com/products/signal.html. [Funnet 10 5 2022].

[31] The MathWorks, Inc., «Mapping Toolbox,» The MathWorks, Inc., 2022. [Internett]. Available: https://se.mathworks.com/products/mapping.html. [Funnet 10 5 2022].

[32] The MathWorks, Inc., «System Identification Toolbox,» The MathWorks, Inc., 2022. [Internett]. Available: https://se.mathworks.com/products/sysid.html. [Funnet 10 5 2022].

[33] Cosmol, «Finite Element Mesh Refinement,» 6. January 2016. [Internett]. Available: https://www.comsol.com/multiphysics/mesh-refinement.

[34] M. Salehi, «Modal identification and finite element model updating of railway bridges considering boundary conditions using artificial neural networks,» Oslo, 2021.

[35] H. Aveyard, Doing a Literature Review in Health and Social Care: A Practical Guide, Berkshire: Great Britain: Open University Press, 2010.

[36] M. Maage, S. Smeplass, P. Gjerp, B. Pedersen, B. Kristiansen og J. Injar, Betong - Regelverk, teknologi og utførelse, Oslo: Byggenæringens forlag AS, 2015.

[37] A. S. AL-Ameeri, M. I. Rafiq, O. Tsioulou og O. Rybdylova, «Impact of climate change on the carbonation in concrete due to carbon,» *Journal of Building Engineering,* p. 15, 2021.

[38] T.-W. Chen, J. Wu og G.-Q. Dong, «Mechanical Properties and Uniaxial Compression,» *Strain Relation of Recycled Coarse Aggregate,* p. 19, 2021.

[39] J. Zhibin, H. Bo, R. Juanjuan og P. Shiling, «Reduction of Vehicle-Induced Vibration of Railway Bridges due to Distribution of Axle Loads through Track,» *Department of Bridge Eng., Southwest Jiaotong University, Chengdu, China & Department of Civil and*

Environmental Eng., Colorado School of Mines, Golden, USA, Vol. %1 av %2Volume 2018, Article ID 2431980, p. 14, 2018.

[40] NS-EN, Eurocode 1, Actions on structures - Part 2: Traffic loads on bridges 19912:2003+NA:2010,, Norsk Standard, 2010.

[41] J. L. Cleve Moler, «A history of MATLAB,» *Proceedings of the ACM on Programming Languages,* vol. 4, nr. HOPL, p. 67, 2020.

[42] The MathWorks, Inc., «What is Matlab?,» Mathworks, 2022. [Internett]. Available: https://se.mathworks.com/discovery/what-is-matlab.html. [Funnet 10 5 2022].

Appendix A

```
clear all; close all; clc;

% get the continuous data first
cd '/Users/benedictenummestad/Desktop/2022.03.02-03/Text Files';
cd '/Users/benedictenummestad/Desktop/2022.03.02-03/Text Files';

% % open the directory for the results docs

testfiledir = '/Users/benedictenummestad/Desktop/2022.03.02-03/Text Files';
files = dir(fullfile(testfiledir,'*.txt'));
nfiles = length(files);
cell_name = struct2cell(files) ;
cd '/Users/benedictenummestad/Desktop/2022.03.02-03/Text Files';
filenames = extractfield(files,'name') ;
fs = 250 ; %Hz
dt = 1/fs;

data = [] ;
for i = 33

    filename = filenames{i} ;
     datatemp = readmatrix(filename) ;
     starttime = filename ;
end

data = datatemp ;
t = (0:(length(data)-1))*dt; % time vector

figure
plot(t,data,'Linewidth',1); grid on; xlabel('Time (sec)'); ylabel('Amplitude (g)');
legend('S1','S2','S3','S4','S5','S6','S9','S10','S11','S12','Location','Southeast')
% starttime = starttime(1:41) ;
title(['Measurement starts at: ', starttime])
set(gcf,'color','w'); set(gcf,'PaperUnits','inches'); set(gcf,'PaperSize',[8 6]);
set(gcf,'PaperPosition',[0 0 8 6]);
set(gcf,'PaperPositionMode','Manual');
set(gca,'FontName', 'Times New Roman');
set(gca,'LooseInset',get(gca,'TightInset'));




% select the starting point and export cursor data to workspace
start_seconds=1;
DI = start_seconds*fs %data index
```

```
train_data = data(DI:DI+30000,:) ; % train crossing data
train_t = (0:(length(train_data)-1))*dt ;

figure
plot(train_t,train_data,'Linewidth',1); grid on; xlabel('Time (sec)'); ylabel('Amplitude (g)');
legend('S1','S2','S3','S4','S5','S6','S9','S10','S11','S12','Location','Southeast')
```

```
name_of_file = ['TrainCrossing_2022-02-25_13-12-00.txt'] % write name of the file manuall
% write them to a .txt file
varNames = {'Sensor 1 [g]','Sensor 2 [g]','Sensor 3 [g]','Sensor 4 [g]','Sensor 5 [g]', 'Sensor 6
[g]','Sensor 7 [g]','Sensor 8 [g]','Sensor 9 [g]','Sensor 10 [g]'};
document = array2table(train_data) ;
document.Properties.VariableNames = varNames ;
document.Properties.Description = 'Acceleration data with fs = 250 Hz, start time of the recording is
the name of the file';

cd '/Users/benedictenummestad/Desktop/2022.03.02-03/TrainCrossings' ;
writetable(document, name_of_file,'Delimiter',' ')
cd '/Users/benedictenummestad/Desktop/2022.03.02-03/TrainCrossings';
```

Appendix B

```
clear all; close all; clc;

% get the continuous data first
cd '/Users/benedictenummestad/Desktop/2022.02.24-25/TrainCrossings';
cd '/Users/benedictenummestad/Desktop/2022.02.24-25/TrainCrossings';

% % open the directory for the results docs
testfiledir = '/Users/benedictenummestad/Desktop/2022.02.24-25/TrainCrossings';
files = dir(fullfile(testfiledir,'*.txt'));
nfiles = length(files);
cell_name = struct2cell(files) ;
cd '/Users/benedictenummestad/Desktop/2022.02.24-25/TrainCrossings';

filenames = extractfield(files,'name') ;
fs = 250 ; %Hz
dt = 1/fs;

data = [] ;
for i = 12
   filename = filenames{i} ;
   datatemp = readmatrix(filename) ;
%     data_all{i,1} = datatemp ;
%     data = [data; datatemp] ;
   starttime = filename ;
end
%
data = datatemp ;
t = (0:(length(data)-1))*dt; % time vector

figure
plot(t,data,'Linewidth',1); grid on; xlabel('Time (sec)'); ylabel('Amplitude (g)');
legend('S1','S2','S3','S4','S5','S6','S9','S10','S11','S12','Location','Southeast')




sensor=1

DI = cursor_info.DataIndex %data index
% check the anomally
check_data = data(DI-3:DI+3, sensor) % select the sensor number from the figure




% delete the anomally
```

```
data(DI, :) = [] ;
t = (0:(length(data)-1))*dt; % time vector

figure
plot(t,data,'Linewidth',1); grid on; xlabel('Time (sec)'); ylabel('Amplitude (g)');
legend('S1','S2','S3','S4','S5','S6','S9','S10','S11','S12','Location','Southeast')
```

```
name_of_file = 'TrainCrossing_2022-02-25_04-16-00.txt' % write name of the file manuall
% write them to a .txt file
varNames = {'Sensor 1 [g]','Sensor 2 [g]','Sensor 3 [g]','Sensor 4 [g]','Sensor 5 [g]','Sensor 6
[g]','Sensor 7 [g]','Sensor 8 [g]','Sensor 9 [g]','Sensor 10 [g]'};
document = array2table(data) ;
document.Properties.VariableNames = varNames ;
document.Properties.Description = 'Acceleration data with fs = 250 Hz, start time of the recording is
the name of the file';

cd '/Users/benedictenummestad/Desktop/2022.02.24-25/TrainCrossings' ;
writetable(document, name_of_file,'Delimiter',' ')
cd '/Users/benedictenummestad/Desktop/2022.02.24-25/TrainCrossings';
```

Appendix C

```
clear all; close all; clc;

cd '/Users/benedictenummestad/Desktop/2022.02.24-25/TrainCrossings';

% open the directory for the results docs
testfiledir = '/Users/benedictenummestad/Desktop/2022.02.24-25/TrainCrossings';
files = dir(fullfile(testfiledir,'*.txt'));
nfiles = length(files);
cell_name = struct2cell(files) ;
cd '/Users/benedictenummestad/Desktop/2022.02.24-25/TrainCrossings';

filenames = extractfield(files,'name') ;
fs = 250 ; %Hz
dt = 1/fs;
data = [] ;

for i = 5
    filename = filenames{i} ;
    data = readmatrix(filename) ;

    starttime = filename ;

%     data(:,1:2) = [] ;
    t = (0:(length(data)-1))*dt;

    figure
    plot(t,data,'Linewidth',1); grid on; xlabel('Time (sec)'); ylabel('Amplitude (m/s^2)');
    legend('S1','S2','S3','S4','S5','S6','S9','S10','S11','S12','Location','Southeast')

    title(['Measurement starts at: ', starttime])
    set(gcf,'color','w'); set(gcf,'PaperUnits','inches'); set(gcf,'PaperSize',[8 6]);
    set(gcf,'PaperPosition',[0 0 8 6]);
    set(gcf,'PaperPositionMode','Manual');
    set(gca,'FontName', 'Times New Roman');
    set(gca,'LooseInset',get(gca,'TightInset'));

    max_Acc(i,:) = max(abs(data)) ;

end




position = cursor_info.DataIndex   % record this to your excel file or .pptx
data = data(position:position+5*250,:) ;  % 5 seconds data
t = (0:(length(data)-1))*dt;
```

```
figure
plot(t,data,'Linewidth',1); grid on; xlabel('Time (sec)'); ylabel('Amplitude (m/s^2)');
legend('S1','S2','S3','S4','S5','S6','S9','S10','S11','S12','Location','Southeast')
data = detrend(data) ;

%%
%%------------ SYSTEM IDENTIFICATION ------------------------------------------%%

% SSI-COV



data = bpfilter(data,dt,2.5,'high');

%Create a stabilization diagram using the function plotstab included in the OoMA toolbox to aid in selection of stable poles and model order. Use a stabilization criteria of 1% error in frequency, 5% error in damping, and 98% confidence in mode shape vectors.
err = [0.01,0.05,0.98];
order = 200;
s = 4*order;
[A,C,G,R0] = ssicov(data,order,s);
```

Appendix D

```
function plotBridgeModes_stange(MS)

global index_
global freq
global ksi
for i = 1:size(MS,2)
    clear fx
%     frekans = freq(index_(i)) ;
%     sonum = ksi(index_(i)) ;
    z = MS(:,i);
    phase = [cos(angle(z)) sin(angle(z))]; % the angles of the mode shape vector
    % choose the mode shape phase that maximizes the displacement
    [~,idx] = max([sum(abs(phase(:,1))) sum(abs(phase(:,2)))]);
    shape = abs(z).*phase(:,idx);
    shape = shape/max(abs(shape)); %normalized shape

    x = [0.30 2.70 10.2 18.1 23.4 29.4 36.9 41.0 46.3 48.3] ; % x-coordinates of the sensors

    fx = fit(x',shape,'cubicinterp') ; % piece-wise cubic interpolation
    x_bar = 0:0.1:48.6 ;

    figure
%     title( ['Frequency = ', num2str(frekans), ' and \ksi = ', num2str(sonum)] )
    plot(fx,'b')
    hold on
    plot(x,shape,'.-','markersize',15)
    legend off
    % plot the 'other side' of the mode shape
    plot(x,-shape,'.-','markersize',15)
    % plot the bridge centerline and supports
    line([0 48.6],[0 0],'color','k','linestyle','--')
    line([18.2 18.2],[-1 0],'color','r','linestyle','-','linewidth',2) %pier
    line([37 37],[-1 0],'color','r','linestyle','-','linewidth',2)%pier
    line([4.5 4.5],[-1 0],'color','k','linestyle','--') %elastomer
    line([44.1 44.1],[-1 0],'color','k','linestyle','--') %elastomer
    hold off
    yticks([-1 0 1])
    xticks([0 0.30 2.70 4.5 10.2 18.2 23.4 29.4 37 41 44.1 46.2 48.3 48.6])
    title( ['Frequency = ', num2str(freq(index_(i))), ' and \ksi = ', num2str(ksi(index_(i)))] )
    % remove axis ticks and resize axes
    inset =  get(gca,'tightinset');
    pos = get(gca,'position');
    set(gca,'FontName', 'Times New Roman');
    set(gca,'LooseInset',get(gca,'TightInset')); set(gcf,'color','w');

%     xlabel(['Mode ' num2str(i)])
    ylabel(['Mode ' num2str(i)])
    axis tight
end
```

Appendix E

i=7 14:51

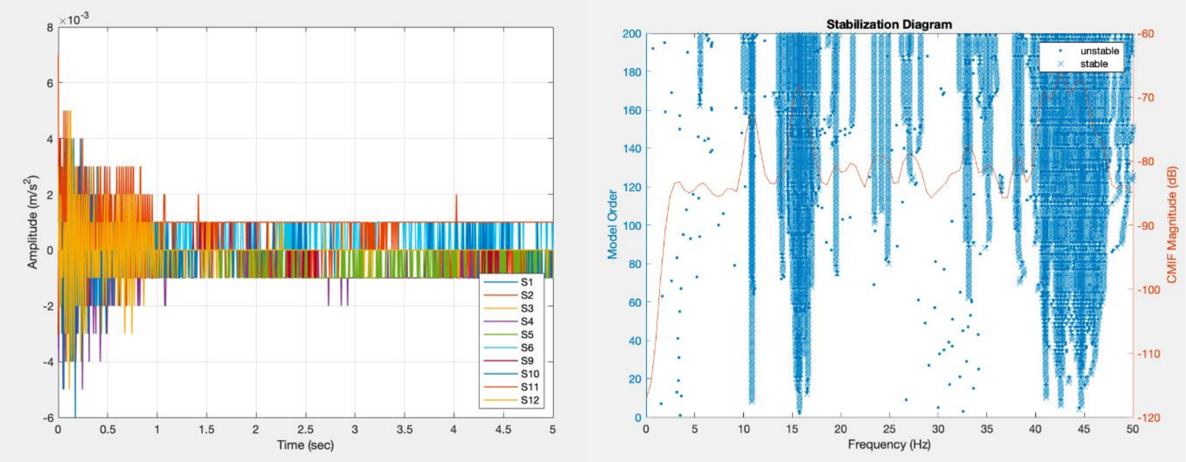

Selected order = 140

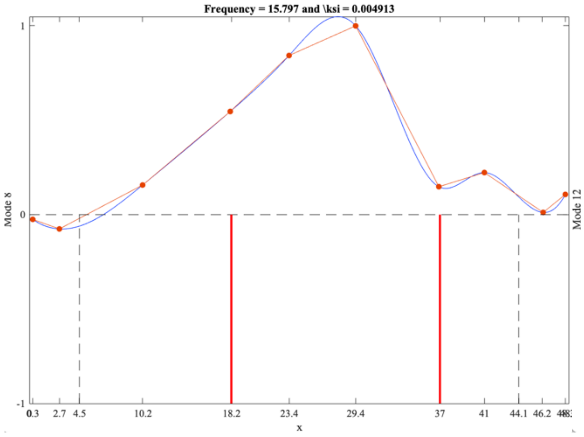

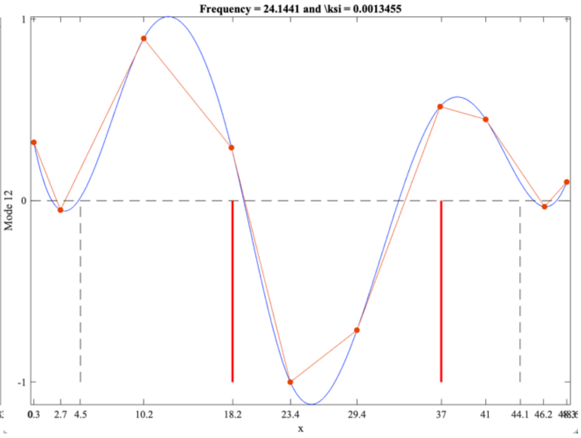

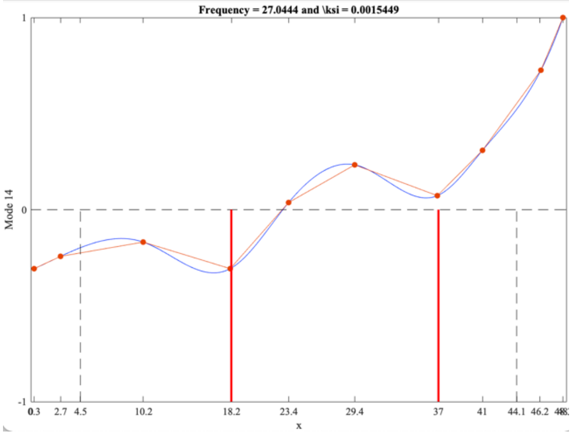

i=8 15:21

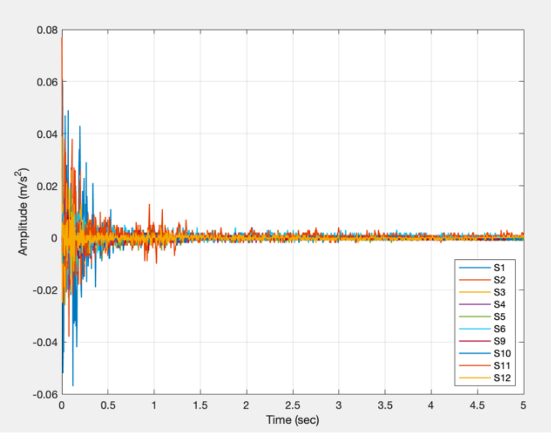

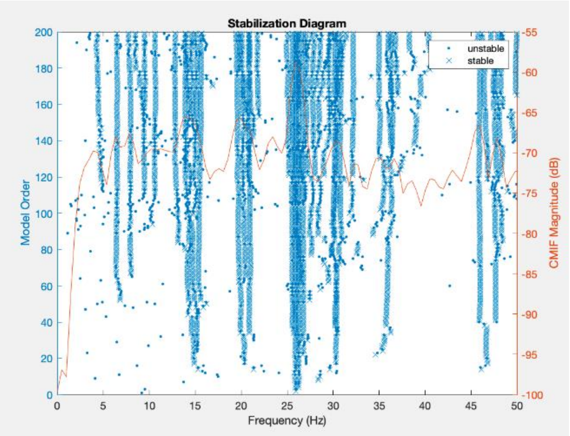

Selected order = 140

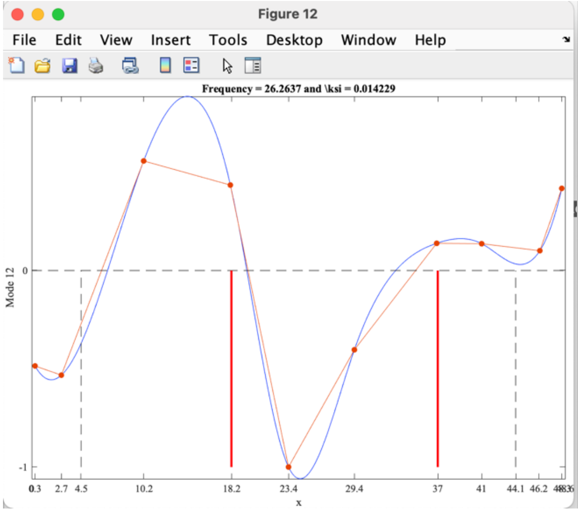

Frequency = 26.2637 and \ksi = 0.014229

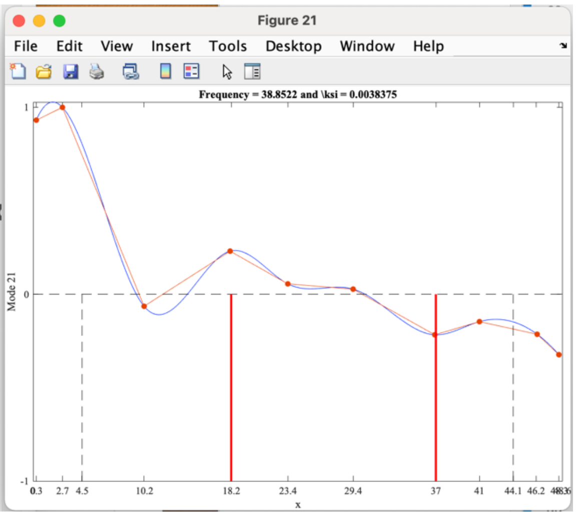

Frequency = 38.8522 and \ksi = 0.0038375

i=10 18:05

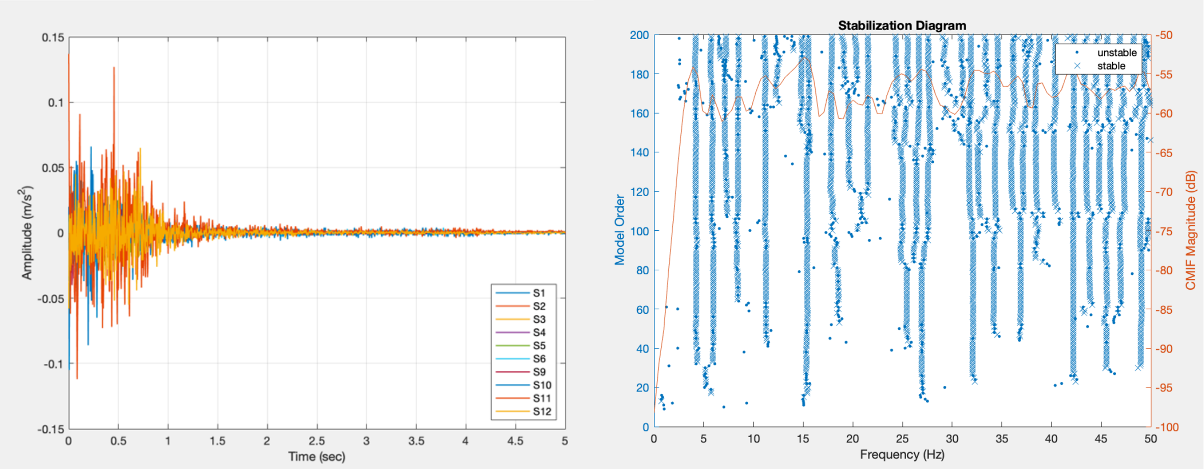

Selected order =140

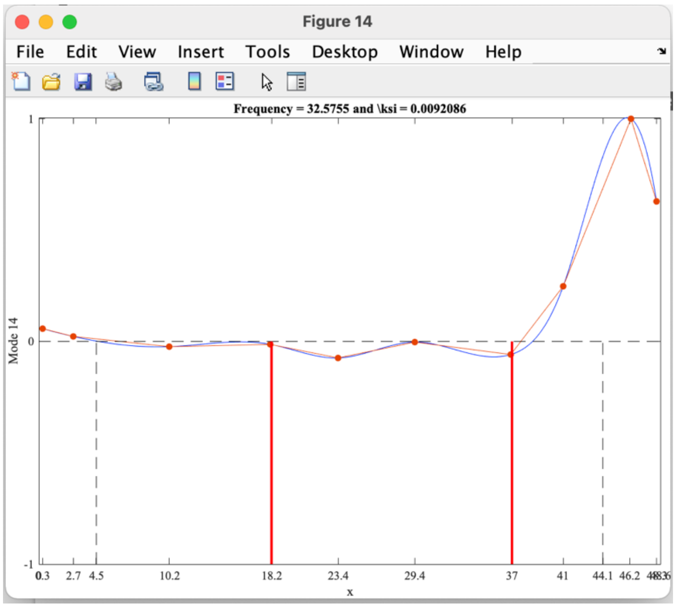

i=11 19:46

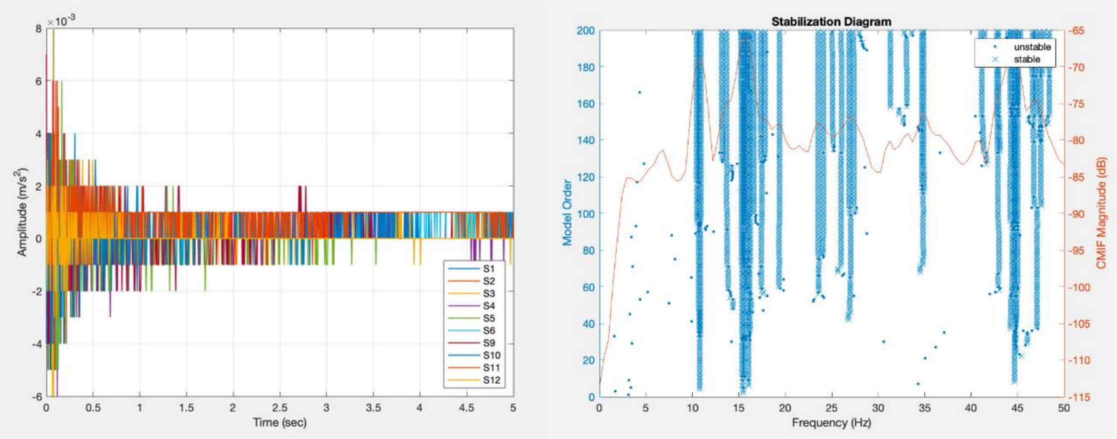

Selected order = 100

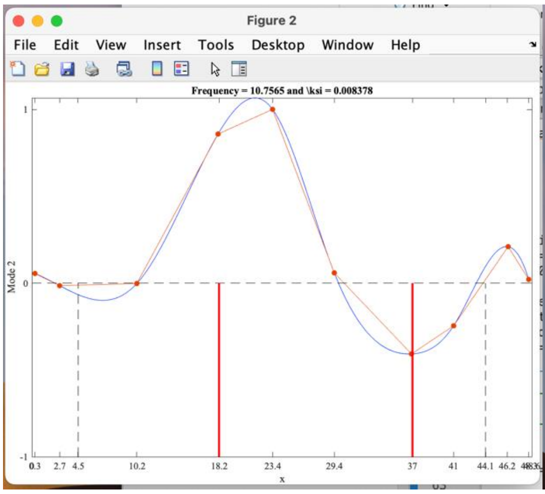

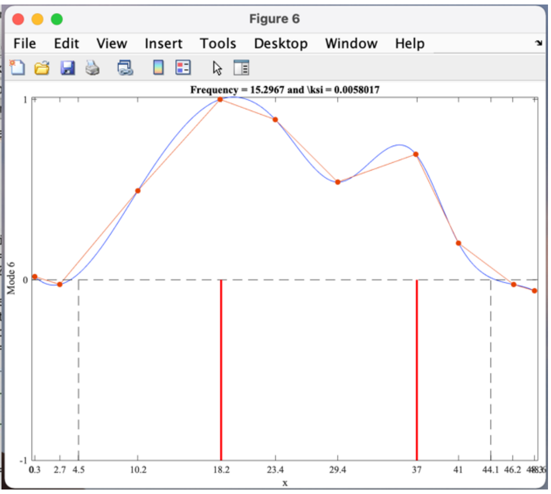

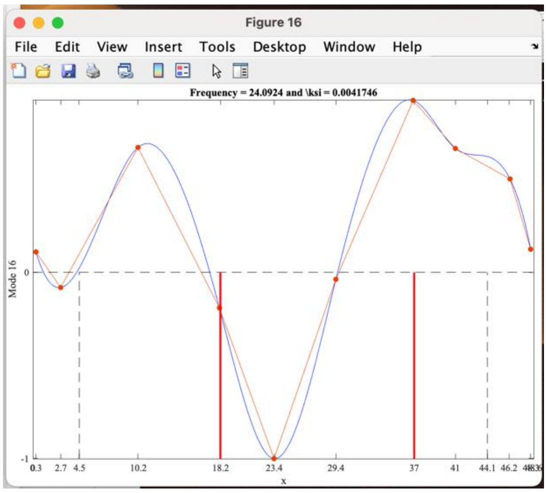

i=13 22:03

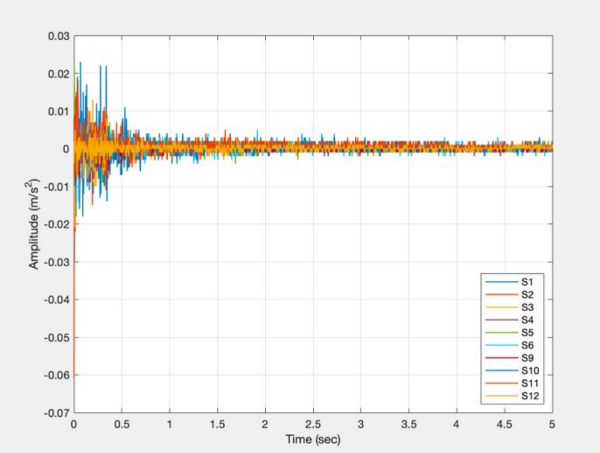

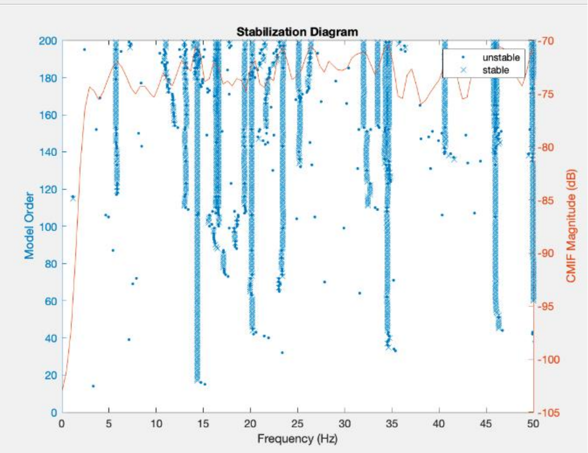

Selected order = 160

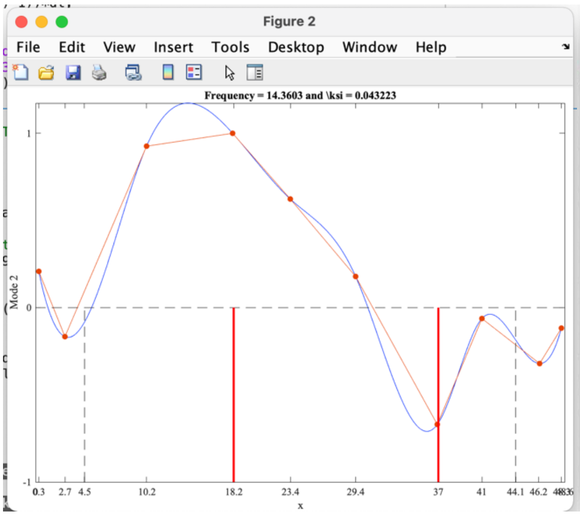

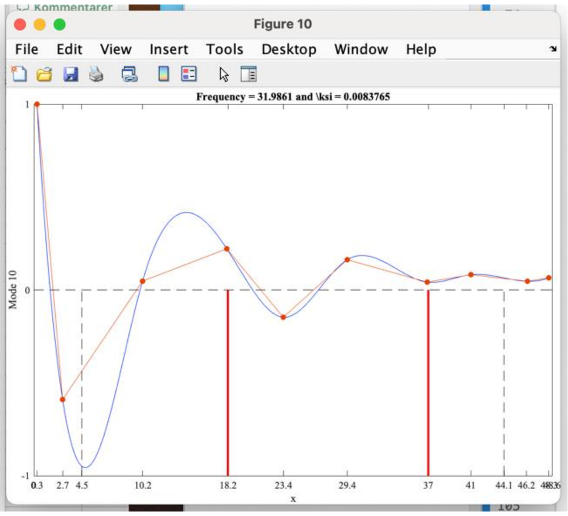

i=15 02:00

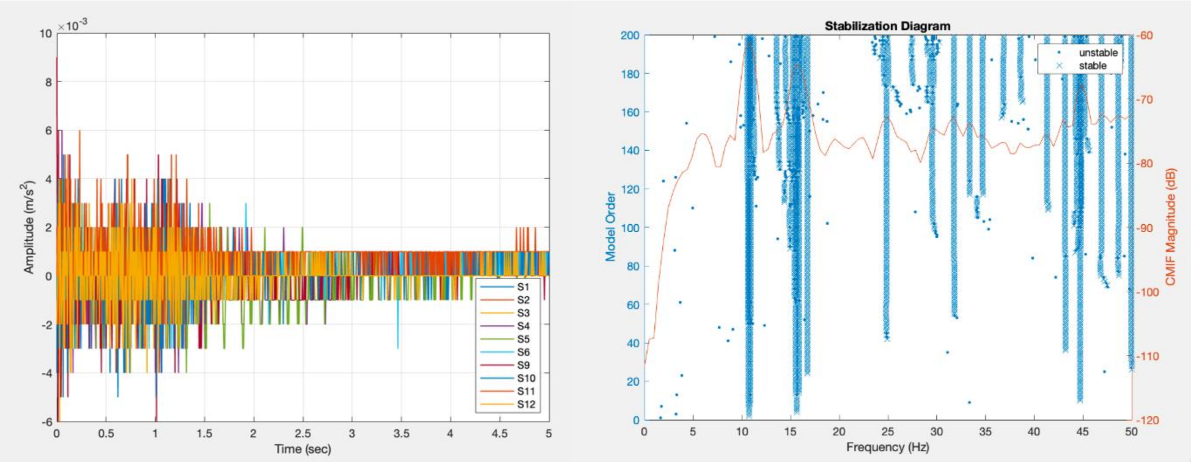

Selected order = 140

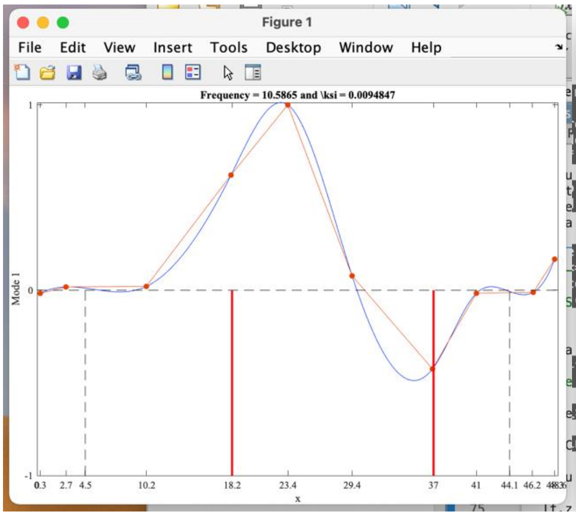
Figure 1
File Edit View Insert Tools Desktop Window Help
Frequency = 10.5865 and \ksi = 0.0094847
Mode 1
x
0.3 2.7 4.5 10.2 18.2 23.4 29.4 37 41 44.1 46.2 48.36

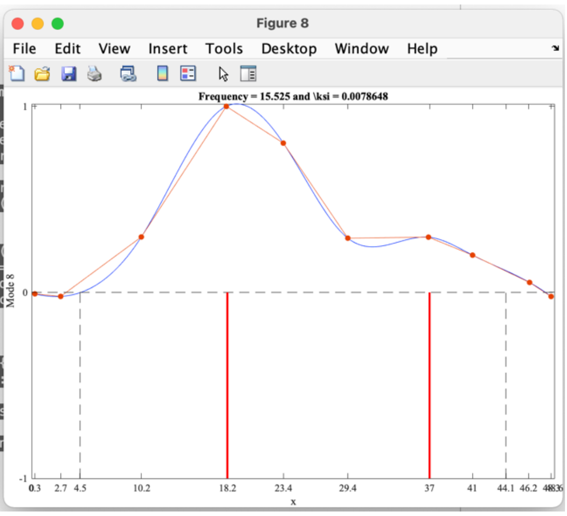
Figure 8
File Edit View Insert Tools Desktop Window Help
Frequency = 15.525 and \ksi = 0.0078648
Mode 8
x
0.3 2.7 4.5 10.2 18.2 23.4 29.4 37 41 44.1 46.2 48.36

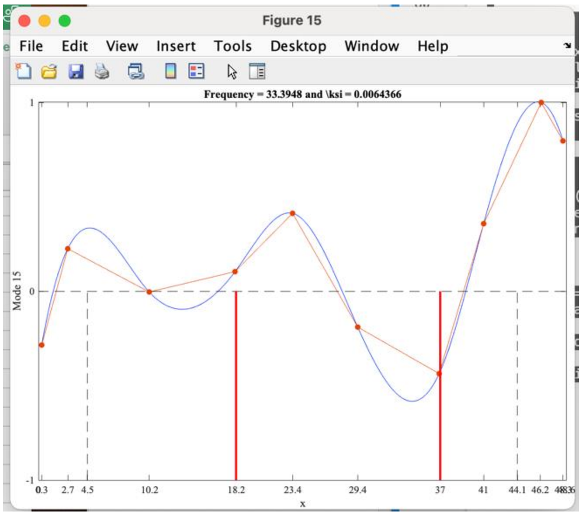
Figure 15
File Edit View Insert Tools Desktop Window Help
Frequency = 33.3948 and \ksi = 0.0064366
Mode 15
x
0.3 2.7 4.5 10.2 18.2 23.4 29.4 37 41 44.1 46.2 48.36

Appendix F

i=1 15:21

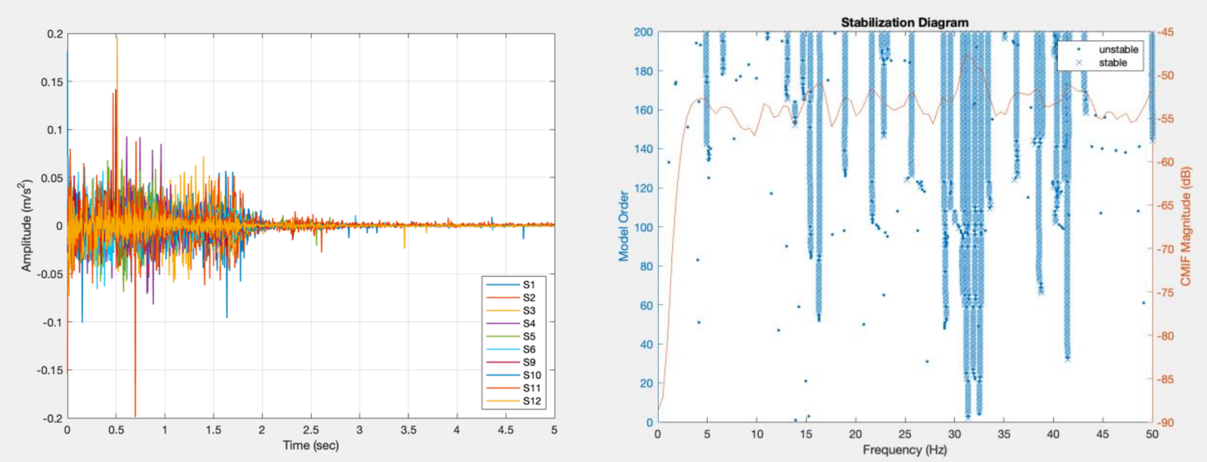

Selected order = 140

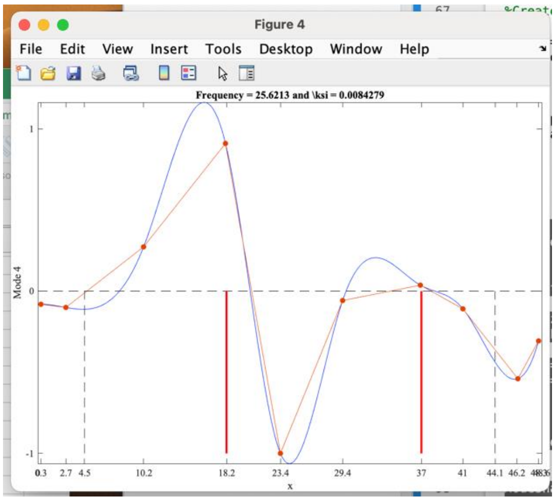

i=3 15:42

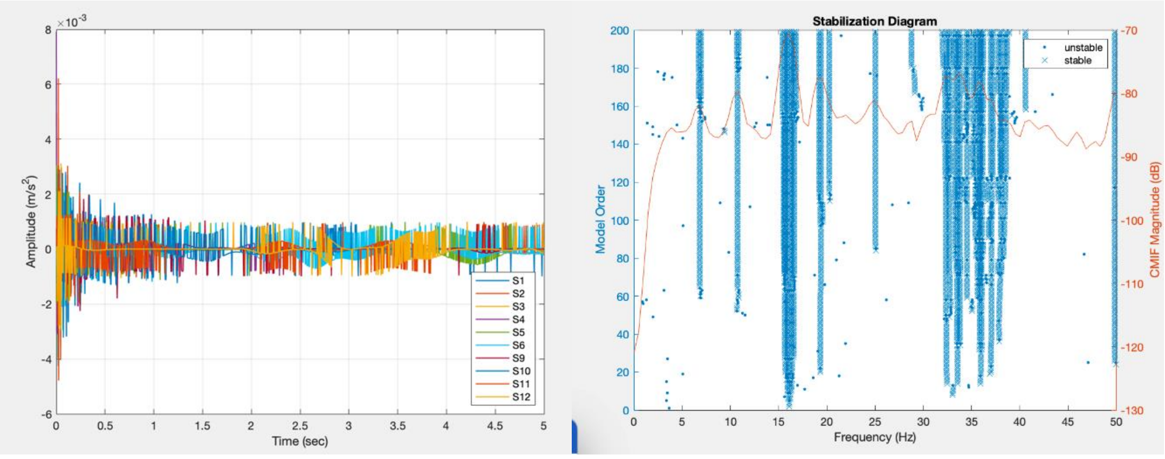

Selected order = 80

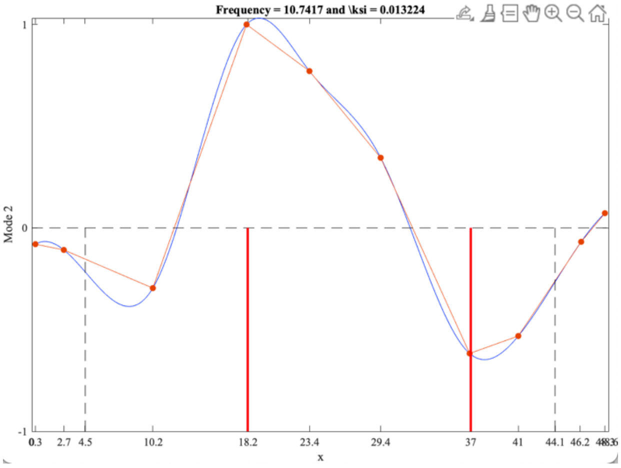

i=4 18:28

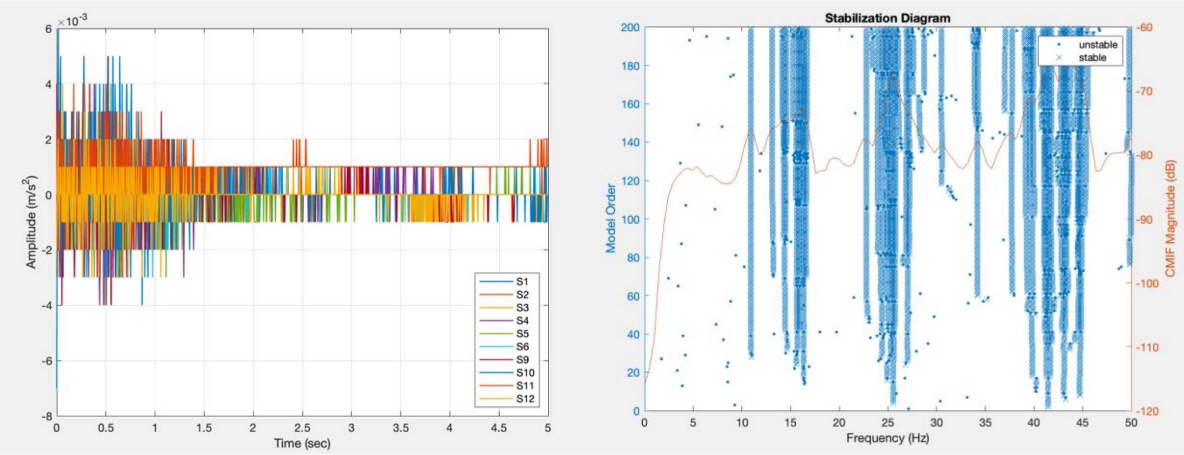

Selected order = 60

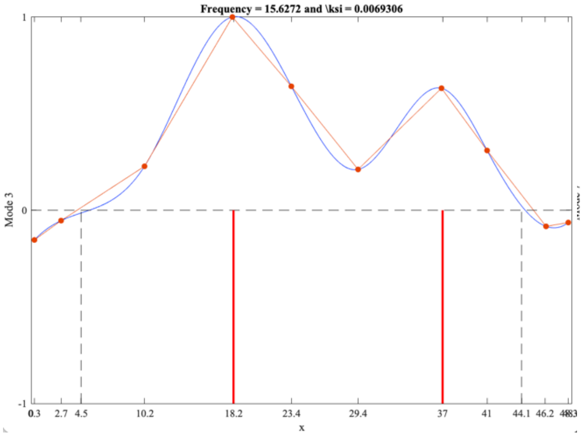

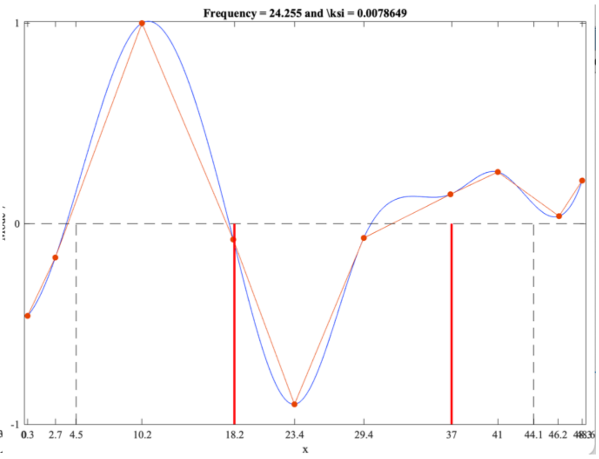

i=5 22:04

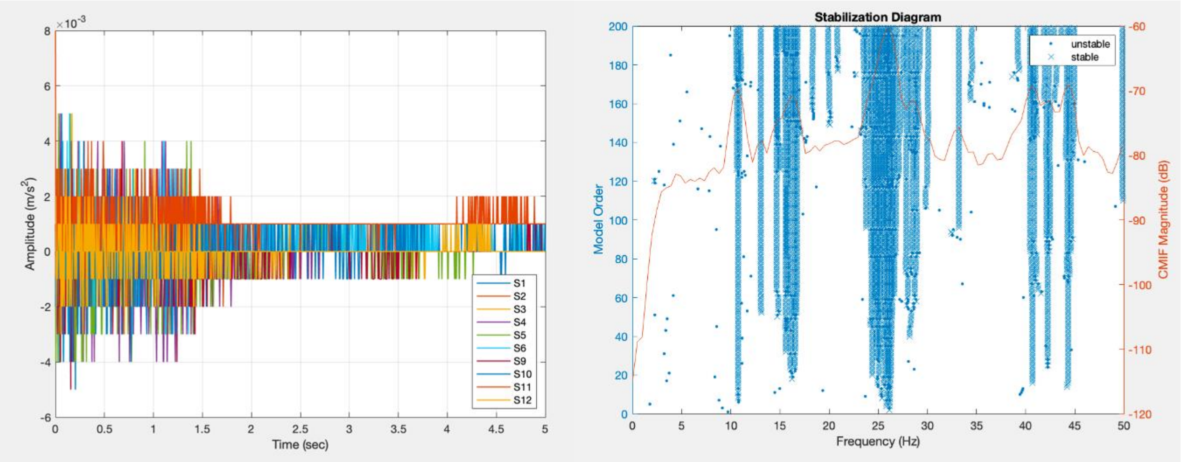

Selected order = 40

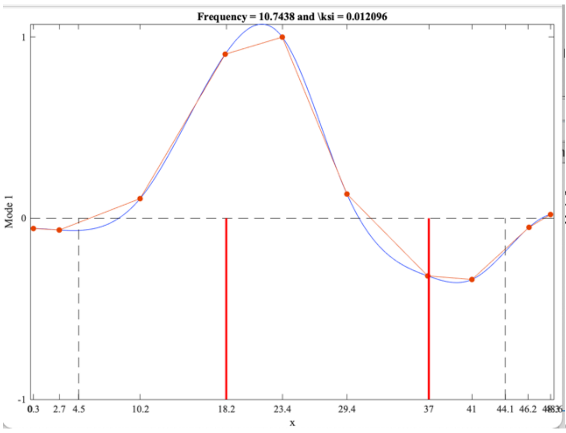

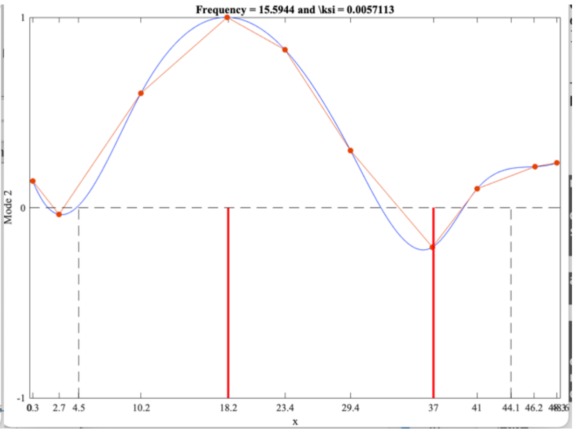

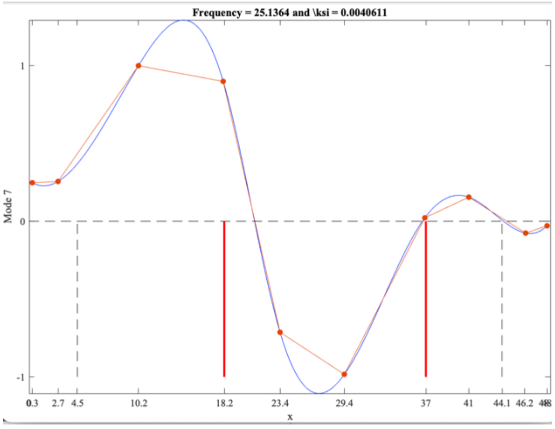

Appendix G

i=1 14:40

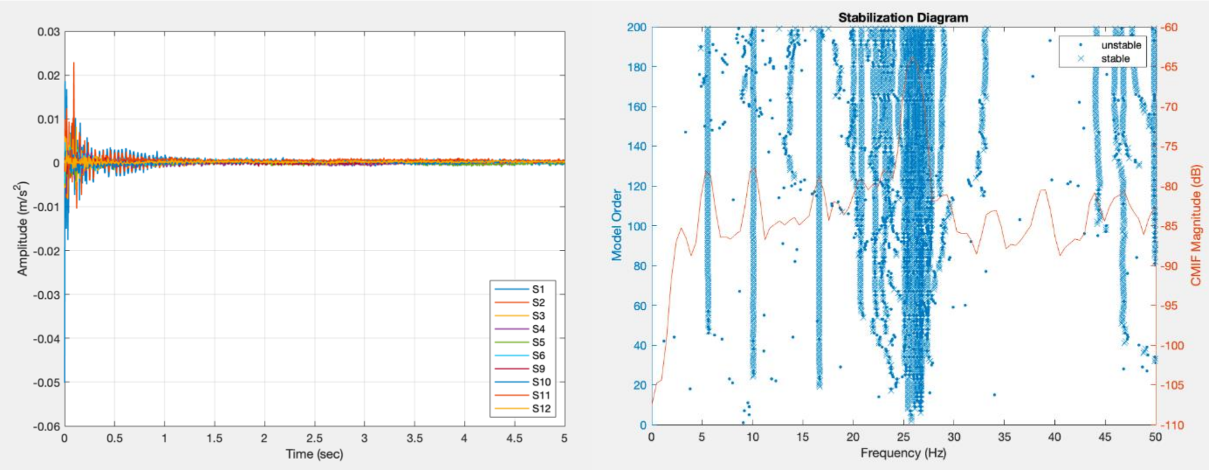

Selected order = 110

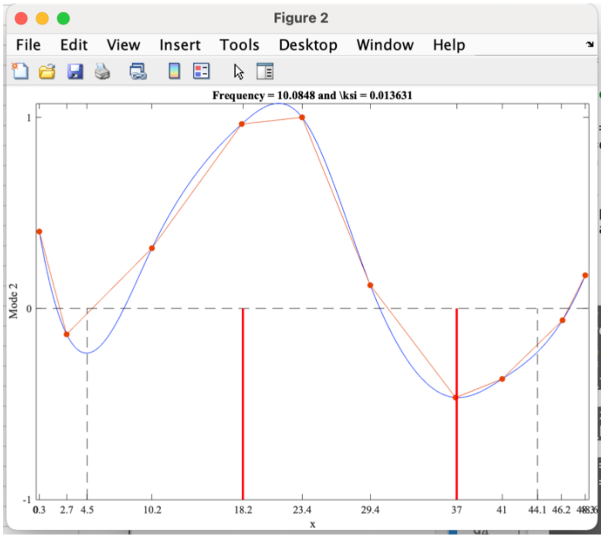

i=2 15:08

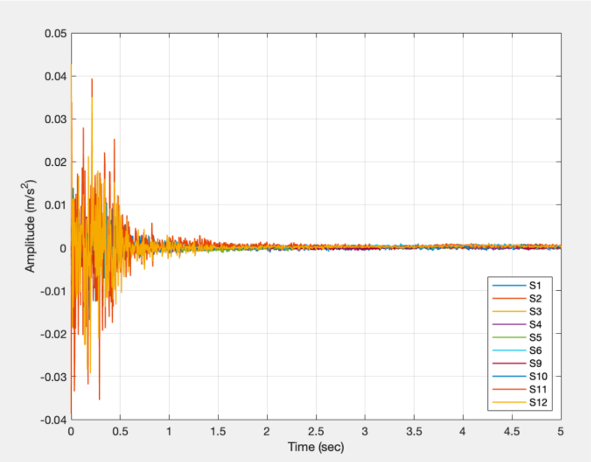

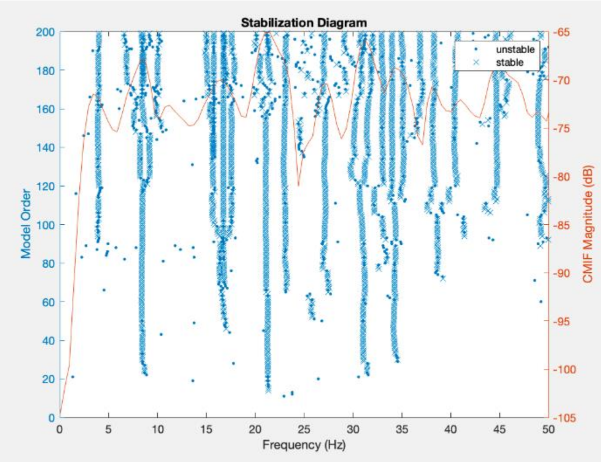

Selected order = 150

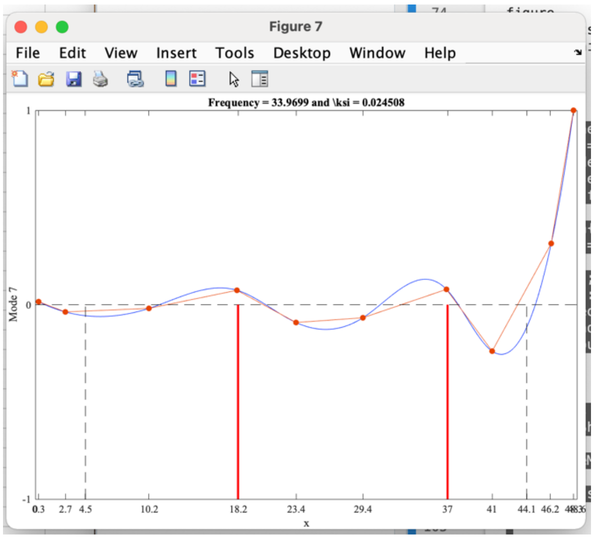

i=3 15:40

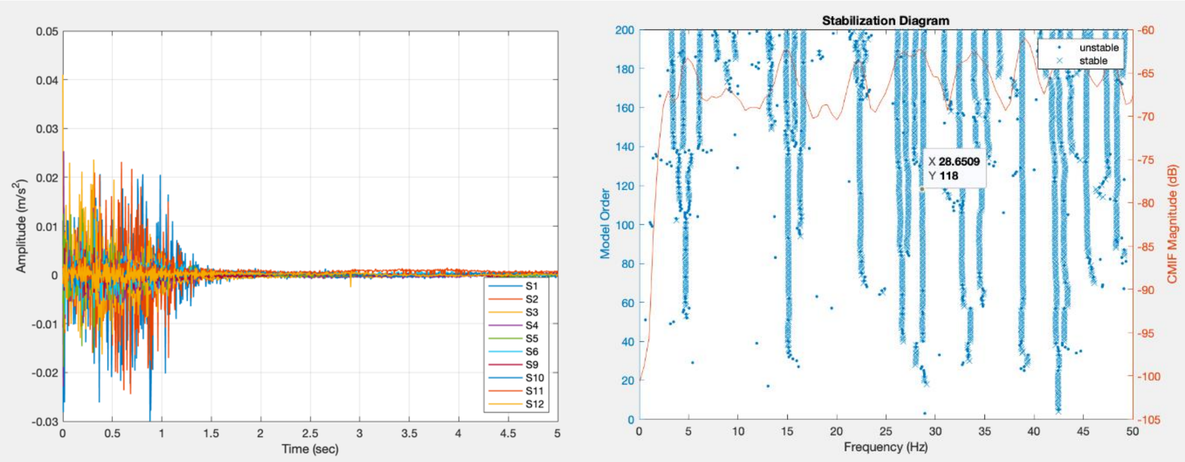

Selected order = 120

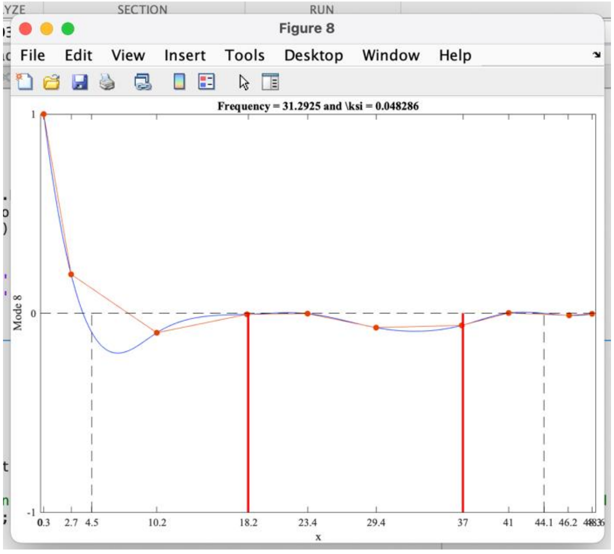

Appendix H

```
figurenumber=7;

z = MS(:,figurenumber);
   phase = [cos(angle(z)) sin(angle(z))]; % the angles of the mode shape vector
   % choose the mode shape phase that maximizes the displacement
   [~,idx] = max([sum(abs(phase(:,1))) sum(abs(phase(:,2)))]);
   shape = abs(z).*phase(:,idx);
   shape = shape/max(abs(shape)) %normalized shape

   x = [0.30 2.70 10.2 18.1 23.4 29.4 36.9 41.0 46.3 48.3] ; % x-coordinates of the sensors

   fx = fit(x',shape,'cubicinterp') ; % piece-wise cubic interpolation
   x_bar = 0:0.1:48.6 ;
```

Appendix I

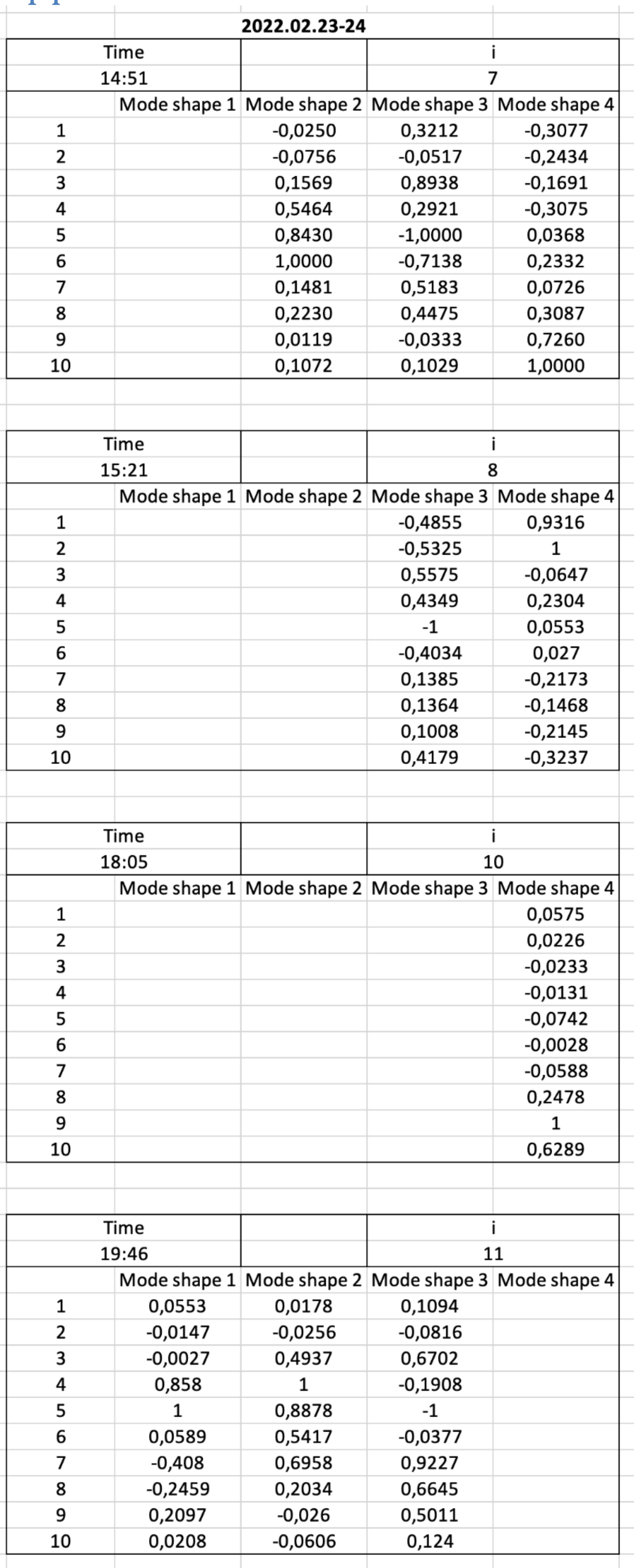

2022.02.23-24

Time			i	
14:51			7	
	Mode shape 1	Mode shape 2	Mode shape 3	Mode shape 4
1		-0,0250	0,3212	-0,3077
2		-0,0756	-0,0517	-0,2434
3		0,1569	0,8938	-0,1691
4		0,5464	0,2921	-0,3075
5		0,8430	-1,0000	0,0368
6		1,0000	-0,7138	0,2332
7		0,1481	0,5183	0,0726
8		0,2230	0,4475	0,3087
9		0,0119	-0,0333	0,7260
10		0,1072	0,1029	1,0000

Time			i	
15:21			8	
	Mode shape 1	Mode shape 2	Mode shape 3	Mode shape 4
1			-0,4855	0,9316
2			-0,5325	1
3			0,5575	-0,0647
4			0,4349	0,2304
5			-1	0,0553
6			-0,4034	0,027
7			0,1385	-0,2173
8			0,1364	-0,1468
9			0,1008	-0,2145
10			0,4179	-0,3237

Time			i	
18:05			10	
	Mode shape 1	Mode shape 2	Mode shape 3	Mode shape 4
1				0,0575
2				0,0226
3				-0,0233
4				-0,0131
5				-0,0742
6				-0,0028
7				-0,0588
8				0,2478
9				1
10				0,6289

Time			i	
19:46			11	
	Mode shape 1	Mode shape 2	Mode shape 3	Mode shape 4
1	0,0553	0,0178	0,1094	
2	-0,0147	-0,0256	-0,0816	
3	-0,0027	0,4937	0,6702	
4	0,858	1	-0,1908	
5	1	0,8878	-1	
6	0,0589	0,5417	-0,0377	
7	-0,408	0,6958	0,9227	
8	-0,2459	0,2034	0,6645	
9	0,2097	-0,026	0,5011	
10	0,0208	-0,0606	0,124	

Time			i	
22:03			13	
	Mode shape 1	Mode shape 2	Mode shape 3	Mode shape 4
1		0,2082		1
2		-0,1663		-0,5902
3		0,9262		0,0472
4		1		0,2212
5		0,6231		-0,1471
6		0,1788		0,1625
7		-0,6696		0,0419
8		-0,0622		0,0821
9		-0,3205		0,0464
10		-0,1173		0,0652

Time			i	
02:00			15	
	Mode shape 1	Mode shape 2	Mode shape 3	Mode shape 4
1	-0,0169	-0,0079		-0,2847
2	0,0177	-0,0218		0,2255
3	0,0206	0,2979		-0,0036
4	0,6214	1		0,1041
5	1	0,8023		0,413
6	0,0776	0,2914		-0,1897
7	-0,4247	0,2968		-0,4361
8	-0,0162	0,2001		0,3582
9	-0,0114	0,0533		1
10	0,1675	-0,0221		0,7963

2022.02.24-25

Time			i	
15.21			1	
	Mode shape 1	Mode shape 2	Mode shape 3	Mode shape 4
1			-0,0808	
2			-0,1006	
3			0,2728	
4			0,9102	
5			-1	
6			-0,0578	
7			0,0367	
8			-0,1091	
9			-0,5401	
10			-0,3068	

Time			i	
15:42			3	
	Mode shape 1	Mode shape 2	Mode shape 3	Mode shape 4
1	-0,0798			
2	-0,108			
3	-0,2957			
4	1			
5	0,771			
6	0,3451			
7	-0,6169			
8	-0,531			
9	-0,068			
10	0,0725			

Time			i	
18:28			4	
	Mode shape 1	Mode shape 2	Mode shape 3	Mode shape 4
1		-0,1539	-0,4594	
2		-0,0538	-0,1686	
3		0,2274	1	
4		1	-0,0786	
5		0,6413	-0,9004	
6		0,211	-0,071	
7		0,6313	0,1467	
8		0,3092	0,258	
9		-0,0836	0,0377	
10		-0,0636	0,215	

Time			i	
22:04			5	
	Mode shape 1	Mode shape 2	Mode shape 3	Mode shape 4
1	-0,0568	0,1398	0,2477	
2	-0,0652	-0,0357	0,2561	
3	0,1082	0,6011	1	
4	0,9057	1	0,8991	
5	1	0,8297	-0,7134	
6	0,1334	0,3001	-0,9835	
7	-0,3186	-0,208	0,0224	
8	-0,3382	0,0993	0,155	
9	-0,0504	0,2154	-0,0758	
10	0,0206	0,2355	-0,029	

2022.03.02-03

Time			i	
14:40			1	
	Mode shape 1	Mode shape 2	Mode shape 3	Mode shape 4
1	0,4024			
2	-0,1355			
3	0,3152			
4	0,9651			
5	1			
6	0,1213			
7	-0,4666			
8	-0,369			
9	-0,062			
10	0,1734			

Time			i	
15:08			2	
	Mode shape 1	Mode shape 2	Mode shape 3	Mode shape 4
1				0,0156
2				-0,0371
3				-0,0188
4				0,0742
5				-0,0916
6				-0,0672
7				0,079
8				-0,239
9				0,3149
10				1

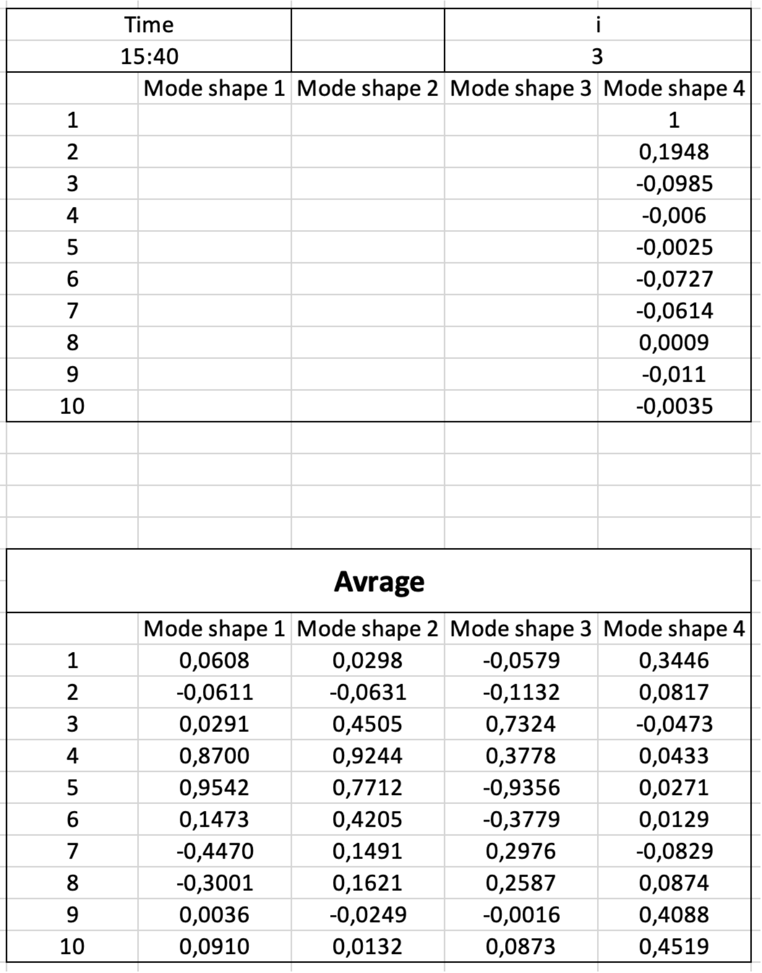

Time			i	
15:40			3	
	Mode shape 1	Mode shape 2	Mode shape 3	Mode shape 4
1				1
2				0,1948
3				-0,0985
4				-0,006
5				-0,0025
6				-0,0727
7				-0,0614
8				0,0009
9				-0,011
10				-0,0035

Avrage

	Mode shape 1	Mode shape 2	Mode shape 3	Mode shape 4
1	0,0608	0,0298	-0,0579	0,3446
2	-0,0611	-0,0631	-0,1132	0,0817
3	0,0291	0,4505	0,7324	-0,0473
4	0,8700	0,9244	0,3778	0,0433
5	0,9542	0,7712	-0,9356	0,0271
6	0,1473	0,4205	-0,3779	0,0129
7	-0,4470	0,1491	0,2976	-0,0829
8	-0,3001	0,1621	0,2587	0,0874
9	0,0036	-0,0249	-0,0016	0,4088
10	0,0910	0,0132	0,0873	0,4519

Appendix J

```
clear all; close all; clc;



y = [0.0608
-0.0611
0.0291
0.8700
0.9542
0.1473
-0.4470
-0.3001
0.0036
0.0910] ;

x = [0.30 2.70 10.2 18.1 23.4 29.4 36.9 41.0 46.3 48.3] ;

plot(x,y)
hold on
line([0 48.6],[0 0],'color','k','linestyle','--')
line([18.2 18.2],[-1 0],'color','r','linestyle','-','linewidth',2) %pier
line([37 37],[-1 0],'color','r','linestyle','-','linewidth',2)%pier
line([4.5 4.5],[-1 0],'color','k','linestyle','--') %elastomer
line([44.1 44.1],[-1 0],'color','k','linestyle','--') %elastomer
hold off
yticks([-1 0 1])
xticks([0 0.30 2.70 4.5 10.2 18.2 23.4 29.4 37 41 44.1 46.2 48.3 48.6])
```

Appendix K

BANE NOR

Ruteplanperiode R22
BLAD NR. 10, EIDSVOLL - DOMBÅS

søndag 12.12.2021 - lørdag 10.12.2022
onsdag, 23. feb. 2022

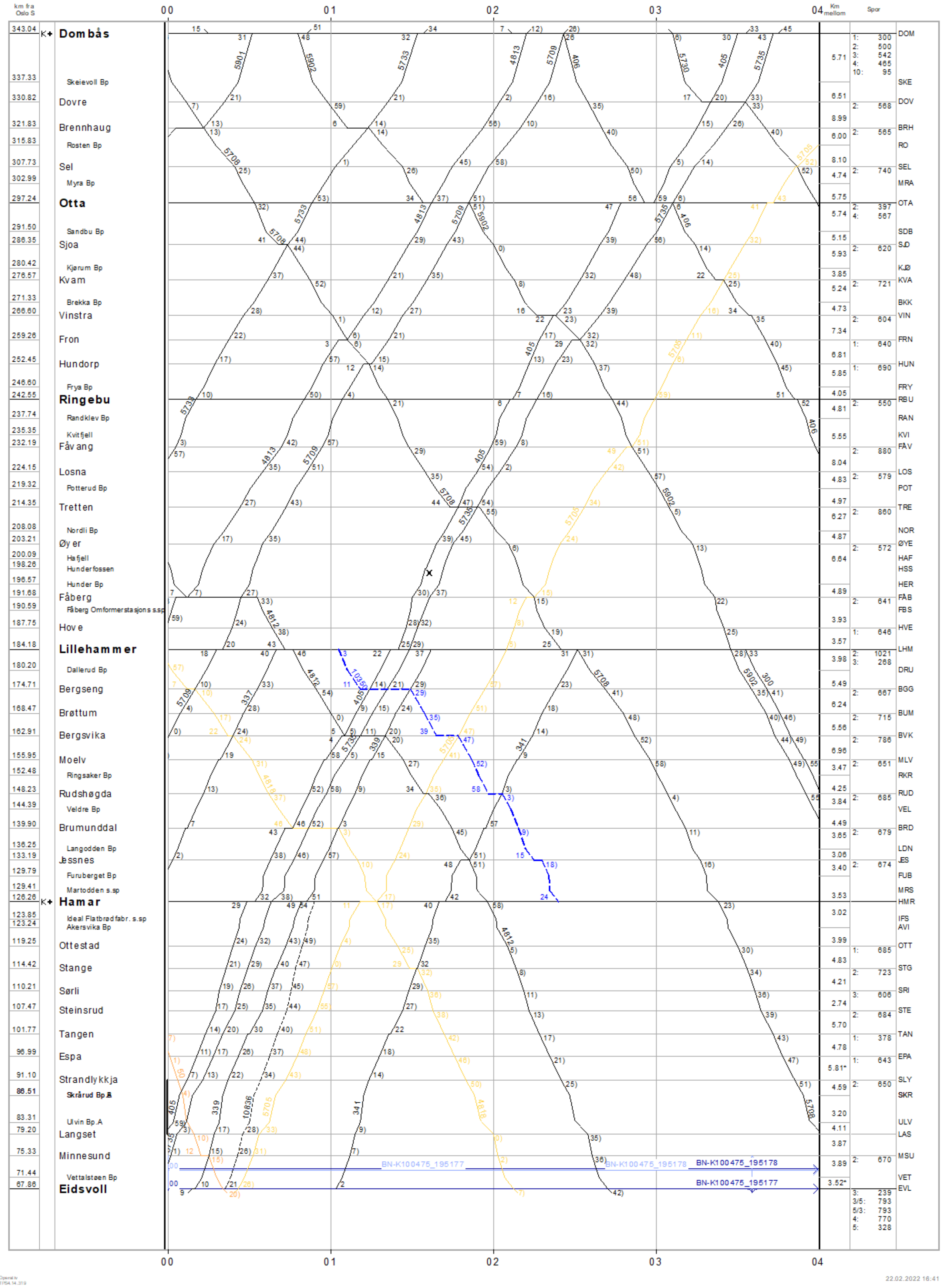

BANE NOR

Ruteplanperiode R22
BLAD NR. 10, EIDSVOLL - DOMBÅS

søndag 12.12.2021 - lørdag 10.12.2022
onsdag, 23. feb. 2022

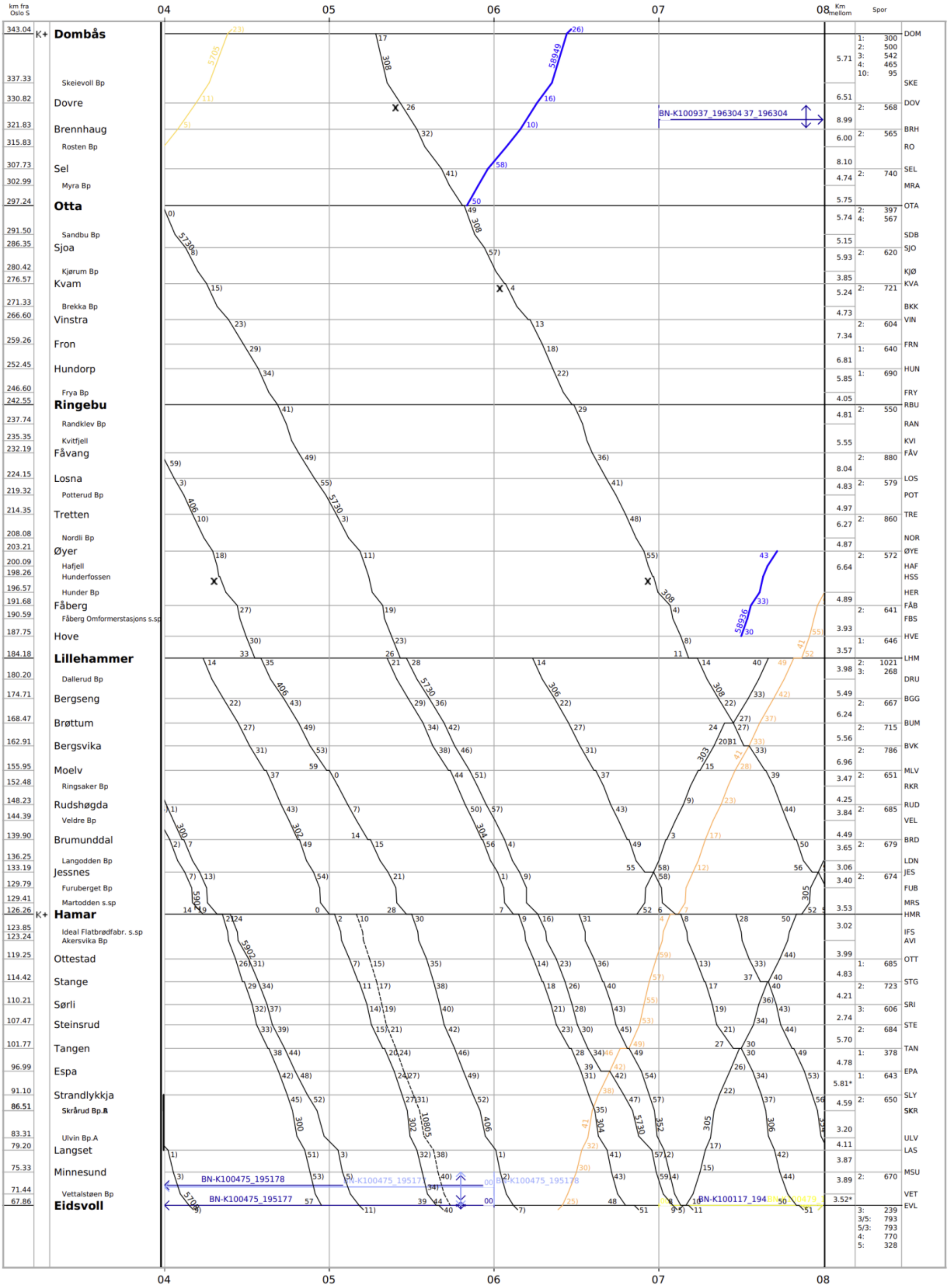

BANE NOR

Ruteplanperiode R22
BLAD NR. 10, EIDSVOLL - DOMBÅS

søndag 12.12.2021 - lørdag 10.12.2022
onsdag, 23. feb. 2022

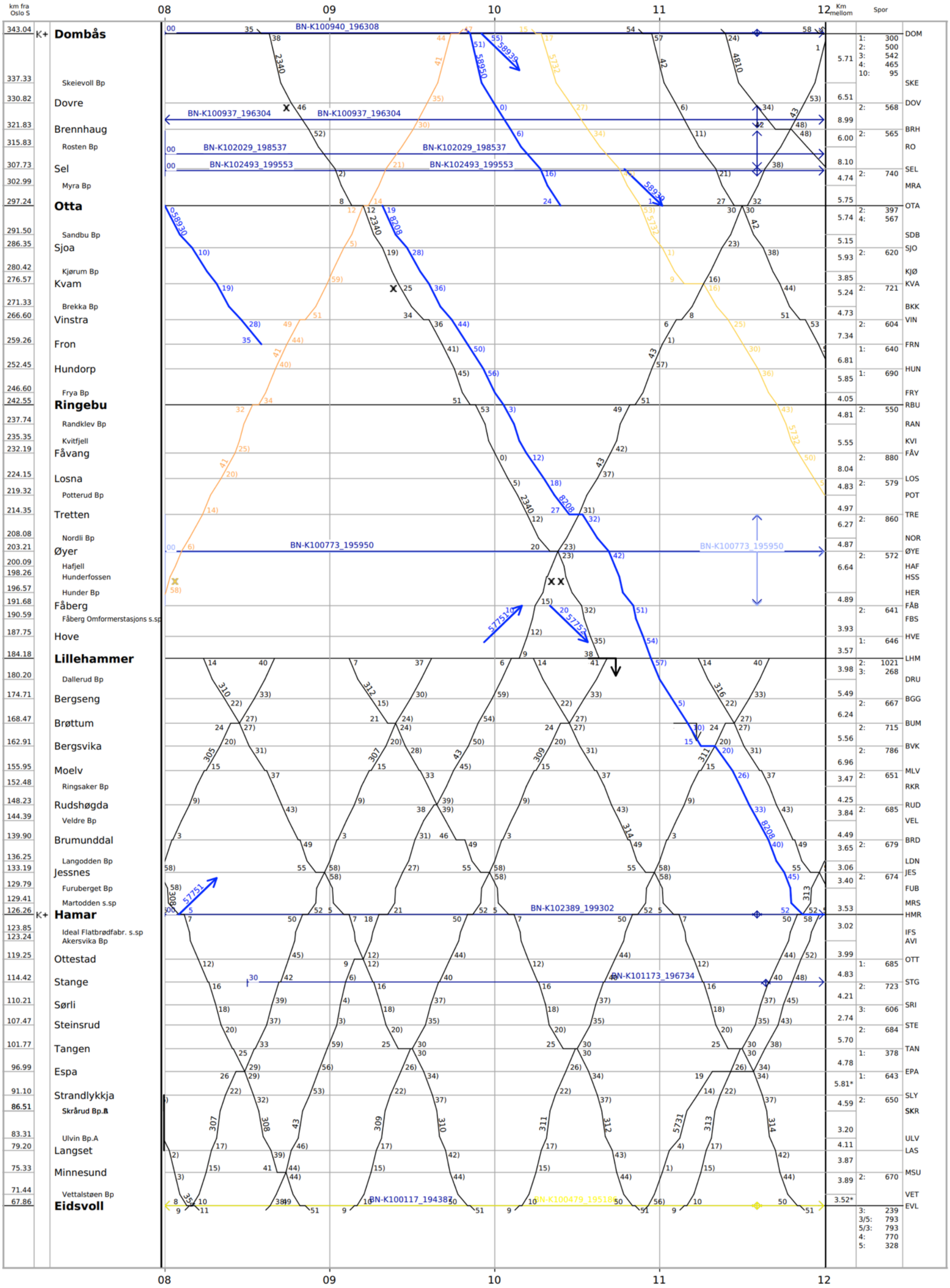

BANE NOR

Ruteplanperiode R22
BLAD NR. 10, EIDSVOLL - DOMBÅS

søndag 12.12.2021 - lørdag 10.12.2022
onsdag, 23. feb. 2022

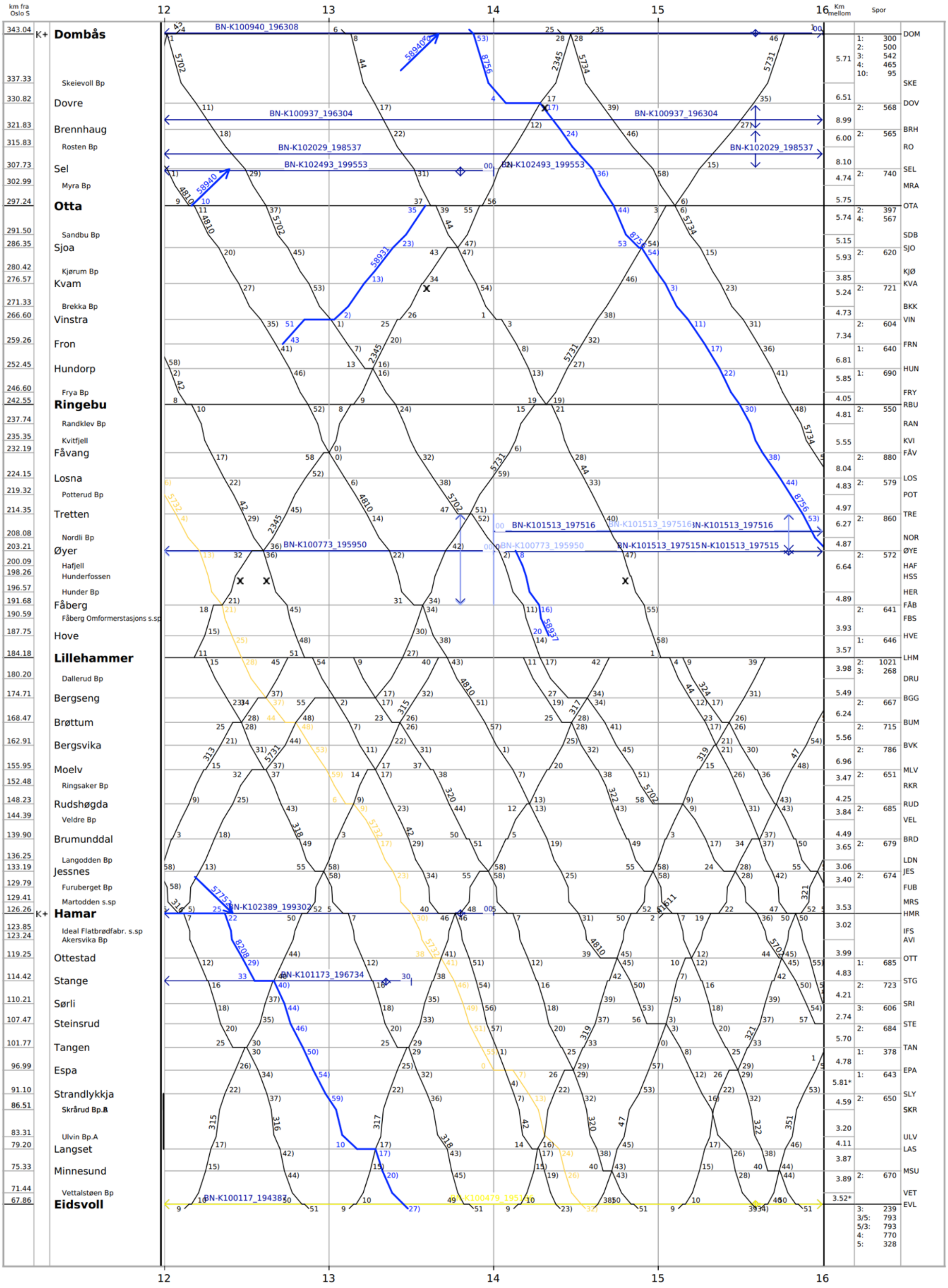

BANE NOR

Ruteplanperiode R22
BLAD NR. 10, EIDSVOLL - DOMBÅS

søndag 12.12.2021 - lørdag 10.12.2022
onsdag, 23. feb. 2022

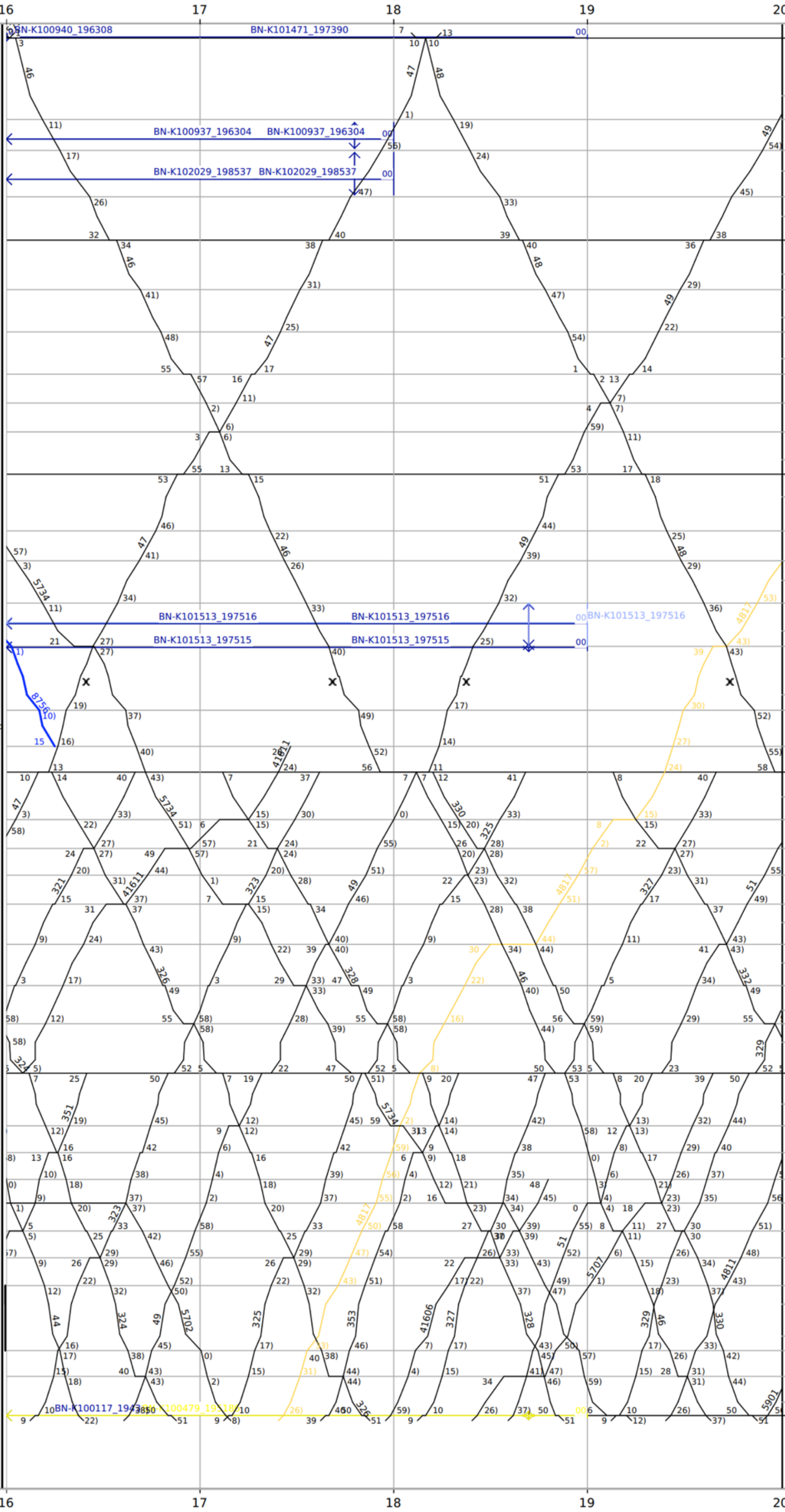

km fra Oslo S			Km mellom	Spor	
343.04	K+	**Dombås**		1: 300 2: 500 3: 542 4: 465 10: 95	DOM
337.33		Skeievoll Bp	5.71		SKE
330.82		Dovre	6.51	2: 568	DOV
321.83		Brennhaug	8.99	2: 565	BRH
315.83		Rosten Bp	6.00		RO
307.73		Sel	8.10	2: 740	SEL
302.99		Myra Bp	4.74		MRA
297.24		**Otta**	5.75	2: 397 4: 567	OTA
291.50		Sandbu Bp	5.74		SDB
286.35		Sjoa	5.15	2: 620	SJO
280.42		Kjørum Bp	5.93		KJØ
276.57		Kvam	3.85	2: 721	KVA
271.33		Brekka Bp	5.24		BKK
266.60		Vinstra	4.73	2: 604	VIN
259.26		Fron	7.34	1: 640	FRN
252.45		Hundorp	6.81	1: 690	HUN
246.60		Frya Bp	5.85		FRY
242.55		**Ringebu**	4.05	2: 550	RBU
237.74		Randklev Bp	4.81		RAN
235.35		Kvitfjell			KVI
232.19		Fåvang	5.55	2: 880	FÅV
224.15		Losna	8.04	2: 579	LOS
219.32		Potterud Bp	4.83		POT
214.35		Tretten	4.97	2: 860	TRE
208.08		Nordli Bp	6.27		NOR
203.21		Øyer	4.87	2: 572	ØYE
200.09		Hafjell			HAF
198.26		Hunderfossen			HSS
196.57		Hunder Bp	6.64		HER
191.68		Fåberg	4.89	2: 641	FÅB
190.59		Fåberg Omformerstasjons s.sp			FBS
187.75		Hove	3.93	1: 646	HVE
184.18		**Lillehammer**	3.57	2: 1021 3: 268	LHM
180.20		Dallerud Bp	3.98		DRU
174.71		Bergseng	5.49	2: 667	BGG
168.47		Brøttum	6.24	2: 715	BUM
162.91		Bergsvika	5.56	2: 786	BVK
155.95		Moelv	6.96	2: 651	MLV
152.48		Ringsaker Bp	3.47		RKR
148.23		Rudshøgda	4.25	2: 685	RUD
144.39		Veldre Bp	3.84		VEL
139.90		Brumunddal	4.49	2: 679	BRD
136.25		Langodden Bp	3.65		LDN
133.19		Jessnes	3.06	2: 674	JES
129.79		Furuberget Bp	3.40		FUB
129.41		Martodden s.sp			MRS
126.26	K+	**Hamar**	3.53		HMR
123.85		Ideal Flatbrødfabr. s.sp			IFS
123.24		Akersvika Bp	3.02		AVI
119.25		Ottestad	3.99	1: 685	OTT
114.42		Stange	4.83	2: 723	STG
110.21		Sørli	4.21	3: 606	SRI
107.47		Steinsrud	2.74	2: 684	STE
101.77		Tangen	5.70	1: 378	TAN
96.99		Espa	4.78	1: 643	EPA
91.10		Strandlykkja	5.81*	2: 650	SLY
86.51		Skrårud Bp.B	4.59		SKR
83.31		Ulvin Bp.A	3.20		ULV
79.20		Langset	4.11		LAS
75.33		Minnesund	3.87	2: 670	MSU
71.44		Vettalstøen Bp	3.89		VET
67.86		**Eidsvoll**	3.52*	3: 239 3/5: 793 5/3: 793 4: 770 5: 328	EVL

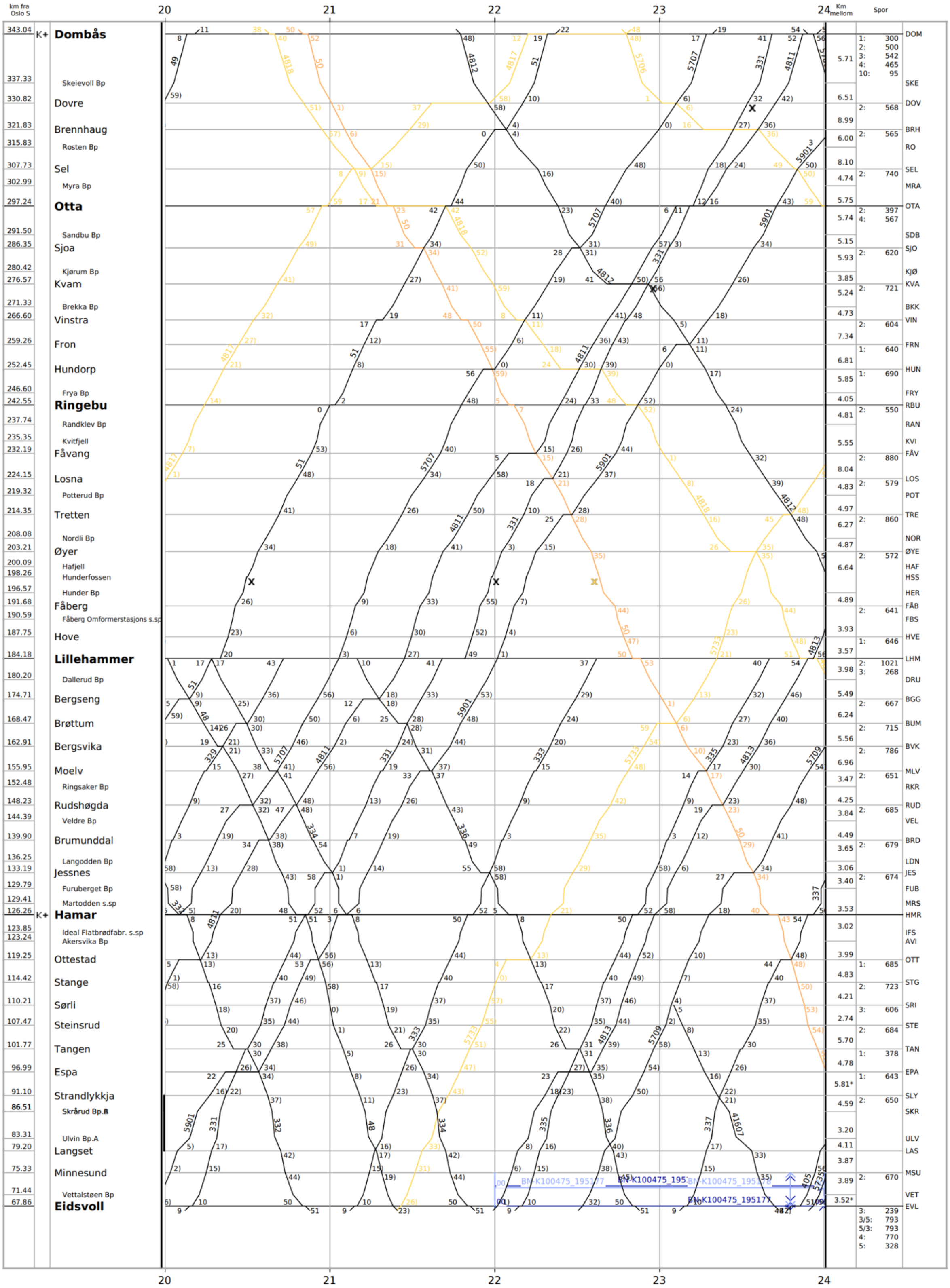
km fra Oslo S
20
21
22
23
24
Km mellom
Spor
343.04 K+ Dombås
337.33 Skeievoll Bp
330.82 Dovre
321.83 Brennhaug
315.83 Rosten Bp
307.73 Sel
302.99 Myra Bp
297.24 Otta
291.50 Sandbu Bp
286.35 Sjoa
280.42 Kjørum Bp
276.57 Kvam
271.33 Brekka Bp
266.60 Vinstra
259.26 Fron
252.45 Hundorp
246.60 Frya Bp
242.55 Ringebu
237.74 Randklev Bp
235.35 Kvitfjell
232.19 Fåvang
224.15 Losna
219.32 Potterud Bp
214.35 Tretten
208.08 Nordli Bp
203.21 Øyer
200.09 Hafjell
198.26 Hunderfossen
196.57 Hunder Bp
191.68 Fåberg
190.59 Fåberg Omformerstasjons s.sp
187.75 Hove
184.18 Lillehammer
180.20 Dallerud Bp
174.71 Bergseng
168.47 Brøttum
162.91 Bergsvika
155.95 Moelv
152.48 Ringsaker Bp
148.23 Rudshøgda
144.39 Veldre Bp
139.90 Brumunddal
136.25 Langodden Bp
133.19 Jessnes
129.79 Furuberget Bp
129.41 Martodden s.sp
126.26 K+ Hamar
123.85 Ideal Flatbrødfabr. s.sp
123.24 Akersvika Bp
119.25 Ottestad
114.42 Stange
110.21 Sørli
107.47 Steinsrud
101.77 Tangen
96.99 Espa
91.10 Strandlykkja
86.51 Skrårud Bp.A
83.31 Ulvin Bp.A
79.20 Langset
75.33 Minnesund
71.44 Vettalstøen Bp
67.86 Eidsvoll
5.71 6.51 8.99 6.00 8.10 4.74 5.75 5.74 5.15 5.93 3.85 5.24 4.73 7.34 6.81 5.85 4.05 4.81 5.55 8.04 4.83 4.97 6.27 4.87 6.64 4.89 3.93 3.57 3.98 5.49 6.24 5.56 6.96 3.47 4.25 3.84 4.49 3.65 3.06 3.40 3.53 3.02 3.99 4.83 4.21 2.74 5.70 4.78 5.81* 4.59 3.20 4.11 3.87 3.89 3.52*
DOM 1: 300 2: 500 3: 542 4: 465 10: 95
SKE
DOV 2: 568
BRH 2: 565
RO
SEL 2: 740
MRA
OTA 2: 397 4: 567
SDB
SJO 2: 620
KJØ
KVA 2: 721
BKK
VIN 2: 604
FRN 1: 640
HUN 1: 690
FRY
RBU 2: 550
RAN
KVI
FÅV 2: 880
LOS 2: 579
POT
TRE 2: 860
NOR
ØYE 2: 572
HAF
HSS
HER
FÅB 2: 641
FBS
HVE 1: 646
LHM 2: 1021 3: 268
DRU
BGG 2: 667
BUM 2: 715
BVK 2: 786
MLV 2: 651
RKR
RUD 2: 685
VEL
BRD 2: 679
LDN
JES 2: 674
FUB
MRS
HMR
IFS
AVI
OTT 1: 685
STG 2: 723
SRI 3: 606
STE 2: 684
TAN 1: 378
EPA 1: 643
SLY 2: 650
SKR
ULV
LAS
MSU 2: 670
VET
EVL 3: 239 3/5: 793 5/3: 793 4: 770 5: 328
BN-K100475_195177

BANE NOR

Ruteplanperiode R22
BLAD NR. 10, EIDSVOLL - DOMBÅS

søndag 12.12.2021 - lørdag 10.12.2022
torsdag, 24. feb. 2022

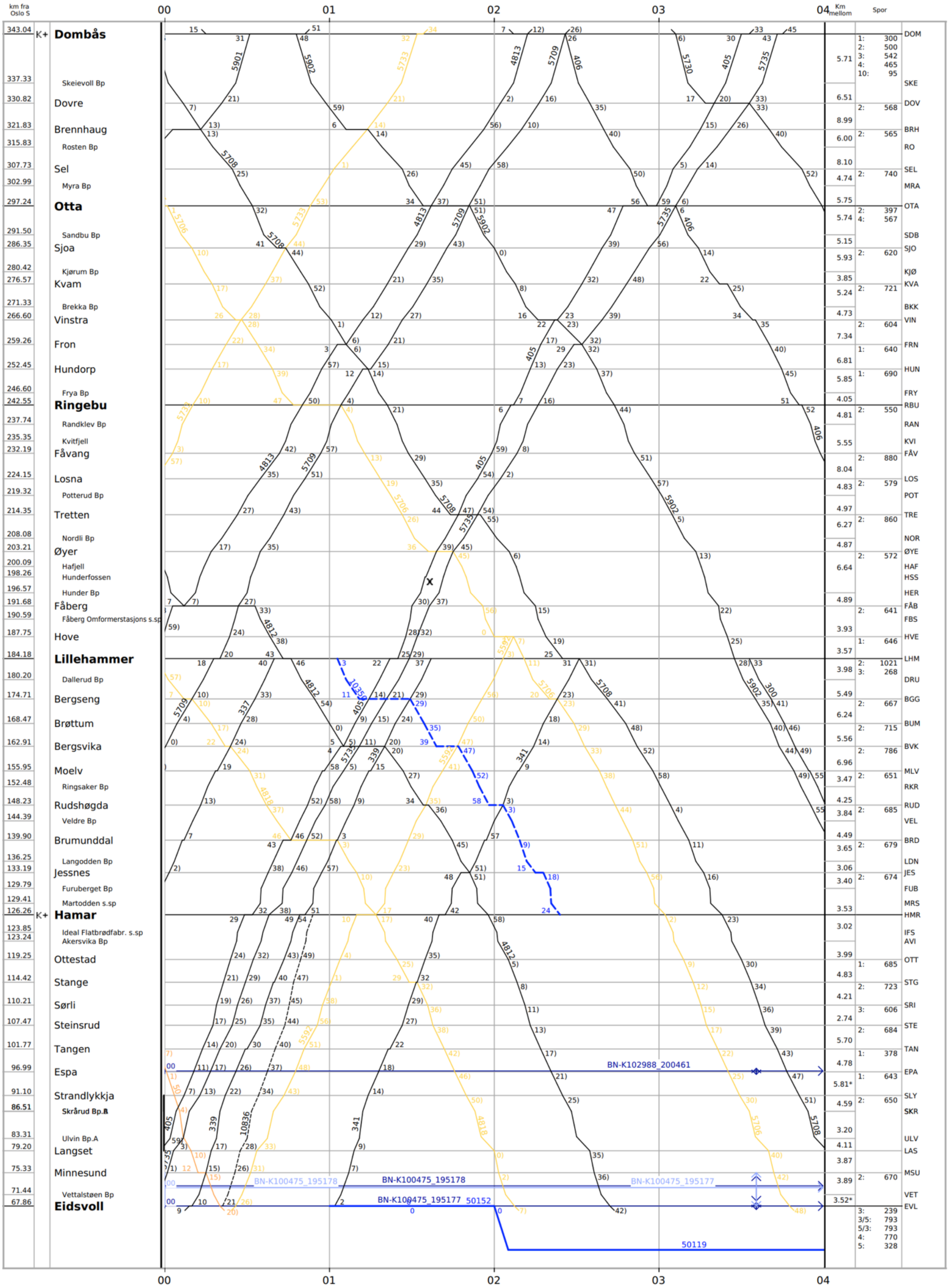

BANE NOR

Ruteplanperiode R22
BLAD NR. 10, EIDSVOLL - DOMBÅS

søndag 12.12.2021 - lørdag 10.12.2022
torsdag, 24. feb. 2022

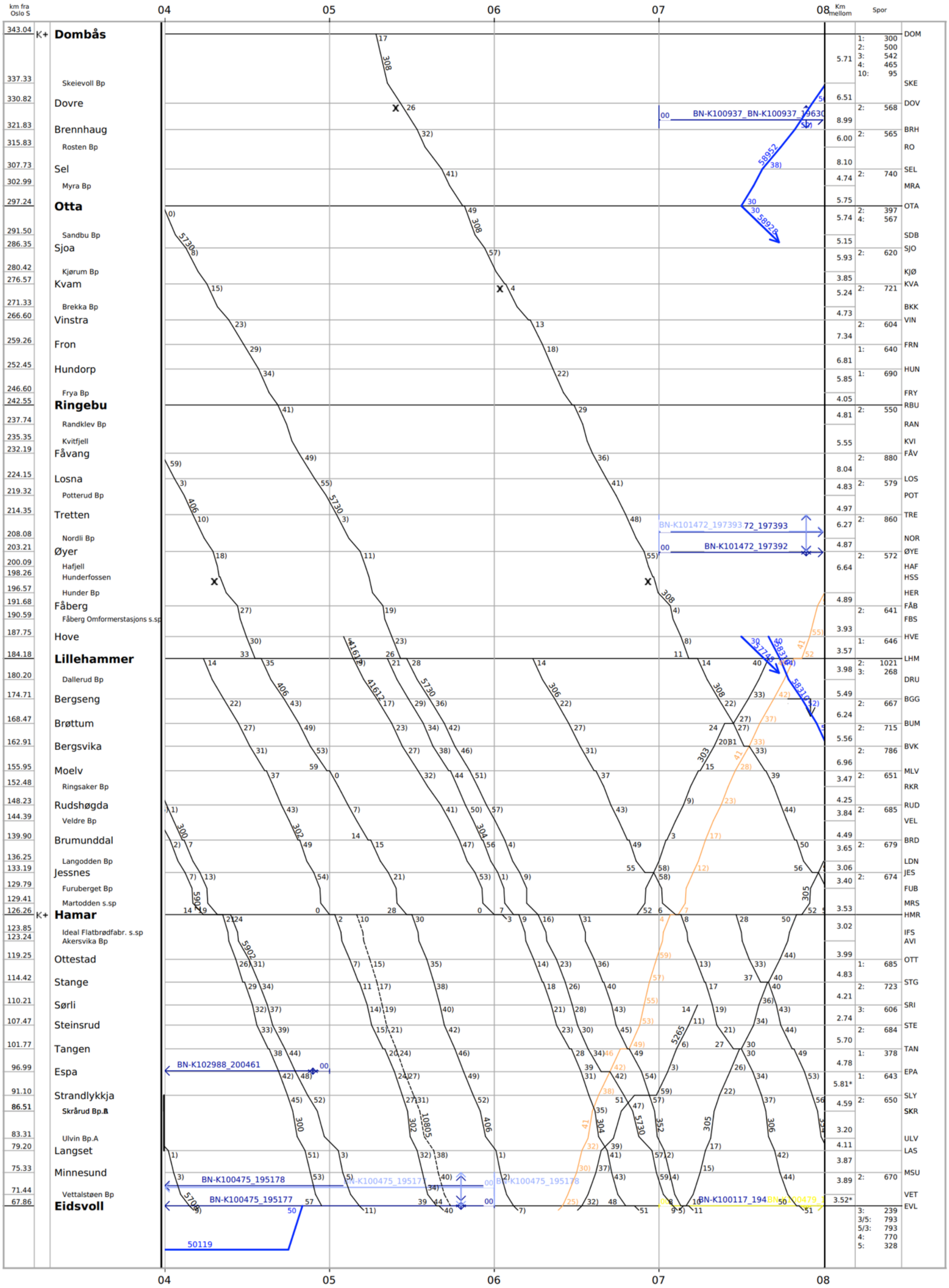

BANE NOR

Ruteplanperiode R22
BLAD NR. 10, EIDSVOLL - DOMBÅS

søndag 12.12.2021 - lørdag 10.12.2022
torsdag, 24. feb. 2022

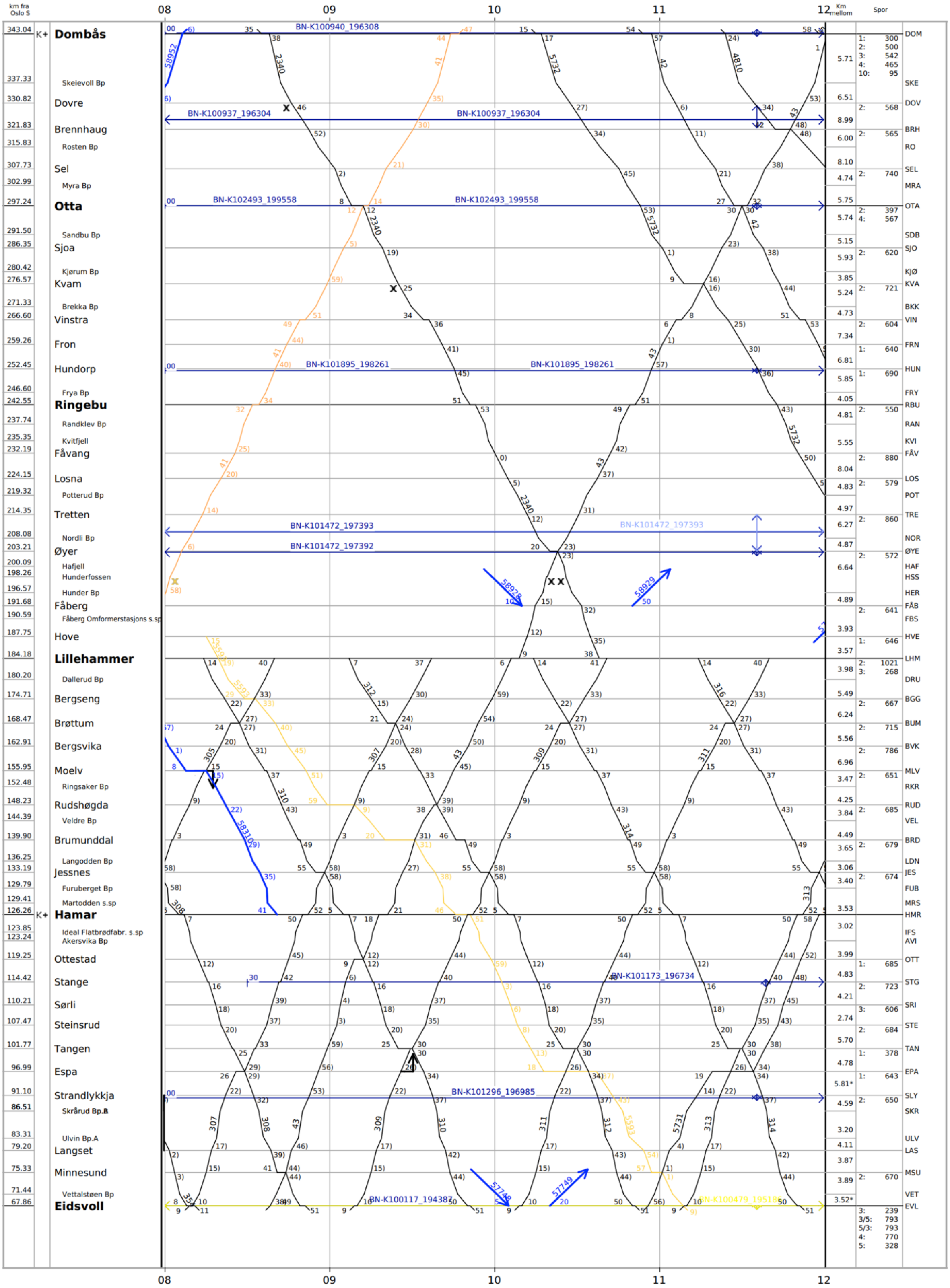

BANE NOR

Ruteplanperiode R22
BLAD NR. 10, EIDSVOLL - DOMBÅS

søndag 12.12.2021 - lørdag 10.12.2022
torsdag, 24. feb. 2022

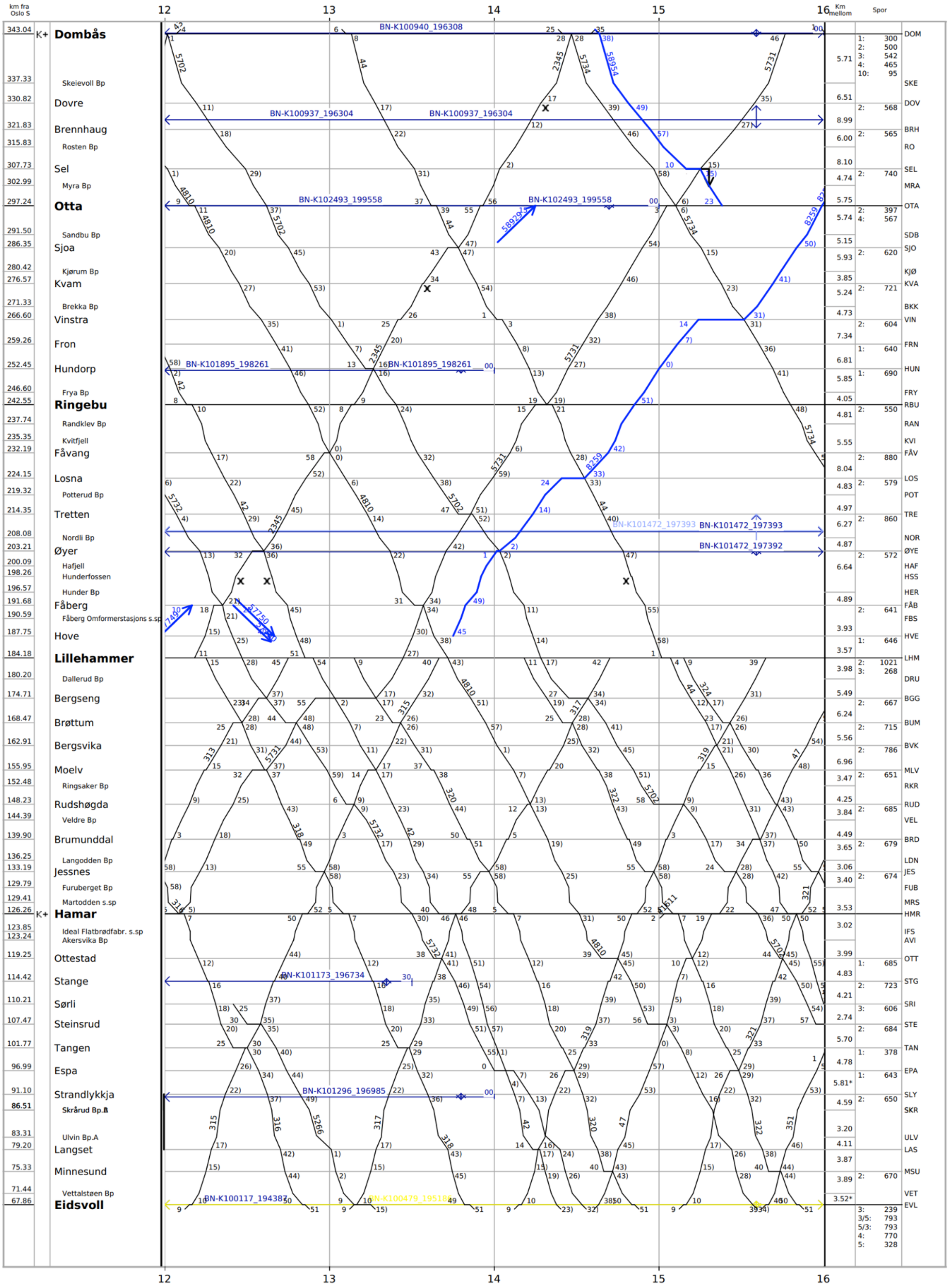

B⩘NE NOR

Ruteplanperiode R22
BLAD NR. 10, EIDSVOLL - DOMBÅS

søndag 12.12.2021 - lørdag 10.12.2022
torsdag, 24. feb. 2022

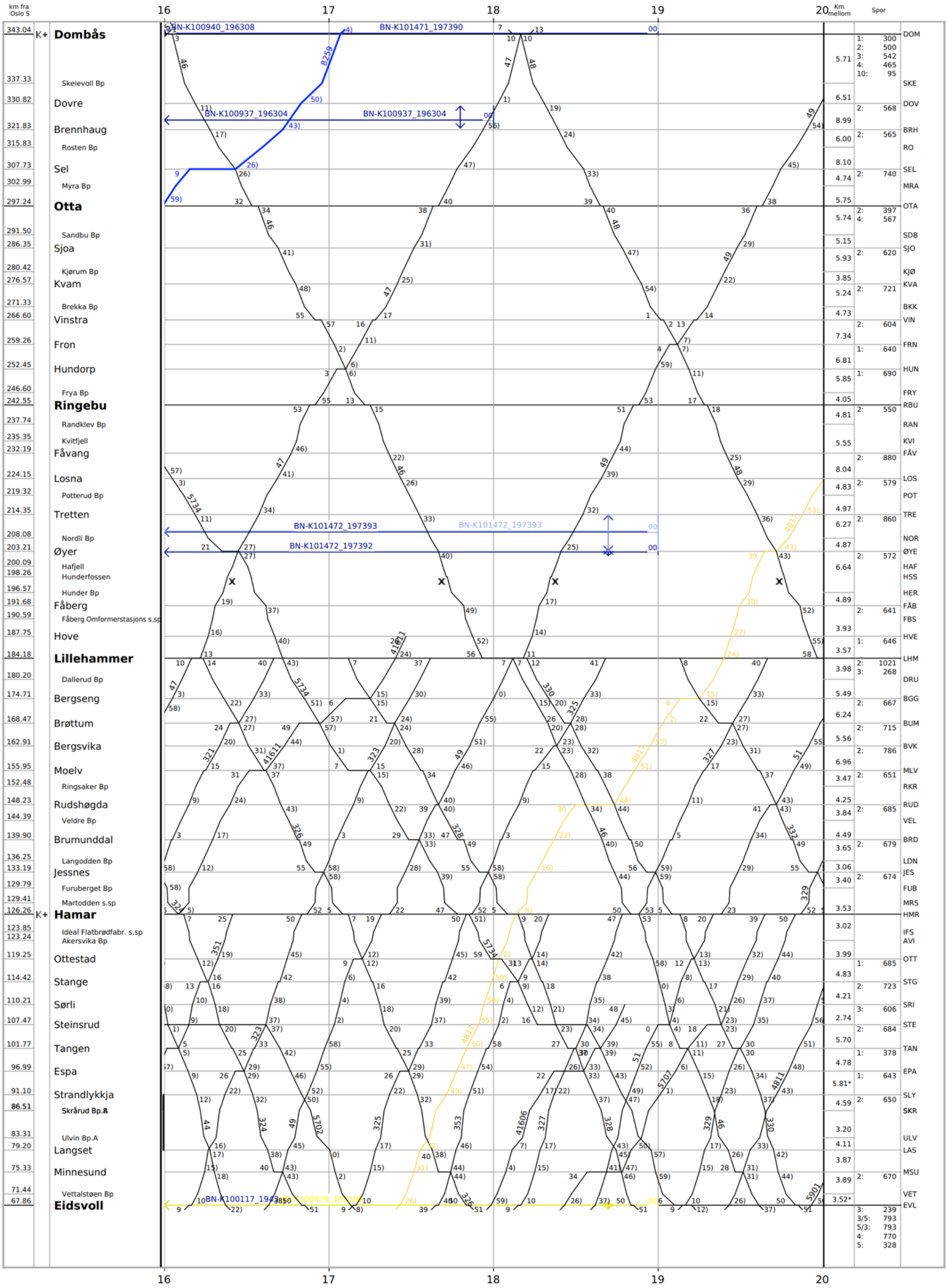

BANE NOR

Ruteplanperiode R22
BLAD NR. 10, EIDSVOLL - DOMBÅS

søndag 12.12.2021 - lørdag 10.12.2022
torsdag, 24. feb. 2022

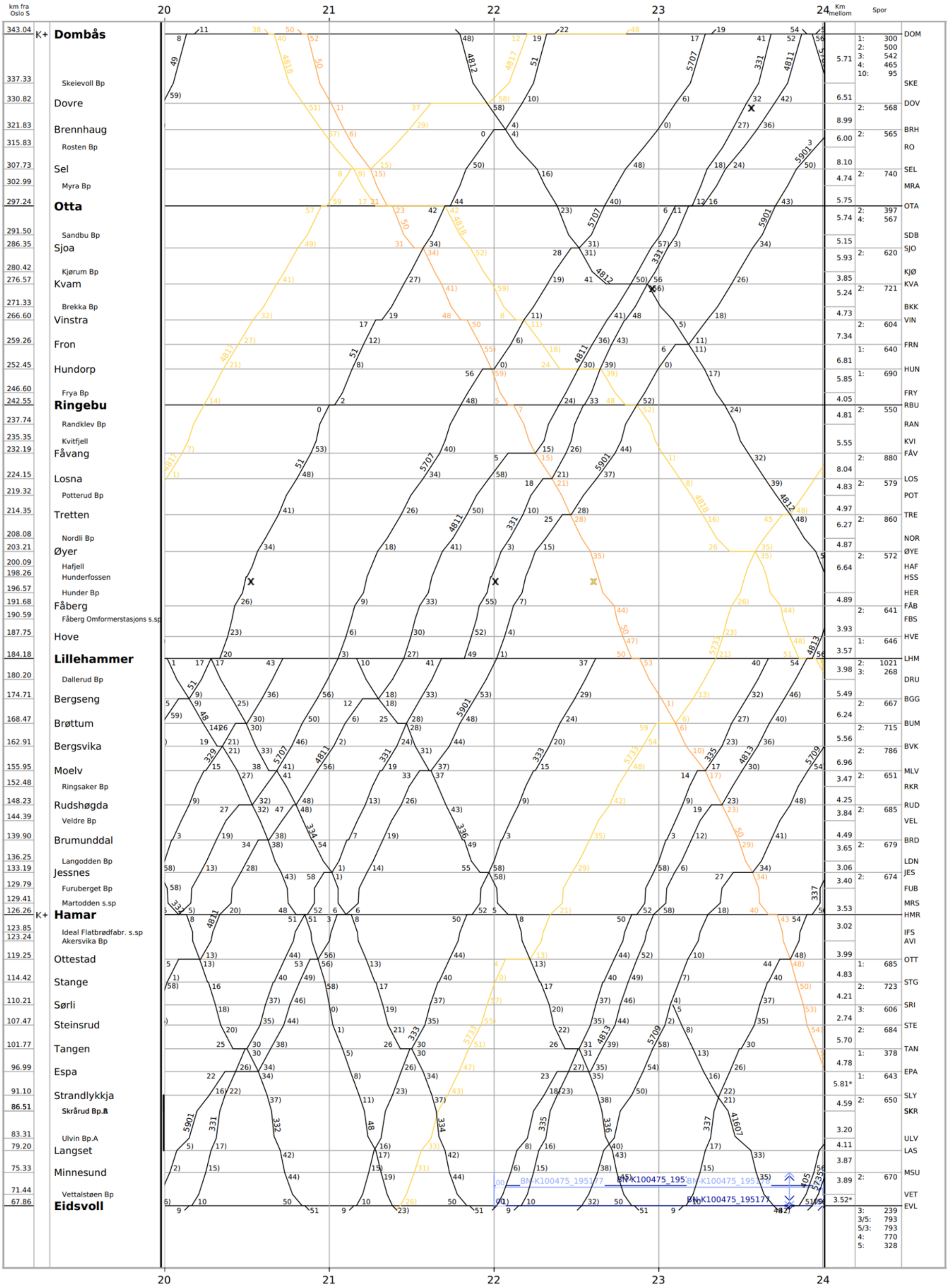

BANE NOR

Ruteplanperiode R22
BLAD NR. 10, EIDSVOLL - DOMBÅS

søndag 12.12.2021 - lørdag 10.12.2022
fredag, 25. feb. 2022

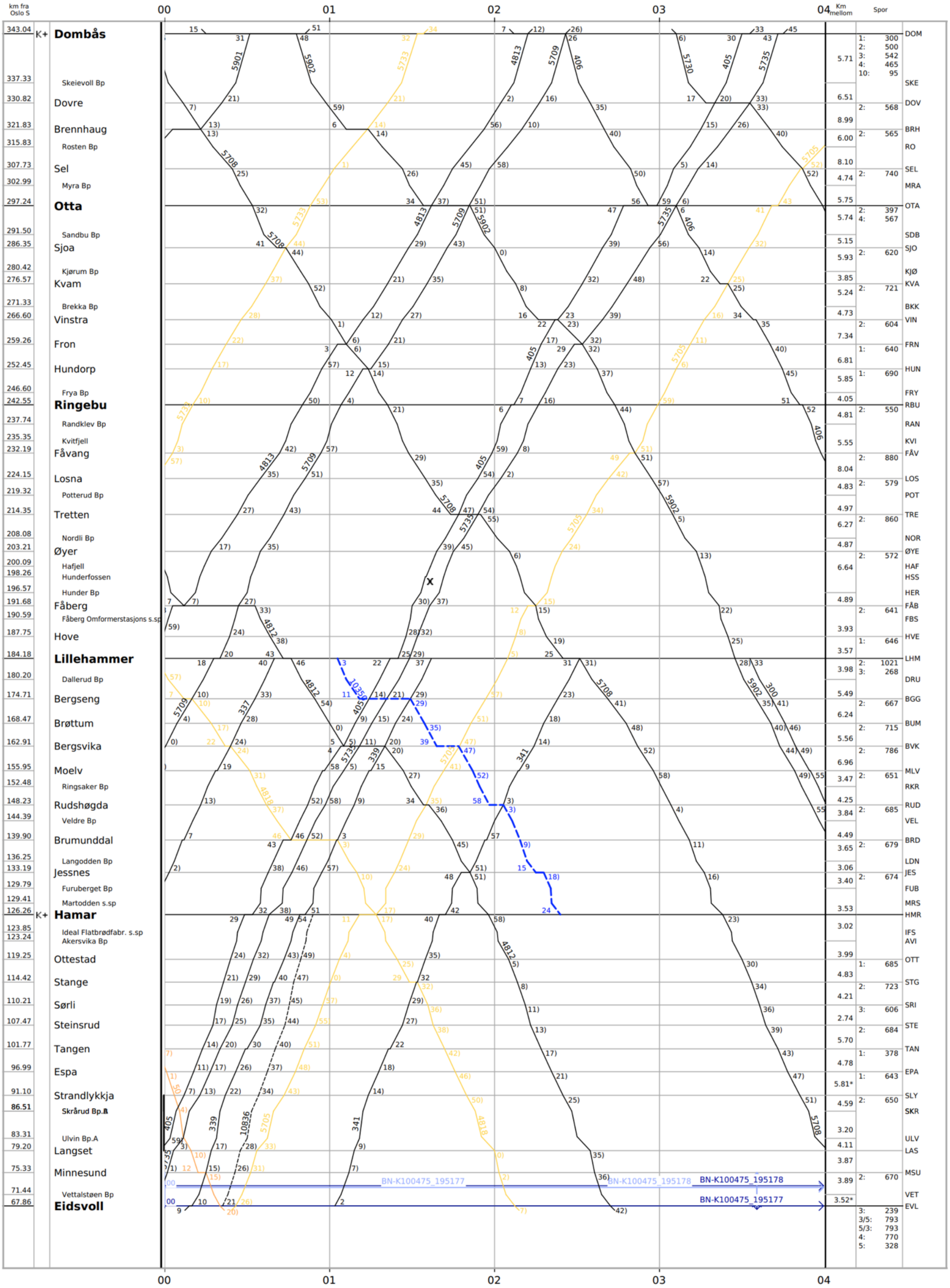

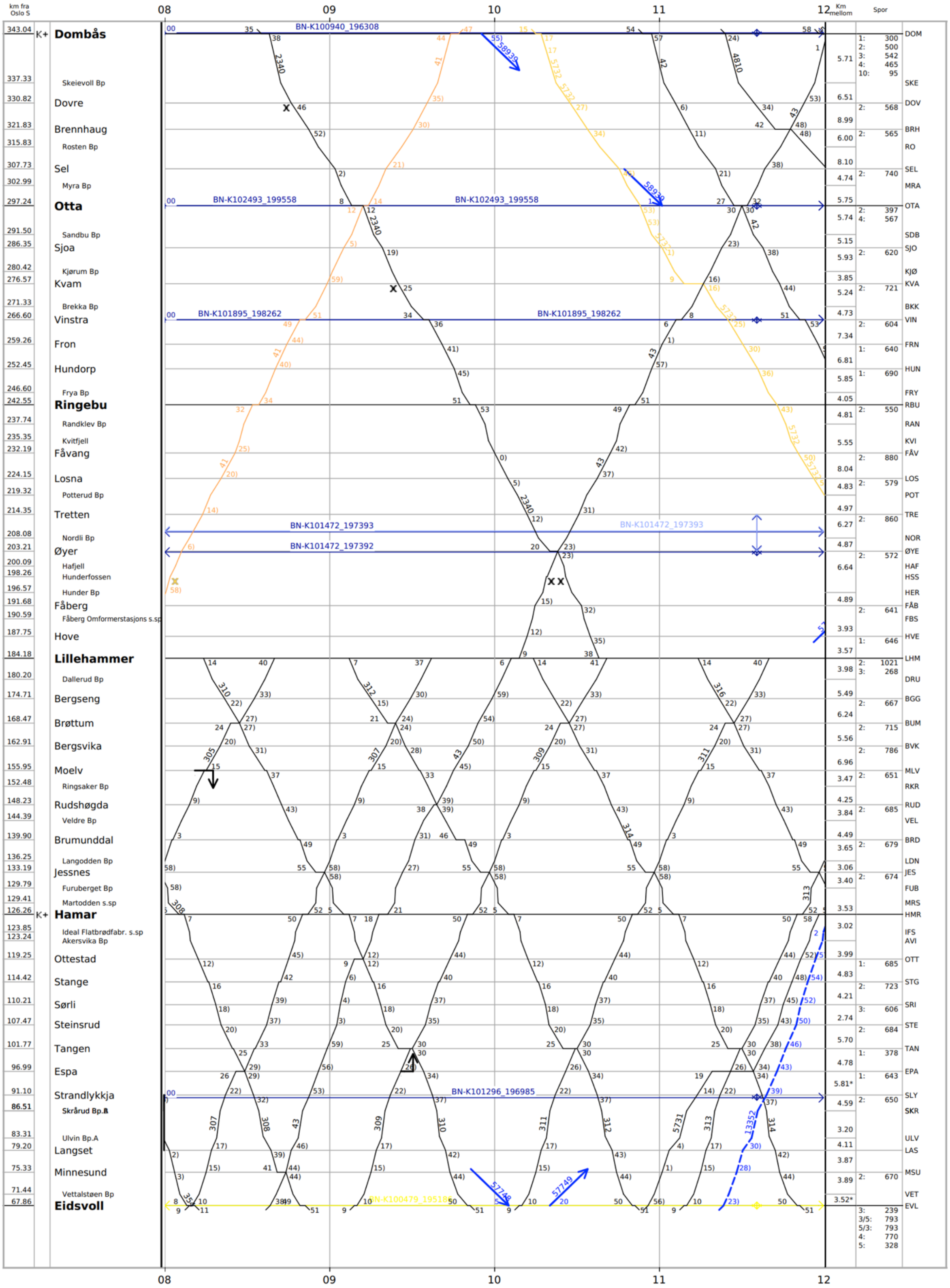
km fra Oslo S
08
09
10
11
12
Km mellom
Spor
343.04 K+ Dombås DOM
337.33 Skeievoll Bp SKE
330.82 Dovre DOV
321.83 Brennhaug BRH
315.83 Rosten Bp RO
307.73 Sel SEL
302.99 Myra Bp MRA
297.24 Otta OTA
291.50 Sandbu Bp SDB
286.35 Sjoa SJO
280.42 Kjørum Bp KJØ
276.57 Kvam KVA
271.33 Brekka Bp BKK
266.60 Vinstra VIN
259.26 Fron FRN
252.45 Hundorp HUN
246.60 Frya Bp FRY
242.55 Ringebu RBU
237.74 Randklev Bp RAN
235.35 Kvitfjell KVI
232.19 Fåvang FÅV
224.15 Losna LOS
219.32 Potterud Bp POT
214.35 Tretten TRE
208.08 Nordli Bp NOR
203.21 Øyer ØYE
200.09 Hafjell HAF
198.26 Hunderfossen HSS
196.57 Hunder Bp HER
191.68 Fåberg FÅB
190.59 Fåberg Omformerstasjons s.sp FBS
187.75 Hove HVE
184.18 Lillehammer LHM
180.20 Dallerud Bp DRU
174.71 Bergseng BGG
168.47 Brøttum BUM
162.91 Bergsvika BVK
155.95 Moelv MLV
152.48 Ringsaker Bp RKR
148.23 Rudshøgda RUD
144.39 Veldre Bp VEL
139.90 Brumunddal BRD
136.25 Langodden Bp LDN
133.19 Jessnes JES
129.79 Furuberget Bp FUB
129.41 Martodden s.sp MRS
126.26 K+ Hamar HMR
123.85 Ideal Flatbrødfabr. s.sp IFS
123.24 Akersvika Bp AVI
119.25 Ottestad OTT
114.42 Stange STG
110.21 Sørli SRI
107.47 Steinsrud STE
101.77 Tangen TAN
96.99 Espa EPA
91.10 Strandlykkja SLY
86.51 Skrårud Bp.A SKR
83.31 Ulvin Bp.A ULV
79.20 Langset LAS
75.33 Minnesund MSU
71.44 Vettalstøen Bp VET
67.86 Eidsvoll EVL
5.71 1: 300 2: 500 3: 542 4: 465 10: 95
6.51 2: 568
8.99
6.00 2: 565
8.10
4.74 2: 740
5.75
5.74 2: 397 4: 567
5.15
5.93 2: 620
3.85
5.24 2: 721
4.73
7.34 2: 604
6.81 1: 640
5.85 1: 690
4.05
4.81 2: 550
5.55
8.04 2: 880
4.83 2: 579
4.97
6.27 2: 860
4.87
6.64 2: 572
4.89 2: 641
3.93 1: 646
3.57
3.98 2: 1021 3: 268
5.49
6.24 2: 667
5.56 2: 715
6.96 2: 786
3.47 2: 651
4.25
3.84 2: 685
4.49
3.65 2: 679
3.06
3.40 2: 674
3.53
3.02
3.99 1: 685
4.83 2: 723
4.21 3: 606
2.74 2: 684
5.70 1: 378
4.78 1: 643
5.81*
4.59 2: 650
3.20
4.11
3.87
3.89 2: 670
3.52* 3: 239 3/5: 793 5/3: 793 4: 770 5: 328
BN-K100940_196308
BN-K102493_199558
BN-K101895_198262
BN-K101472_197393
BN-K101472_197392
BN-K101296_196985
BN-K100479_195186
2340
4810
5732
5893
42
43
41
305
306
307
308
309
310
311
312
313
314
316
5731
13352
57749

BANE NOR

Ruteplanperiode R22
BLAD NR. 10, EIDSVOLL - DOMBÅS

søndag 12.12.2021 - lørdag 10.12.2022
fredag, 25. feb. 2022

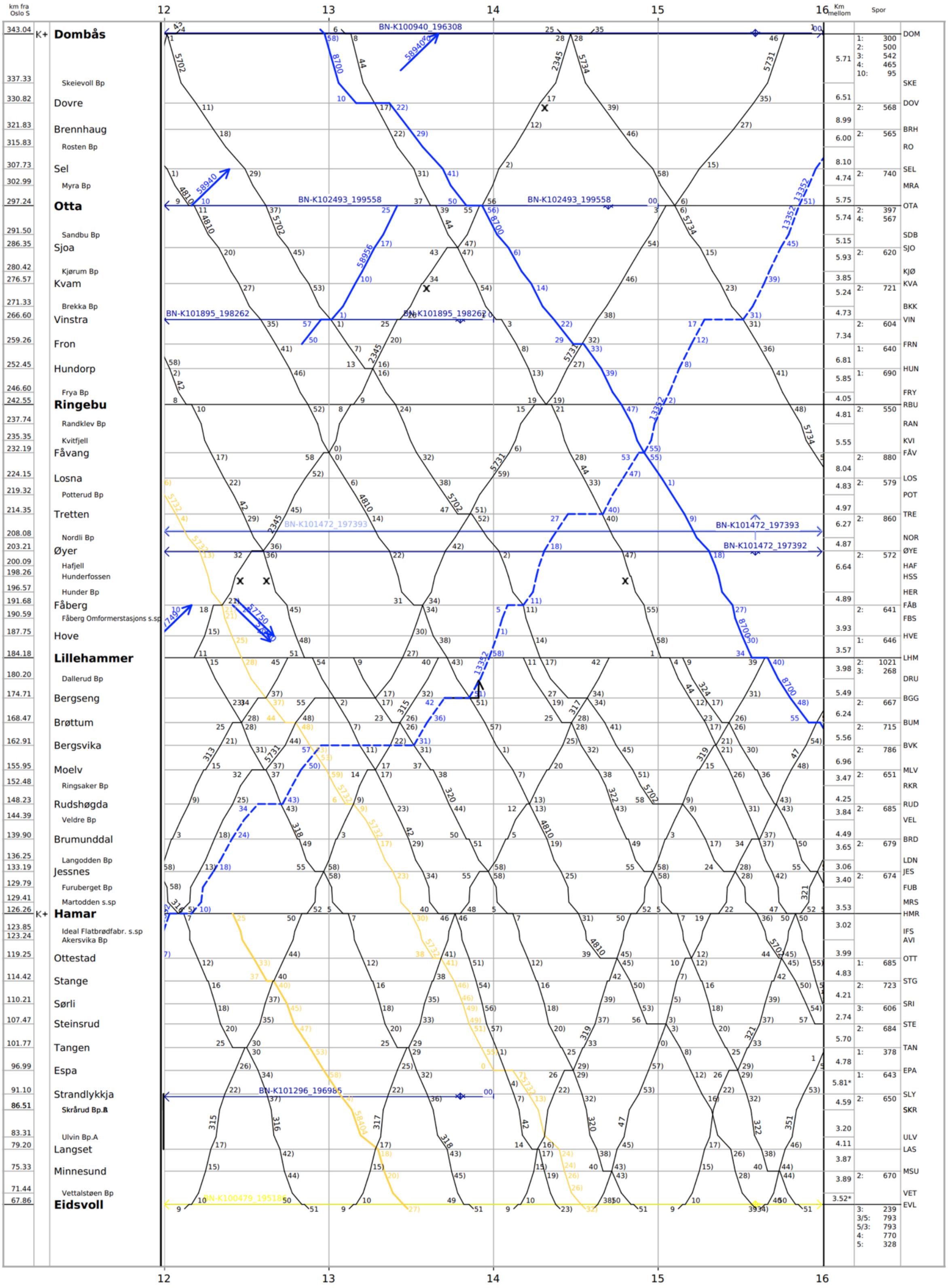

Ruteplanperiode R22
BLAD NR. 10, EIDSVOLL - DOMBÅS

søndag 12.12.2021 - lørdag 10.12.2022
fredag, 25. feb. 2022

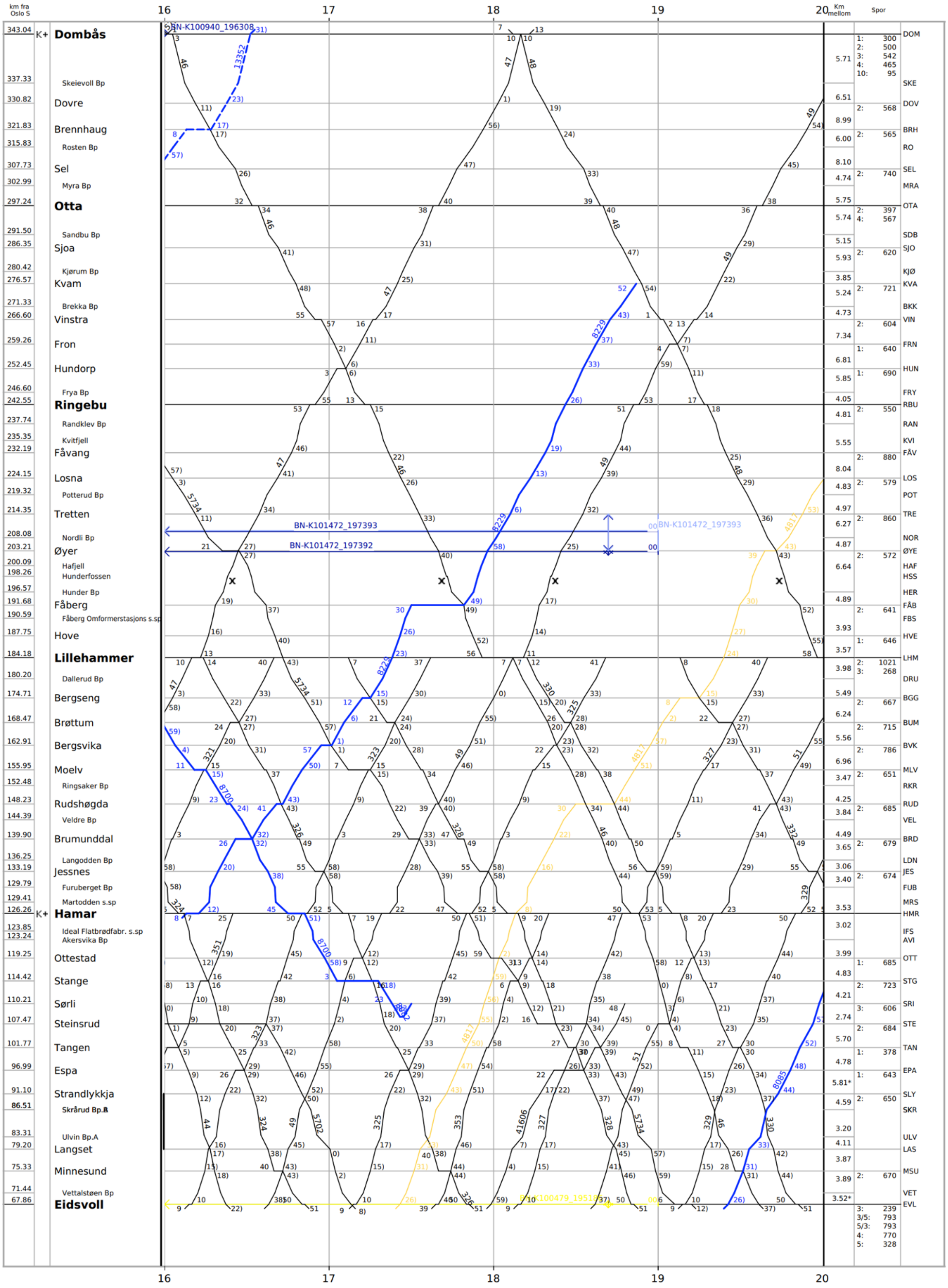

BANE NOR

Ruteplanperiode R22
BLAD NR. 10, EIDSVOLL - DOMBÅS

søndag 12.12.2021 - lørdag 10.12.2022
fredag, 25. feb. 2022

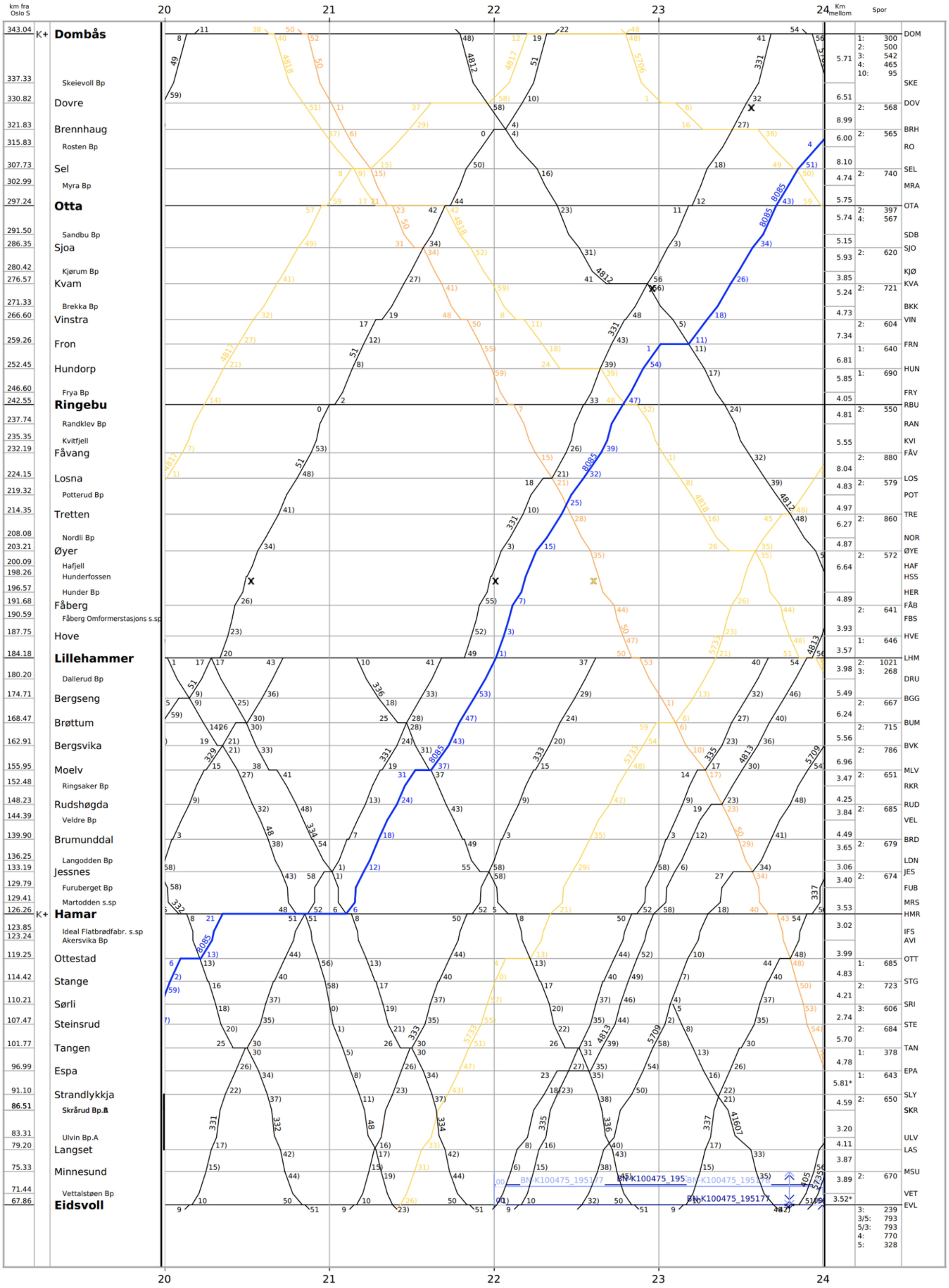

BANE NOR

Ruteplanperiode R22
BLAD NR. 10, EIDSVOLL - DOMBÅS

søndag 12.12.2021 - lørdag 10.12.2022
onsdag, 2. mar. 2022

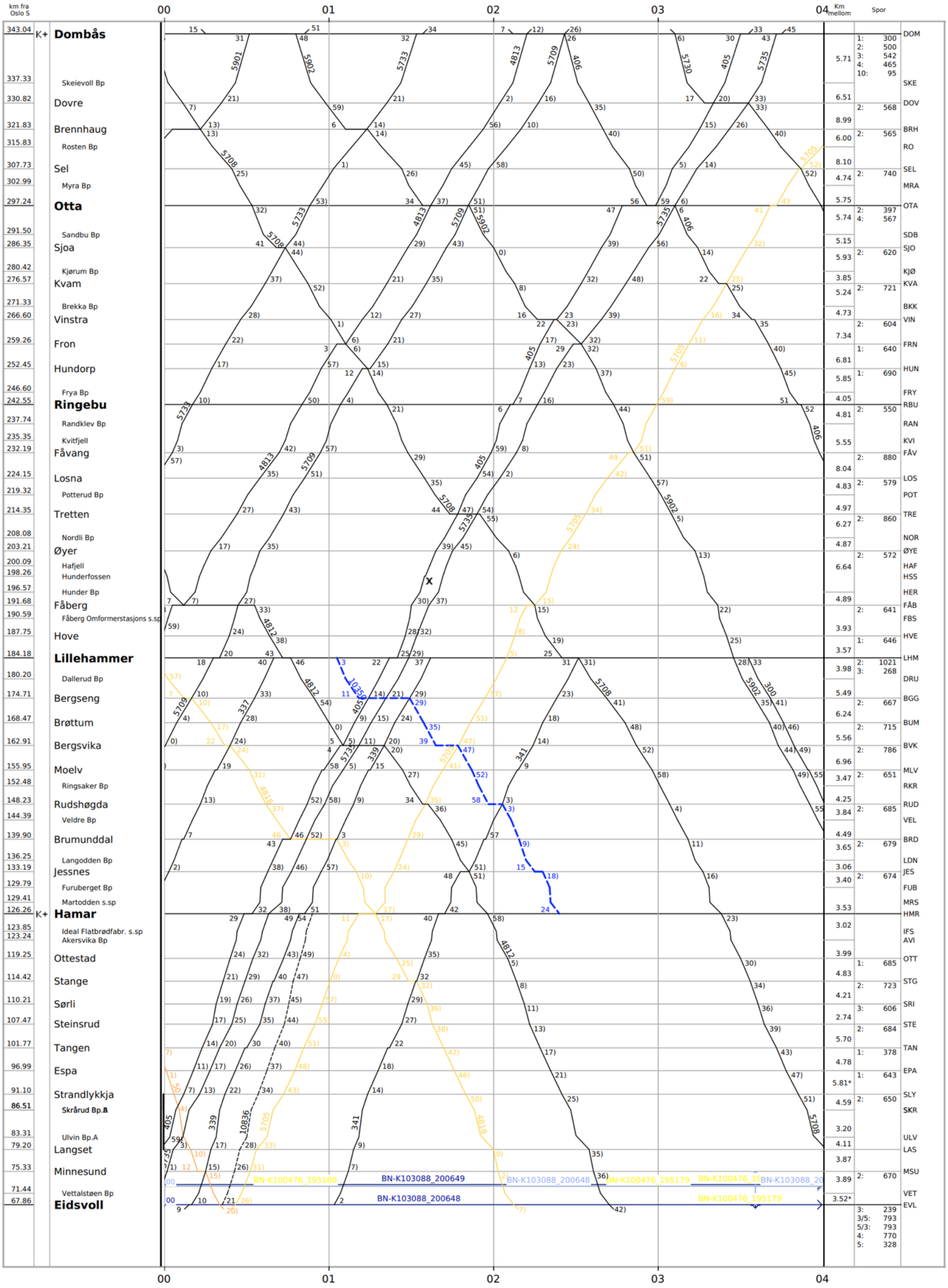

BANE NOR

Ruteplanperiode R22
BLAD NR. 10, EIDSVOLL - DOMBÅS

søndag 12.12.2021 - lørdag 10.12.2022
onsdag, 2. mar. 2022

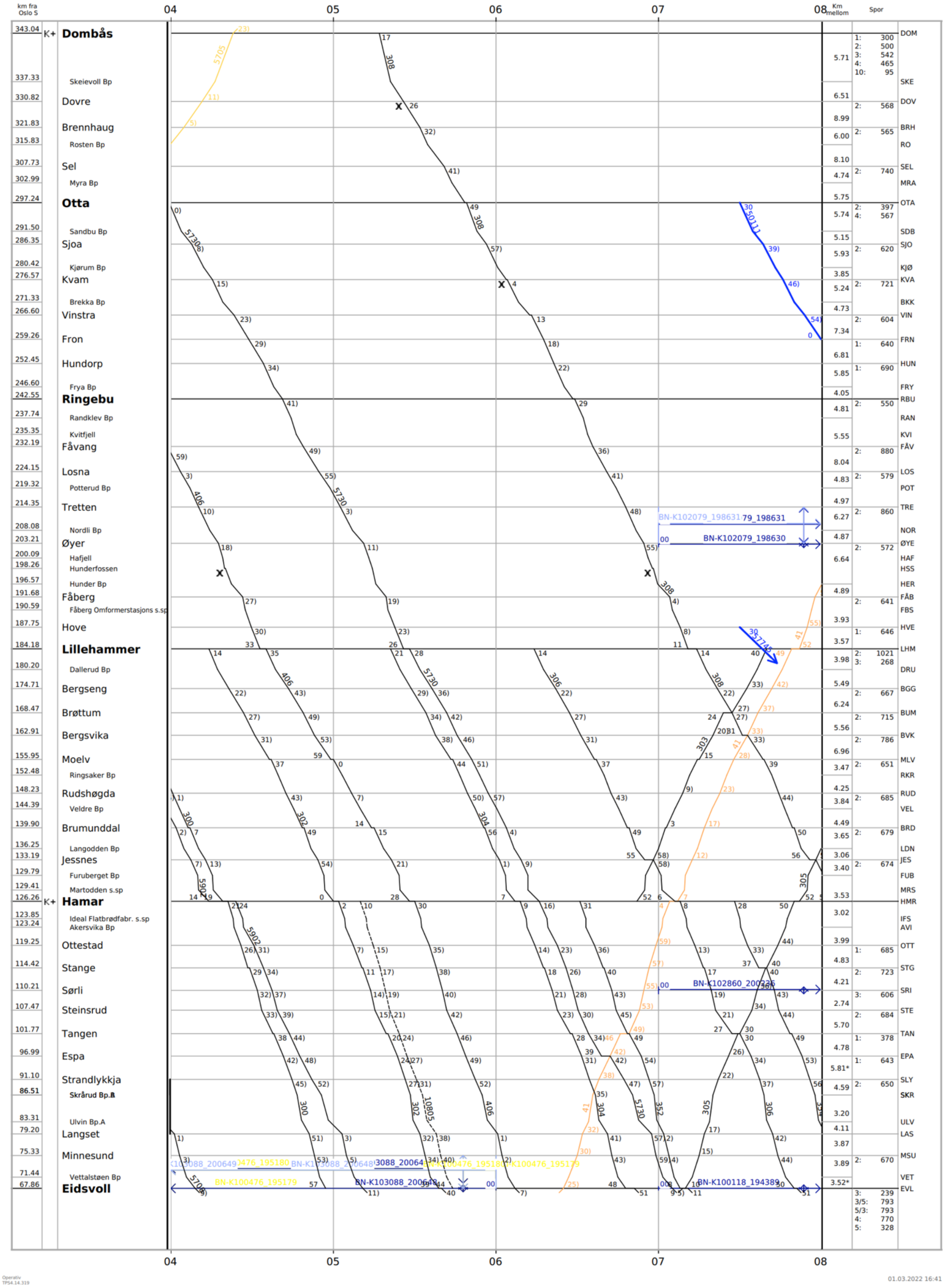

Operativ
TPS4.14.319

01.03.2022 16:41

Ruteplanperiode R22
BLAD NR. 10, EIDSVOLL - DOMBÅS

søndag 12.12.2021 - lørdag 10.12.2022
onsdag, 2. mar. 2022

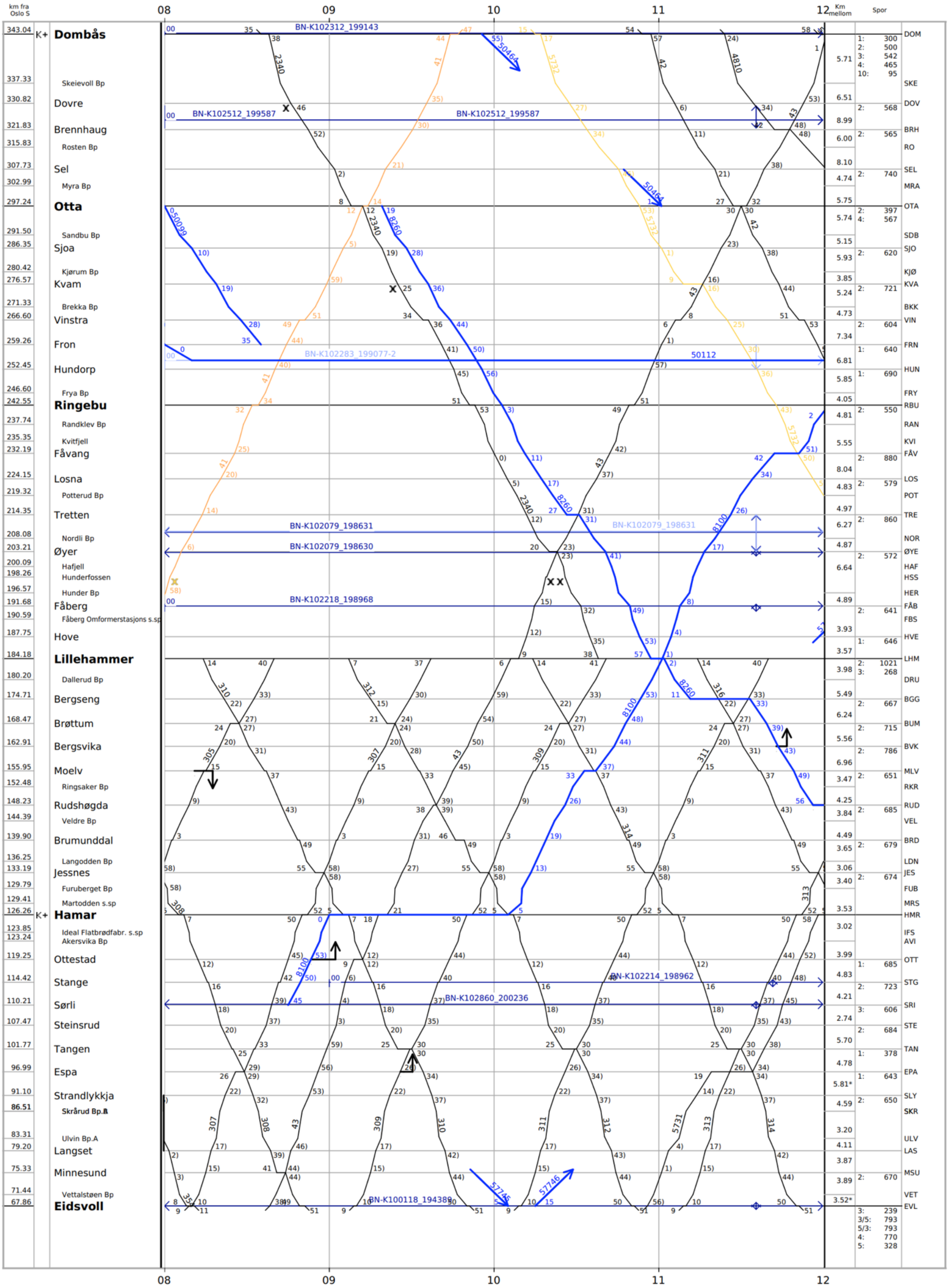

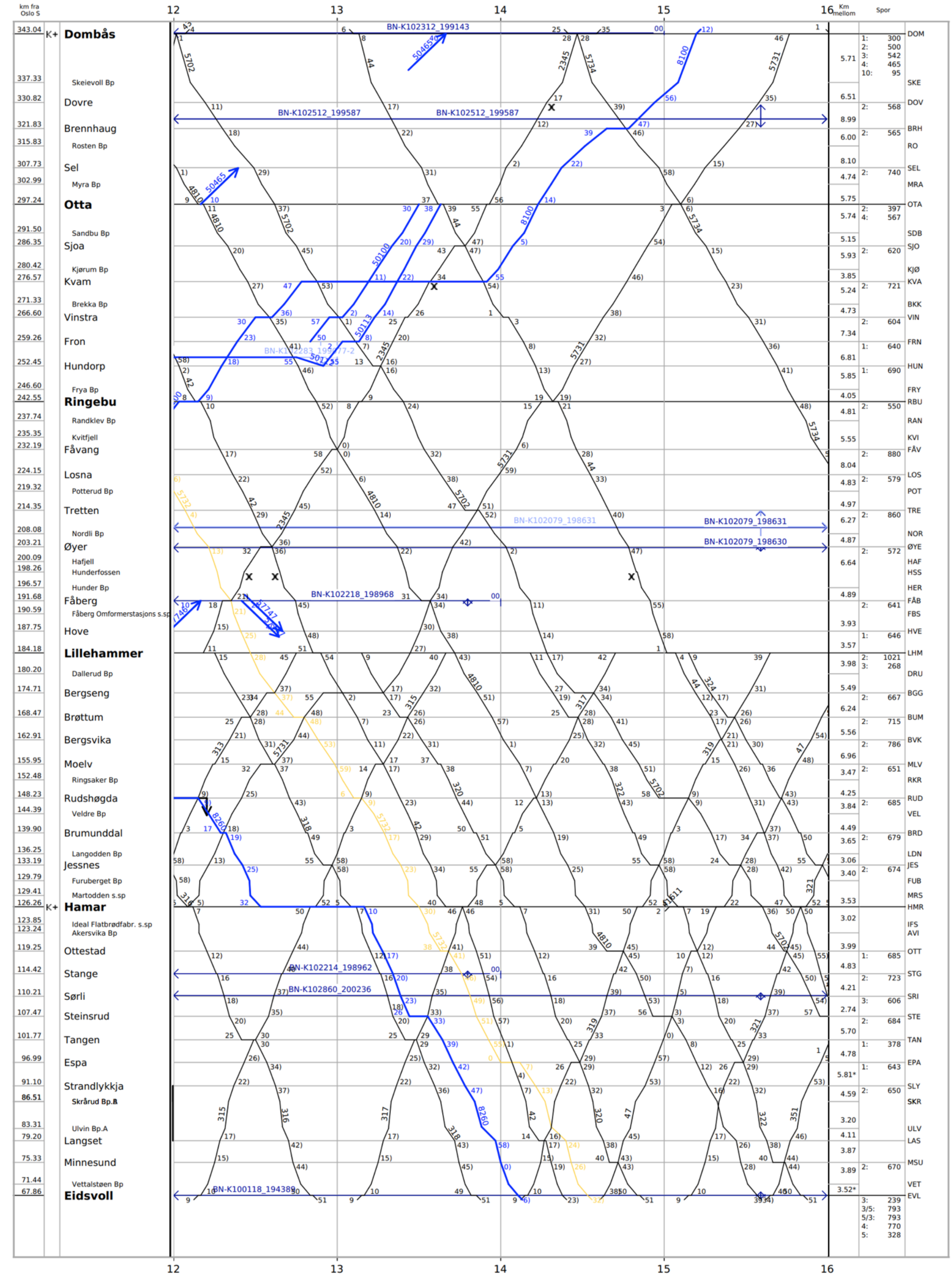
km fra Oslo S
12
13
14
15
16
Km mellom
Spor
343.04 K+ Dombås DOM
337.33 Skeievoll Bp SKE
330.82 Dovre DOV
321.83 Brennhaug BRH
315.83 Rosten Bp RO
307.73 Sel SEL
302.99 Myra Bp MRA
297.24 Otta OTA
291.50 Sandbu Bp SDB
286.35 Sjoa SJO
280.42 Kjørum Bp KJØ
276.57 Kvam KVA
271.33 Brekka Bp BKK
266.60 Vinstra VIN
259.26 Fron FRN
252.45 Hundorp HUN
246.60 Frya Bp FRY
242.55 Ringebu RBU
237.74 Randklev Bp RAN
235.35 Kvitfjell KVI
232.19 Fåvang FÅV
224.15 Losna LOS
219.32 Potterud Bp POT
214.35 Tretten TRE
208.08 Nordli Bp NOR
203.21 Øyer ØYE
200.09 Hafjell HAF
198.26 Hunderfossen HSS
196.57 Hunder Bp HER
191.68 Fåberg FÅB
190.59 Fåberg Omformerstasjons s.sp FBS
187.75 Hove HVE
184.18 Lillehammer LHM
180.20 Dallerud Bp DRU
174.71 Bergseng BGG
168.47 Brøttum BUM
162.91 Bergsvika BVK
155.95 Moelv MLV
152.48 Ringsaker Bp RKR
148.23 Rudshøgda RUD
144.39 Veldre Bp VEL
139.90 Brumunddal BRD
136.25 Langodden Bp LDN
133.19 Jessnes JES
129.79 Furuberget Bp FUB
129.41 Martodden s.sp MRS
126.26 K+ Hamar HMR
123.85 Ideal Flatbrødfabr. s.sp IFS
123.24 Akersvika Bp AVI
119.25 Ottestad OTT
114.42 Stange STG
110.21 Sørli SRI
107.47 Steinsrud STE
101.77 Tangen TAN
96.99 Espa EPA
91.10 Strandlykkja SLY
86.51 Skrårud Bp.B SKR
83.31 Ulvin Bp.A ULV
79.20 Langset LAS
75.33 Minnesund MSU
71.44 Vettalstøen Bp VET
67.86 Eidsvoll EVL
BN-K102312_199143
BN-K102512_199587
BN-K102079_198631
BN-K102079_198630
BN-K102218_198968
BN-K102214_198962
BN-K102860_200236
BN-K100118_194389
5702
44
2345
5734
8100
5731
4810
50465
50100
50113
8260
7747
318
320
322

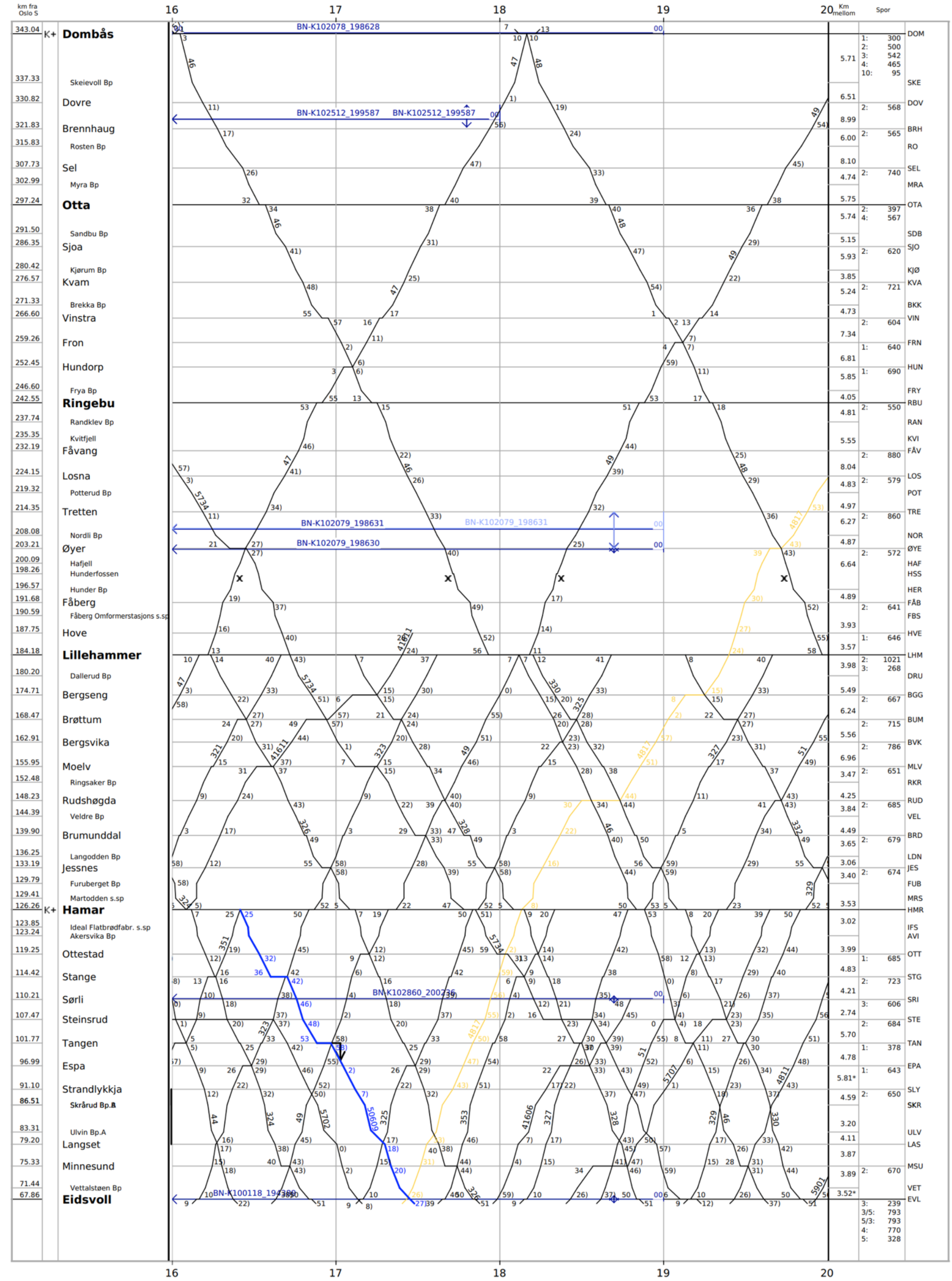
km fra Oslo S
16
17
18
19
20
Km mellom
Spor
343.04 K+ Dombås
337.33 Skeievoll Bp
330.82 Dovre
321.83 Brennhaug
315.83 Rosten Bp
307.73 Sel
302.99 Myra Bp
297.24 Otta
291.50 Sandbu Bp
286.35 Sjoa
280.42 Kjørum Bp
276.57 Kvam
271.33 Brekka Bp
266.60 Vinstra
259.26 Fron
252.45 Hundorp
246.60 Frya Bp
242.55 Ringebu
237.74 Randklev Bp
235.35 Kvitfjell
232.19 Fåvang
224.15 Losna
219.32 Potterud Bp
214.35 Tretten
208.08 Nordli Bp
203.21 Øyer
200.09 Hafjell
198.26 Hunderfossen
196.57 Hunder Bp
191.68 Fåberg
190.59 Fåberg Omformerstasjons s.sp
187.75 Hove
184.18 Lillehammer
180.20 Dallerud Bp
174.71 Bergseng
168.47 Brøttum
162.91 Bergsvika
155.95 Moelv
152.48 Ringsaker Bp
148.23 Rudshøgda
144.39 Veldre Bp
139.90 Brumunddal
136.25 Langodden Bp
133.19 Jessnes
129.79 Furuberget Bp
129.41 Martodden s.sp
126.26 K+ Hamar
123.85 Ideal Flatbrødfabr. s.sp
123.24 Akersvika Bp
119.25 Ottestad
114.42 Stange
110.21 Sørli
107.47 Steinsrud
101.77 Tangen
96.99 Espa
91.10 Strandlykkja
86.51 Skråurd Bp.A
83.31 Ulvin Bp.A
79.20 Langset
75.33 Minnesund
71.44 Vettalstøen Bp
67.86 Eidsvoll
BN-K102078_198628
BN-K102512_199587
BN-K102512_199587
BN-K102079_198631
BN-K102079_198631
BN-K102079_198630
BN-K102860_200236
BN-K100118_194380
5.71 6.51 8.99 6.00 8.10 4.74 5.75 5.74 5.15 5.93 3.85 5.24 4.73 7.34 6.81 5.85 4.05 4.81 5.55 8.04 4.83 4.97 6.27 4.87 6.64 4.89 3.93 3.57 3.98 5.49 6.24 5.56 6.96 3.47 4.25 3.84 4.49 3.65 3.06 3.40 3.53 3.02 3.99 4.83 4.21 2.74 5.70 4.78 5.81* 4.59 3.20 4.11 3.87 3.89 3.52*
DOM 1: 300 2: 500 3: 542 4: 465 10: 95
SKE
DOV 2: 568
BRH 2: 565
RO
SEL 2: 740
MRA
OTA 2: 397 4: 567
SDB
SJO 2: 620
KJØ
KVA 2: 721
BKK
VIN 2: 604
FRN 1: 640
HUN 1: 690
FRY
RBU 2: 550
RAN
KVI
FÅV 2: 880
LOS 2: 579
POT
TRE 2: 860
NOR
ØYE 2: 572
HAF
HSS
HER
FÅB 2: 641
FBS
HVE 1: 646
LHM 2: 1021 3: 268
DRU
BGG 2: 667
BUM 2: 715
BVK 2: 786
MLV 2: 651
RKR
RUD 2: 685
VEL
BRD 2: 679
LDN
JES 2: 674
FUB
MRS
HMR
IFS
AVI
OTT 1: 685
STG 2: 723
SRI 3: 606
STE 2: 684
TAN 1: 378
EPA 1: 643
SLY 2: 650
SKR
ULV
LAS
MSU 2: 670
VET
EVL 3: 239 3/5: 793 5/3: 793 4: 770 5: 328

BANE NOR

Ruteplanperiode R22
BLAD NR. 10, EIDSVOLL - DOMBÅS

søndag 12.12.2021 - lørdag 10.12.2022
torsdag, 3. mar. 2022

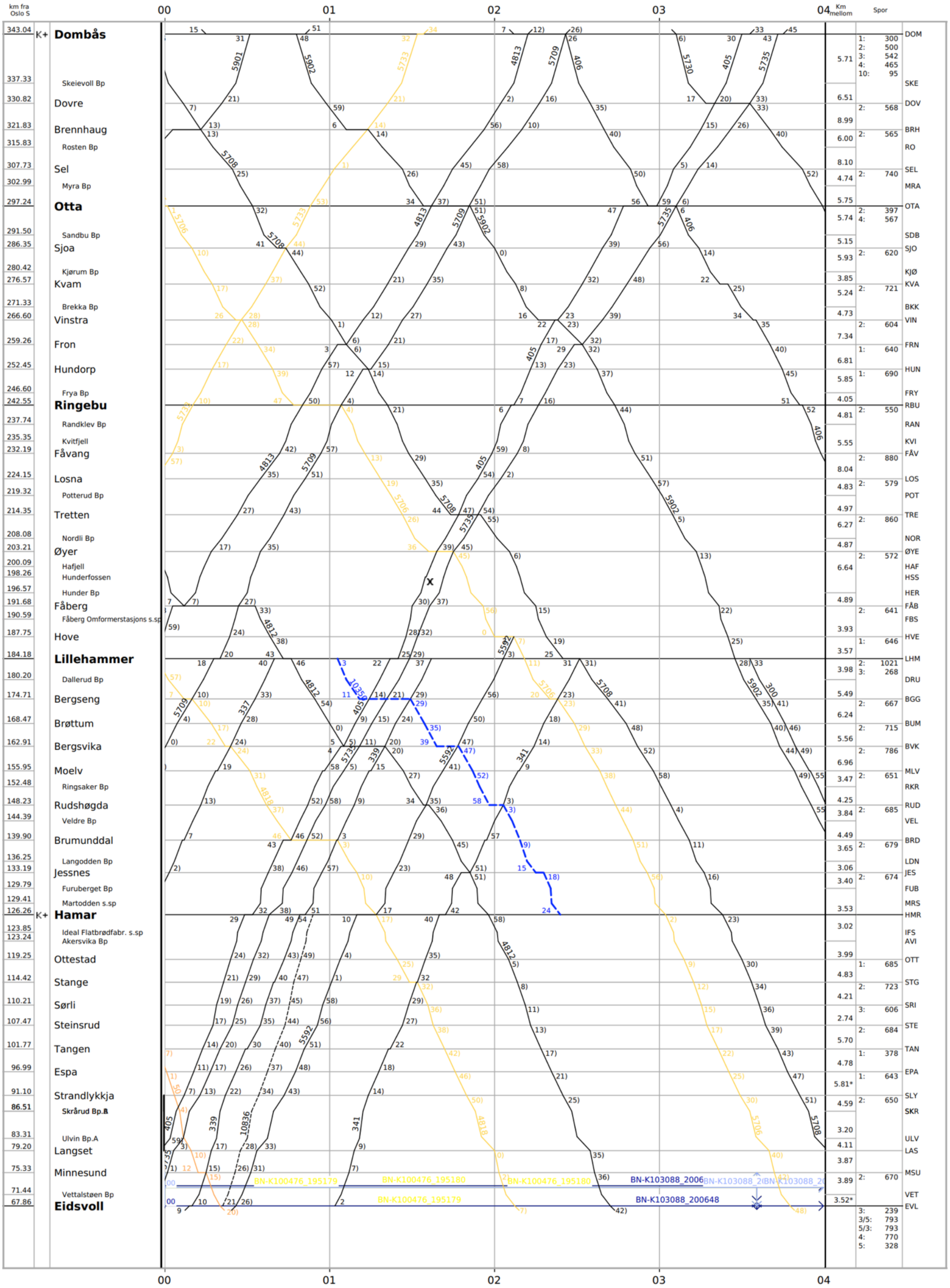

BANE NOR

Ruteplanperiode R22
BLAD NR. 10, EIDSVOLL - DOMBÅS

søndag 12.12.2021 - lørdag 10.12.2022
torsdag, 3. mar. 2022

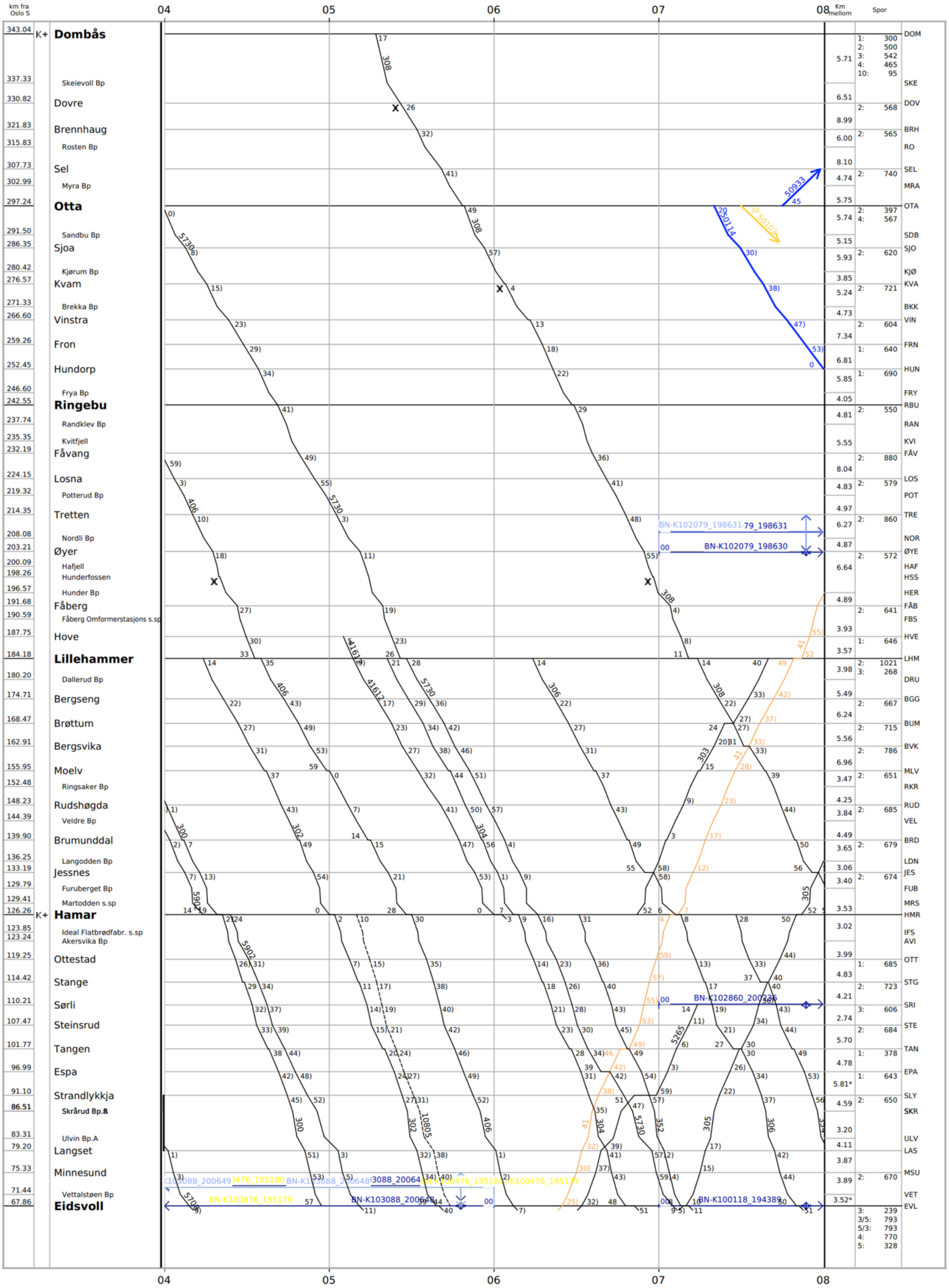

Operativ
TPS4.14.319

02.03.2022 16:41

Ruteplanperiode R22
BLAD NR. 10, EIDSVOLL - DOMBÅS

søndag 12.12.2021 - lørdag 10.12.2022
torsdag, 3. mar. 2022

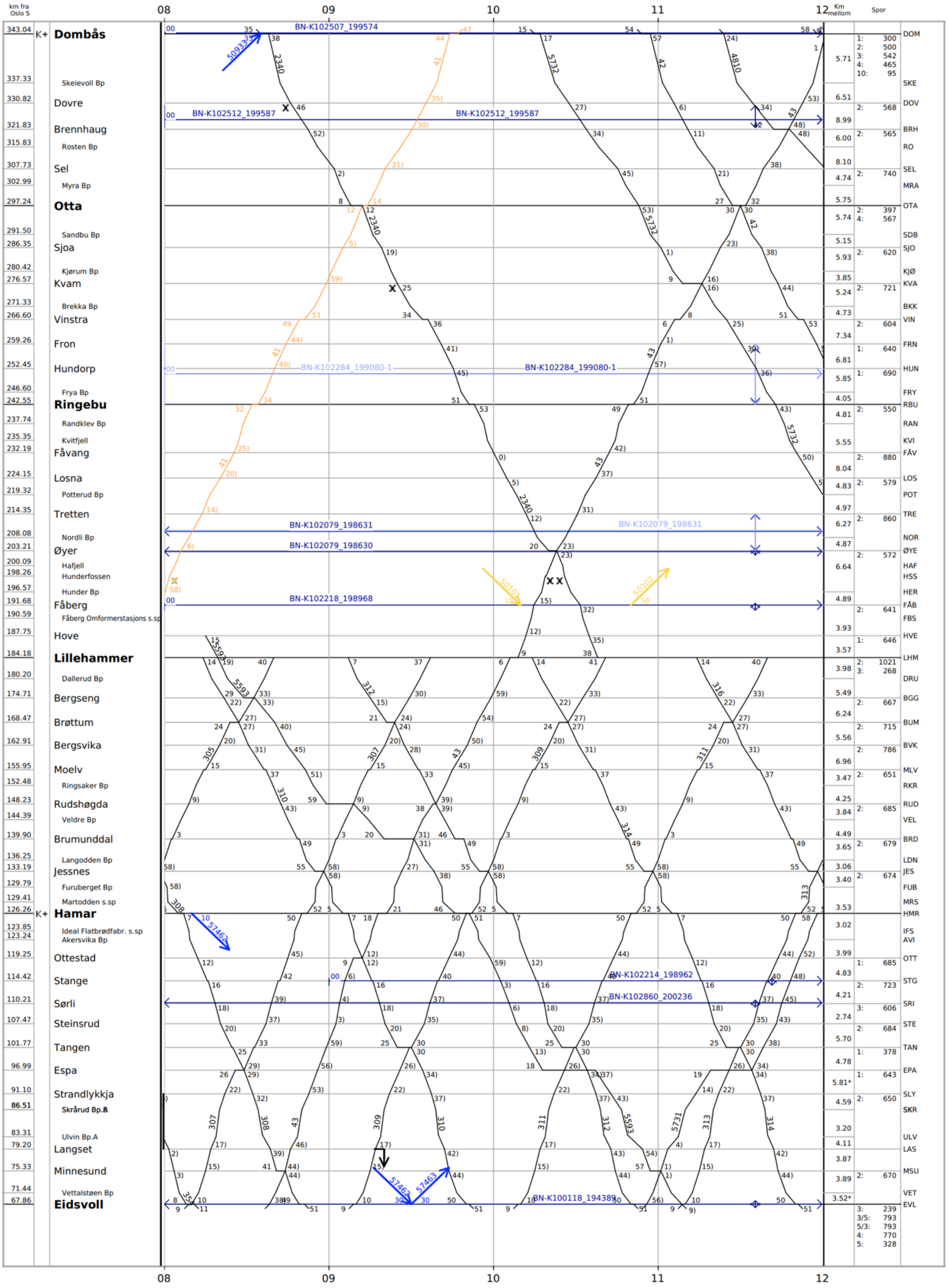

08 09 10 11 12

BANE NOR

Ruteplanperiode R22
BLAD NR. 10, EIDSVOLL - DOMBÅS

søndag 12.12.2021 - lørdag 10.12.2022
torsdag, 3. mar. 2022

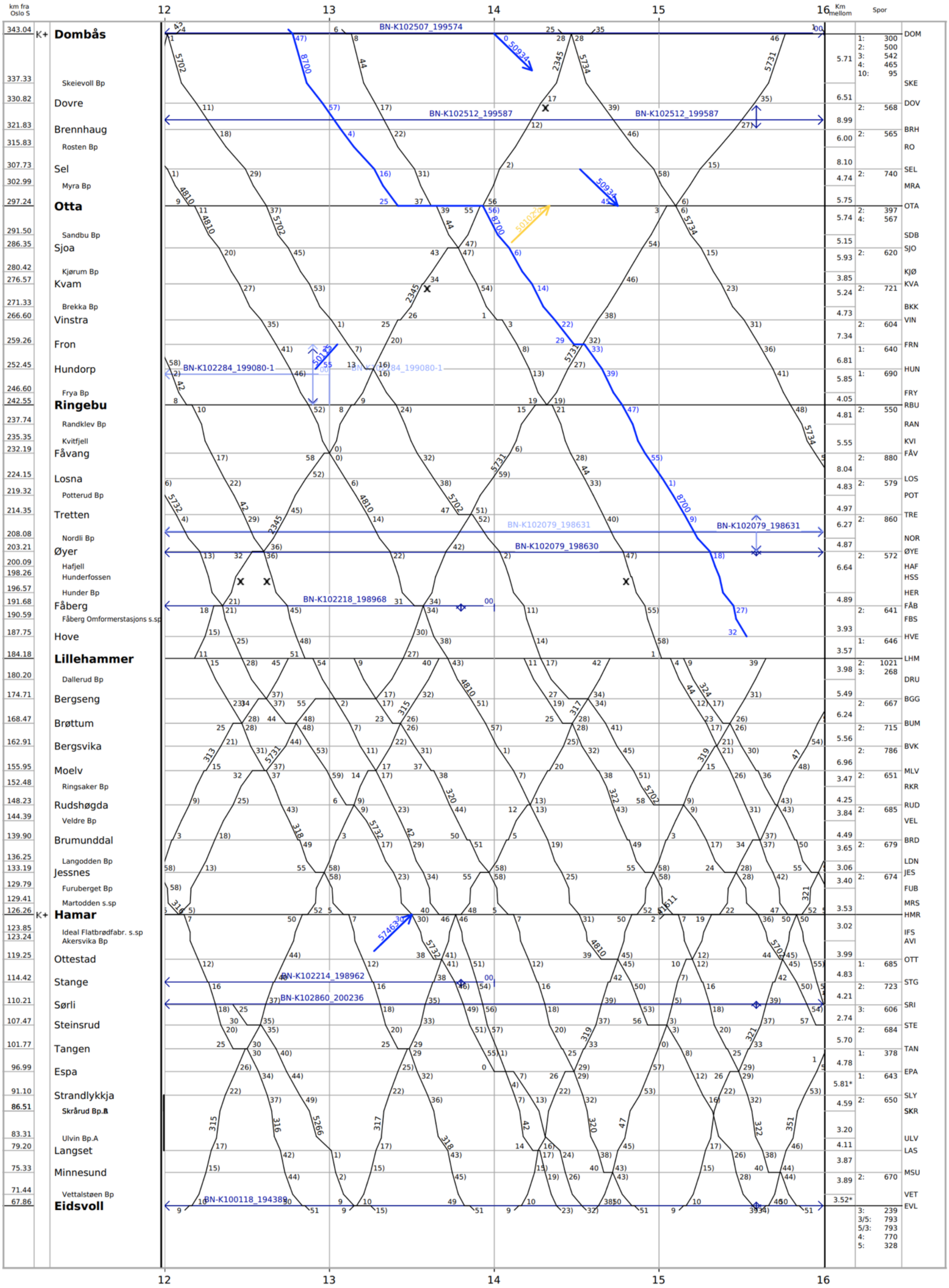

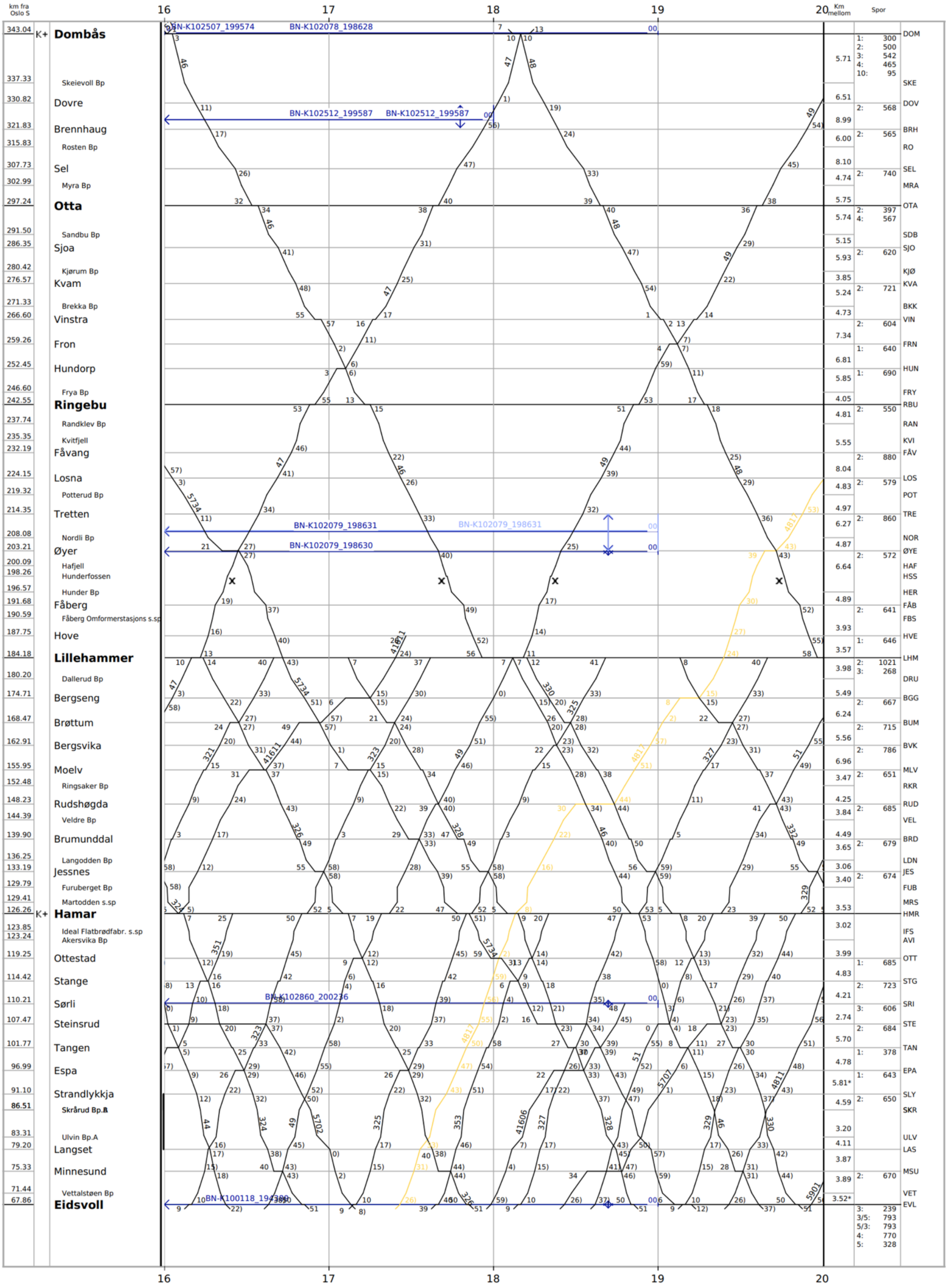
km fra Oslo S
16
17
18
19
20
Km mellom
Spor
343.04 K+ Dombås 5.71 1: 300 2: 500 3: 542 4: 465 10: 95 DOM
337.33 Skeievoll Bp 6.51 SKE
330.82 Dovre 8.99 2: 568 DOV
321.83 Brennhaug 6.00 2: 565 BRH
315.83 Rosten Bp 8.10 RO
307.73 Sel 4.74 2: 740 SEL
302.99 Myra Bp 5.75 MRA
297.24 Otta 5.74 2: 397 4: 567 OTA
291.50 Sandbu Bp 5.15 SDB
286.35 Sjoa 5.93 2: 620 SJO
280.42 Kjørum Bp 3.85 KJØ
276.57 Kvam 5.24 2: 721 KVA
271.33 Brekka Bp 4.73 BKK
266.60 Vinstra 7.34 2: 604 VIN
259.26 Fron 6.81 1: 640 FRN
252.45 Hundorp 5.85 1: 690 HUN
246.60 Frya Bp 4.05 FRY
242.55 Ringebu 4.81 2: 550 RBU
237.74 Randklev Bp RAN
235.35 Kvitfjell 5.55 KVI
232.19 Fåvang 8.04 2: 880 FÅV
224.15 Losna 4.83 2: 579 LOS
219.32 Potterud Bp 4.97 POT
214.35 Tretten 6.27 2: 860 TRE
208.08 Nordli Bp 4.87 NOR
203.21 Øyer 6.64 2: 572 ØYE
200.09 Hafjell HAF
198.26 Hunderfossen HSS
196.57 Hunder Bp 4.89 HER
191.68 Fåberg 2: 641 FÅB
190.59 Fåberg Omformerstasjons s.sp FBS
187.75 Hove 3.93 1: 646 HVE
184.18 Lillehammer 3.57 2: 1021 3: 268 LHM
180.20 Dallerud Bp 3.98 DRU
174.71 Bergseng 5.49 2: 667 BGG
168.47 Brøttum 6.24 2: 715 BUM
162.91 Bergsvika 5.56 2: 786 BVK
155.95 Moelv 6.96 2: 651 MLV
152.48 Ringsaker Bp 3.47 RKR
148.23 Rudshøgda 4.25 2: 685 RUD
144.39 Veldre Bp 3.84 VEL
139.90 Brumunddal 4.49 2: 679 BRD
136.25 Langodden Bp 3.65 LDN
133.19 Jessnes 3.06 2: 674 JES
129.79 Furuberget Bp 3.40 FUB
129.41 Martodden s.sp MRS
126.26 K+ Hamar 3.53 HMR
123.85 Ideal Flatbrødfabr. s.sp 3.02 IFS
123.24 Akersvika Bp AVI
119.25 Ottestad 3.99 1: 685 OTT
114.42 Stange 4.83 2: 723 STG
110.21 Sørli 4.21 3: 606 SRI
107.47 Steinsrud 2.74 2: 684 STE
101.77 Tangen 5.70 1: 378 TAN
96.99 Espa 4.78 1: 643 EPA
91.10 Strandlykkja 5.81* SLY
86.51 Skrårud Bp.B 4.59 2: 650 SKR
83.31 Ulvin Bp.A 3.20 ULV
79.20 Langset 4.11 LAS
75.33 Minnesund 3.87 2: 670 MSU
71.44 Vettalstøen Bp 3.89 VET
67.86 Eidsvoll 3.52* 3: 239 3/5: 793 5/3: 793 4: 770 5: 328 EVL
BN-K102507_199574
BN-K102078_198628
BN-K102512_199587
BN-K102512_199587
BN-K102079_198631
BN-K102079_198631
BN-K102079_198630
BN-K102860_200236
BN-K100118_194380

BANE NOR

Ruteplanperiode R22
BLAD NR. 10, EIDSVOLL - DOMBÅS

søndag 12.12.2021 - lørdag 10.12.2022
torsdag, 3. mar. 2022

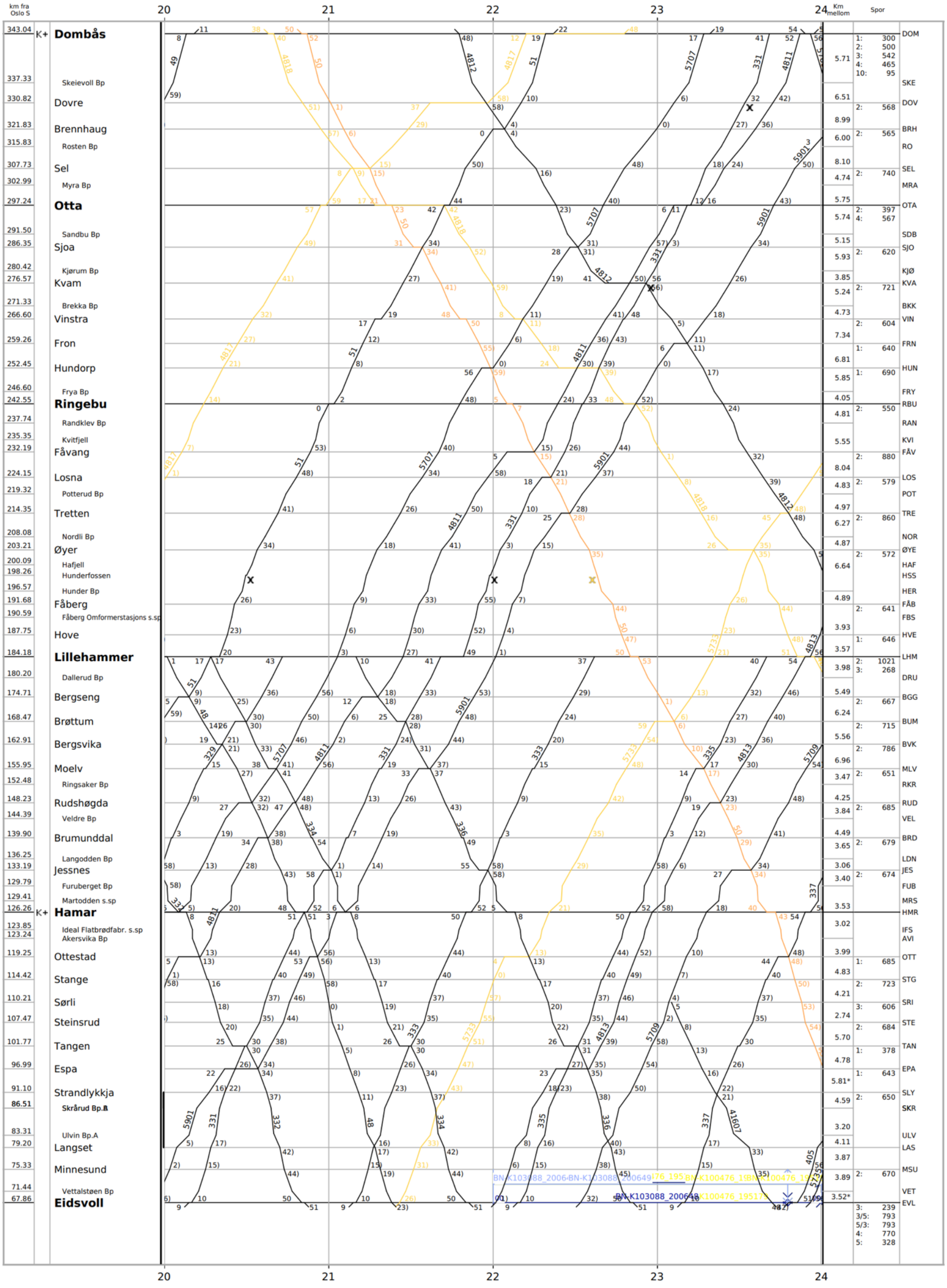

B NE NOR

Ruteplanperiode R22
BLAD NR. 10, EIDSVOLL - DOMBÅS

søndag 12.12.2021 - lørdag 10.12.2022
fredag, 4. mar. 2022

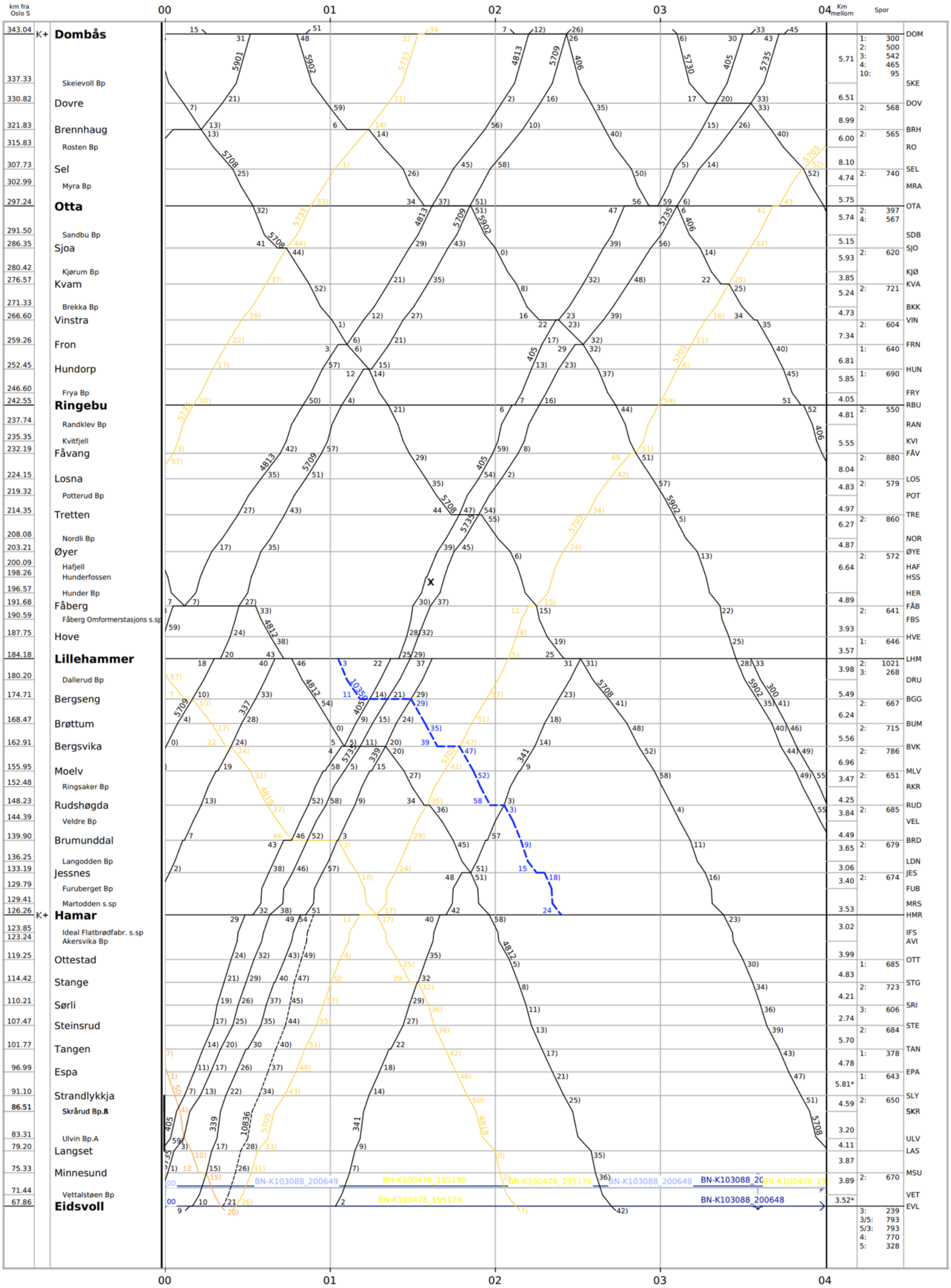

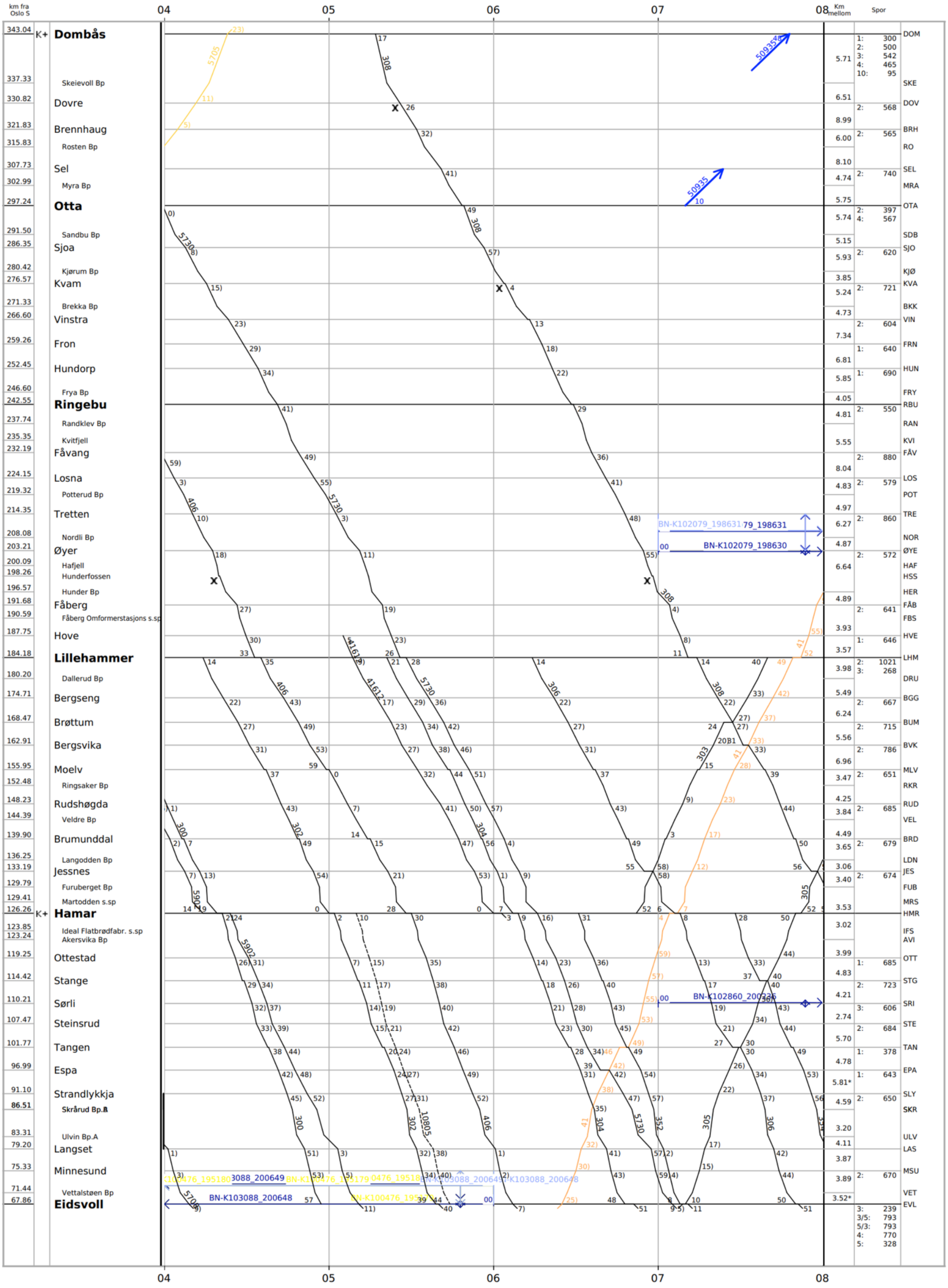
km fra Oslo S
04
05
06
07
08
Km mellom
Spor
343.04 K+ Dombås DOM
337.33 Skeievoll Bp SKE
330.82 Dovre DOV
321.83 Brennhaug BRH
315.83 Rosten Bp RO
307.73 Sel SEL
302.99 Myra Bp MRA
297.24 Otta OTA
291.50 Sandbu Bp SDB
286.35 Sjoa SJO
280.42 Kjørum Bp KJØ
276.57 Kvam KVA
271.33 Brekka Bp BKK
266.60 Vinstra VIN
259.26 Fron FRN
252.45 Hundorp HUN
246.60 Frya Bp FRY
242.55 Ringebu RBU
237.74 Randklev Bp RAN
235.35 Kvitfjell KVI
232.19 Fåvang FÅV
224.15 Losna LOS
219.32 Potterud Bp POT
214.35 Tretten TRE
208.08 Nordli Bp NOR
203.21 Øyer ØYE
200.09 Hafjell HAF
198.26 Hunderfossen HSS
196.57 Hunder Bp HER
191.68 Fåberg FÅB
190.59 Fåberg Omformerstasjons s.sp FBS
187.75 Hove HVE
184.18 Lillehammer LHM
180.20 Dallerud Bp DRU
174.71 Bergseng BGG
168.47 Brøttum BUM
162.91 Bergsvika BVK
155.95 Moelv MLV
152.48 Ringsaker Bp RKR
148.23 Rudshøgda RUD
144.39 Veldre Bp VEL
139.90 Brumunddal BRD
136.25 Langodden Bp LDN
133.19 Jessnes JES
129.79 Furuberget Bp FUB
129.41 Martodden s.sp MRS
126.26 K+ Hamar HMR
123.85 Ideal Flatbrødfabr. s.sp IFS
123.24 Akersvika Bp AVI
119.25 Ottestad OTT
114.42 Stange STG
110.21 Sørli SRI
107.47 Steinsrud STE
101.77 Tangen TAN
96.99 Espa EPA
91.10 Strandlykkja SLY
86.51 Skårud Bp.A SKR
83.31 Ulvin Bp.A ULV
79.20 Langset LAS
75.33 Minnesund MSU
71.44 Vettalstøen Bp VET
67.86 Eidsvoll EVL
5.71 1: 300 2: 500 3: 542 4: 465 10: 95
6.51 2: 568
8.99 2: 565
6.00
8.10 2: 740
4.74
5.75 2: 397 4: 567
5.74
5.15
5.93 2: 620
3.85
5.24 2: 721
4.73 2: 604
7.34 1: 640
6.81 1: 690
5.85
4.05
4.81 2: 550
5.55
2: 880
8.04
4.83 2: 579
4.97
6.27 2: 860
4.87
6.64 2: 572
4.89 2: 641
3.93 1: 646
3.57
3.98 2: 1021 3: 268
5.49 2: 667
6.24 2: 715
5.56 2: 786
6.96
3.47 2: 651
4.25
3.84 2: 685
4.49
3.65 2: 679
3.06
3.40 2: 674
3.53
3.02
3.99
4.83 1: 685
4.21 2: 723
2.74 3: 606
5.70 2: 684
4.78 1: 378
5.81* 1: 643
4.59 2: 650
3.20
4.11
3.87
3.89 2: 670
3.52*
3: 239 3/5: 793 5/3: 793 4: 770 5: 328
BN-K102079_198631
79_198631
BN-K102079_198630
BN-K102860_200236
BN-K103088_200648
BN-K103088_200649
BN-K100476_195188
BN-K100476_195179
BN-K100476_195180
50935
50935
5705
5730
308
406
416
5730
306
303
2081
302
300
304
5902
10805
406
5730
352
305
306
300
302
5706
305

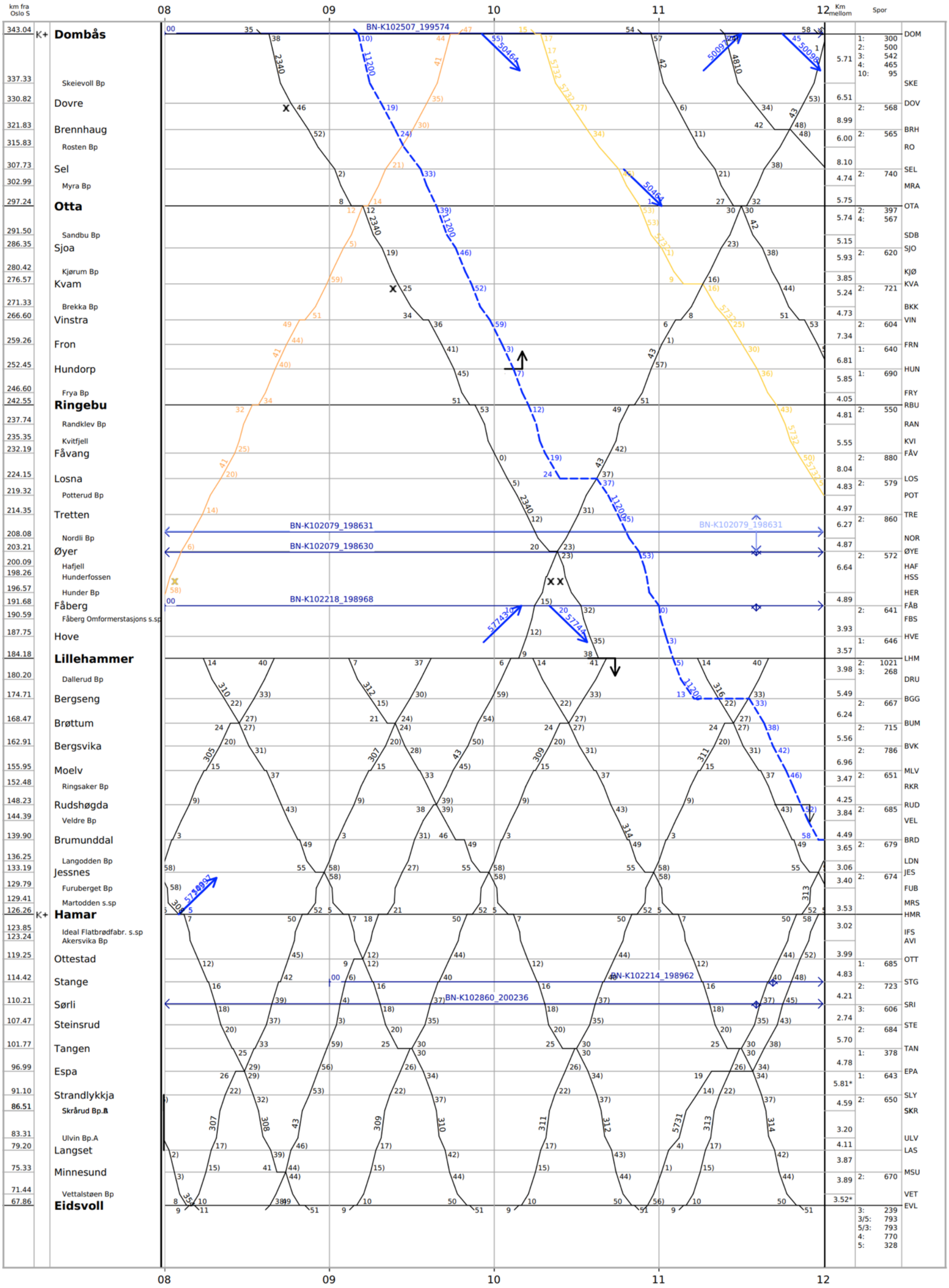
km fra Oslo S
08
09
10
11
12
Km mellom
Spor
343.04 K+ Dombås DOM
337.33 Skeievoll Bp SKE
330.82 Dovre DOV
321.83 Brennhaug BRH
315.83 Rosten Bp RO
307.73 Sel SEL
302.99 Myra Bp MRA
297.24 Otta OTA
291.50 Sandbu Bp SDB
286.35 Sjoa SJO
280.42 Kjørum Bp KJØ
276.57 Kvam KVA
271.33 Brekka Bp BKK
266.60 Vinstra VIN
259.26 Fron FRN
252.45 Hundorp HUN
246.60 Frya Bp FRY
242.55 Ringebu RBU
237.74 Randklev Bp RAN
235.35 Kvitfjell KVI
232.19 Fåvang FÅV
224.15 Losna LOS
219.32 Potterud Bp POT
214.35 Tretten TRE
208.08 Nordli Bp NOR
203.21 Øyer ØYE
200.09 Hafjell HAF
198.26 Hunderfossen HSS
196.57 Hunder Bp HER
191.68 Fåberg FÅB
190.59 Fåberg Omformerstasjons s.sp FBS
187.75 Hove HVE
184.18 Lillehammer LHM
180.20 Dallerud Bp DRU
174.71 Bergseng BGG
168.47 Brøttum BUM
162.91 Bergsvika BVK
155.95 Moelv MLV
152.48 Ringsaker Bp RKR
148.23 Rudshøgda RUD
144.39 Veldre Bp VEL
139.90 Brumunddal BRD
136.25 Langodden Bp LDN
133.19 Jessnes JES
129.79 Furuberget Bp FUB
129.41 Martodden s.sp MRS
126.26 K+ Hamar HMR
123.85 Ideal Flatbrødfabr. s.sp IFS
123.24 Akersvika Bp AVI
119.25 Ottestad OTT
114.42 Stange STG
110.21 Sørli SRI
107.47 Steinsrud STE
101.77 Tangen TAN
96.99 Espa EPA
91.10 Strandlykkja SLY
86.51 Skrårud Bp.A SKR
83.31 Ulvin Bp.A ULV
79.20 Langset LAS
75.33 Minnesund MSU
71.44 Vettalstøen Bp VET
67.86 Eidsvoll EVL
BN-K102507_199574
BN-K102079_198631
BN-K102079_198630
BN-K102218_198968
BN-K102214_198962
BN-K102860_200236
2340
11200
5732
5046
4810
5009
5731
5774
305
307
309
311
313
310
312
314
316
308
43
41

BANE NOR

Ruteplanperiode R22
BLAD NR. 10, EIDSVOLL - DOMBÅS

søndag 12.12.2021 - lørdag 10.12.2022
fredag, 4. mar. 2022

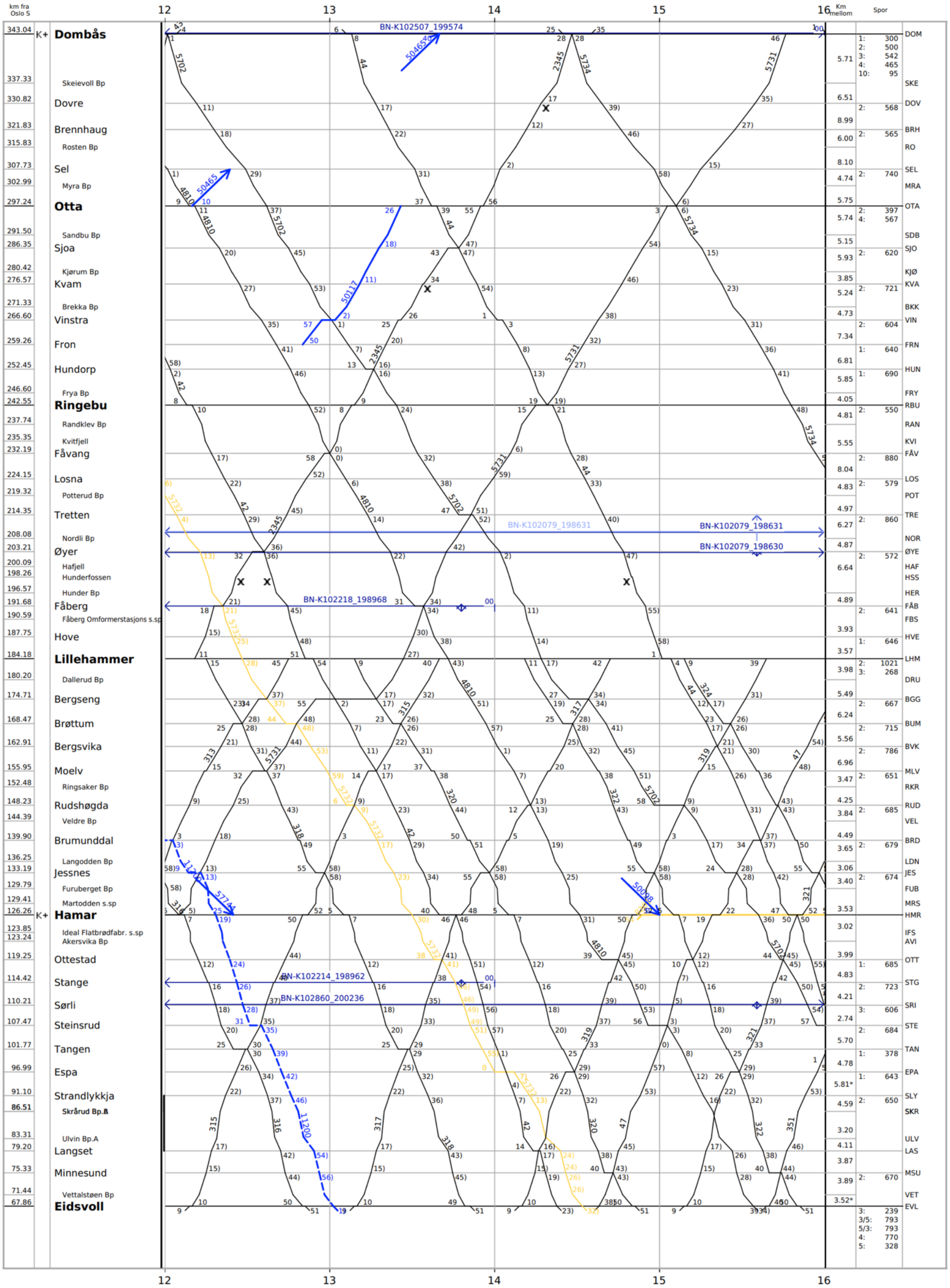

BANE NOR

Ruteplanperiode R22
BLAD NR. 10, EIDSVOLL - DOMBÅS

søndag 12.12.2021 - lørdag 10.12.2022
fredag, 4. mar. 2022

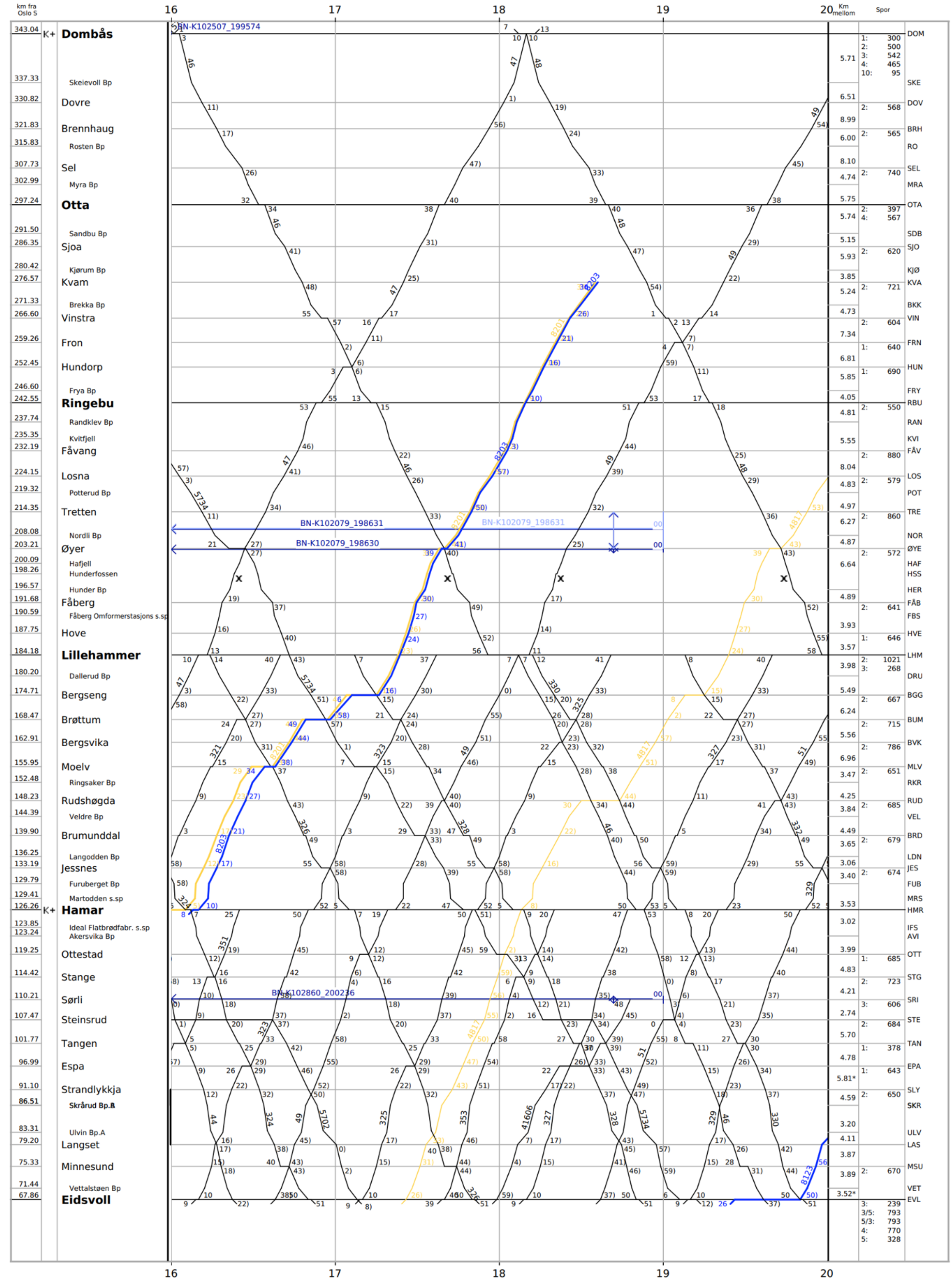

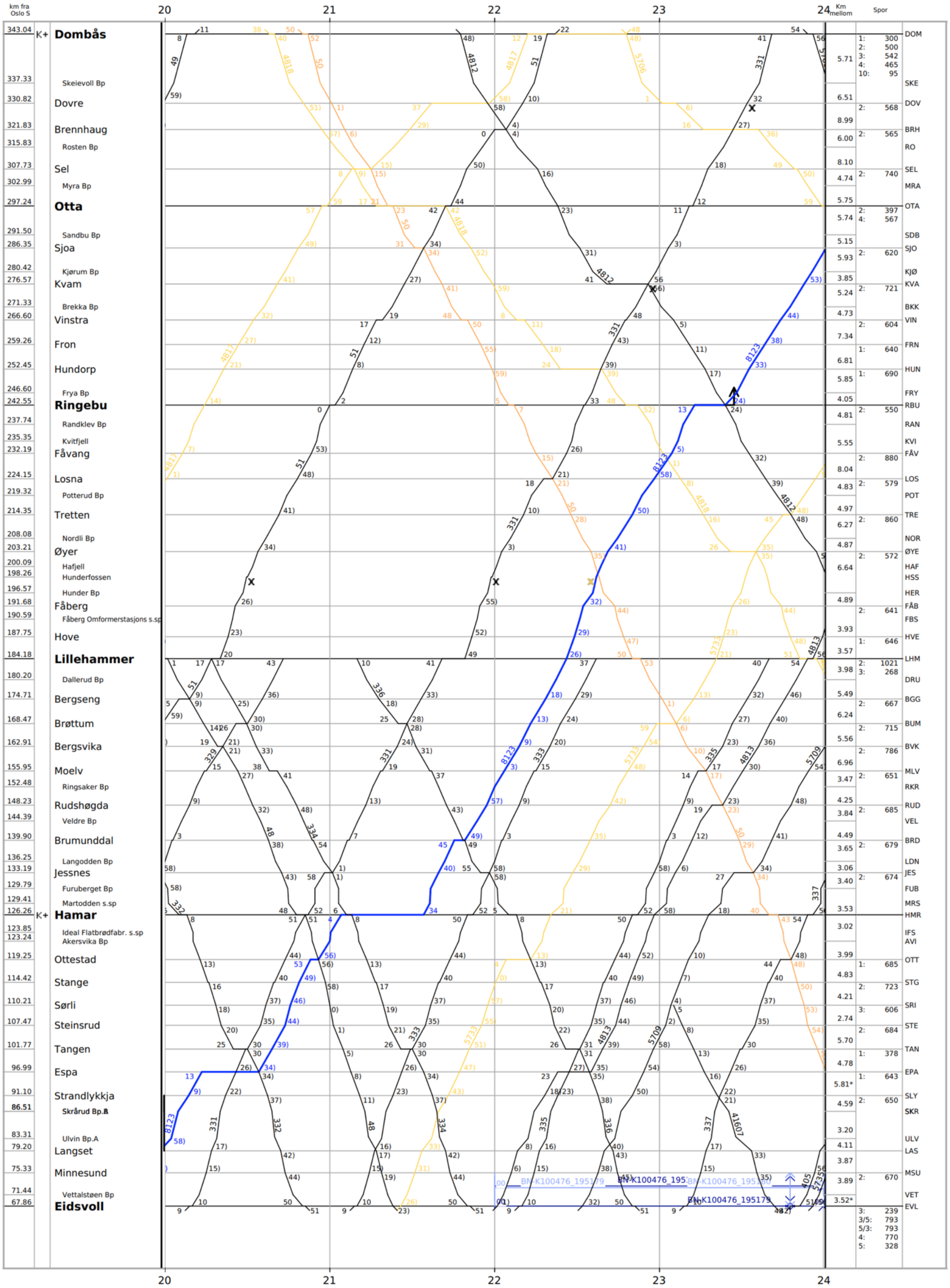
km fra Oslo S
20
21
22
23
24
Km mellom
Spor
343.04 K+ Dombås DOM
337.33 Skeievoll Bp SKE
330.82 Dovre DOV
321.83 Brennhaug BRH
315.83 Rosten Bp RO
307.73 Sel SEL
302.99 Myra Bp MRA
297.24 Otta OTA
291.50 Sandbu Bp SDB
286.35 Sjoa SJO
280.42 Kjørum Bp KJØ
276.57 Kvam KVA
271.33 Brekka Bp BKK
266.60 Vinstra VIN
259.26 Fron FRN
252.45 Hundorp HUN
246.60 Frya Bp FRY
242.55 Ringebu RBU
237.74 Randklev Bp RAN
235.35 Kvitfjell KVI
232.19 Fåvang FÅV
224.15 Losna LOS
219.32 Potterud Bp POT
214.35 Tretten TRE
208.08 Nordli Bp NOR
203.21 Øyer ØYE
200.09 Hafjell HAF
198.26 Hunderfossen HSS
196.57 Hunder Bp HER
191.68 Fåberg FÅB
190.59 Fåberg Omformerstasjons s.sp FBS
187.75 Hove HVE
184.18 Lillehammer LHM
180.20 Dallerud Bp DRU
174.71 Bergseng BGG
168.47 Brøttum BUM
162.91 Bergsvika BVK
155.95 Moelv MLV
152.48 Ringsaker Bp RKR
148.23 Rudshøgda RUD
144.39 Veldre Bp VEL
139.90 Brumunddal BRD
136.25 Langodden Bp LDN
133.19 Jessnes JES
129.79 Furuberget Bp FUB
129.41 Martodden s.sp MRS
126.26 K+ Hamar HMR
123.85 Ideal Flatbrødfabr. s.sp IFS
123.24 Akersvika Bp AVI
119.25 Ottestad OTT
114.42 Stange STG
110.21 Sørli SRI
107.47 Steinsrud STE
101.77 Tangen TAN
96.99 Espa EPA
91.10 Strandlykkja SLY
86.51 Skrårud Bp.B SKR
83.31 Ulvin Bp.A ULV
79.20 Langset LAS
75.33 Minnesund MSU
71.44 Vettalstøen Bp VET
67.86 Eidsvoll EVL
5.71 6.51 8.99 6.00 8.10 4.74 5.75 5.74 5.15 5.93 3.85 5.24 4.73 7.34 6.81 5.85 4.05 4.81 5.55 8.04 4.83 4.97 6.27 4.87 6.64 4.89 3.93 3.57 3.98 5.49 6.24 5.56 6.96 3.47 4.25 3.84 4.49 3.65 3.06 3.40 3.53 3.02 3.99 4.83 4.21 2.74 5.70 4.78 5.81* 4.59 3.20 4.11 3.87 3.89 3.52*
1: 300 2: 500 3: 542 4: 465 10: 95
2: 568
2: 565
2: 740
2: 397 4: 567
2: 620
2: 721
2: 604
1: 640
1: 690
2: 550
2: 880
2: 579
2: 860
2: 572
2: 641
1: 646
2: 1021 3: 268
2: 667
2: 715
2: 786
2: 651
2: 685
2: 679
2: 674
1: 685
2: 723
3: 606
2: 684
1: 378
1: 643
2: 650
2: 670
3: 239 3/5: 793 5/3: 793 4: 770 5: 328
4812
4817
4818
5706
5709
5733
8123
4813
41607
BN-K100476_195179

Appendix L

Track 2

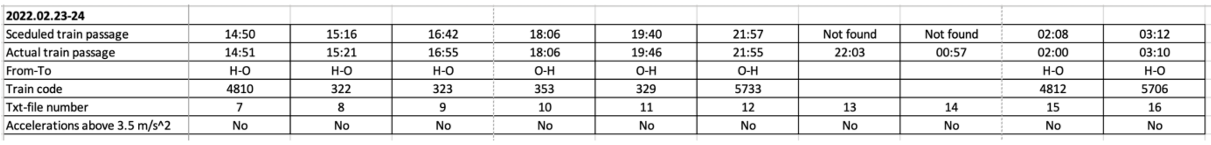

2022.02.23-24										
Sceduled train passage	14:50	15:16	16:42	18:06	19:40	21:57	Not found	Not found	02:08	03:12
Actual train passage	14:51	15:21	16:55	18:06	19:46	21:55	22:03	00:57	02:00	03:10
From-To	H-O	H-O	H-O	O-H	O-H	O-H			H-O	H-O
Train code	4810	322	323	353	329	5733			4812	5706
Txt-file number	7	8	9	10	11	12	13	14	15	16
Accelerations above 3.5 m/s^2	No	No	No	No	No	No	No	No	No	No

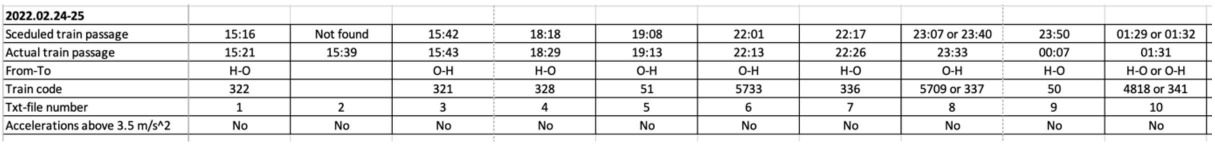

2022.02.24-25										
Sceduled train passage	15:16	Not found	15:42	18:18	19:08	22:01	22:17	23:07 or 23:40	23:50	01:29 or 01:32
Actual train passage	15:21	15:39	15:43	18:29	19:13	22:13	22:26	23:33	00:07	01:31
From-To	H-O		O-H	H-O	O-H	O-H	H-O	O-H	H-O	H-O or O-H
Train code	322		321	328	51	5733	336	5709 or 337	50	4818 or 341
Txt-file number	1	2	3	4	5	6	7	8	9	10
Accelerations above 3.5 m/s^2	No	No	No	No	No	No	No	No	No	No

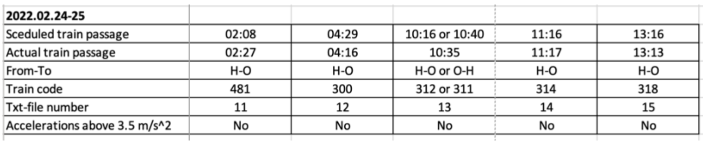

2022.02.24-25					
Sceduled train passage	02:08	04:29	10:16 or 10:40	11:16	13:16
Actual train passage	02:27	04:16	10:35	11:17	13:13
From-To	H-O	H-O	H-O or O-H	H-O	H-O
Train code	481	300	312 or 311	314	318
Txt-file number	11	12	13	14	15
Accelerations above 3.5 m/s^2	No	No	No	No	No

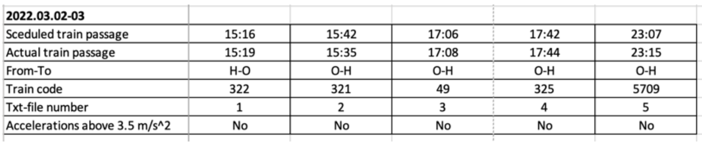

2022.03.02-03					
Sceduled train passage	15:16	15:42	17:06	17:42	23:07
Actual train passage	15:19	15:35	17:08	17:44	23:15
From-To	H-O	O-H	O-H	O-H	O-H
Train code	322	321	49	325	5709
Txt-file number	1	2	3	4	5
Accelerations above 3.5 m/s^2	No	No	No	No	No

Track 1

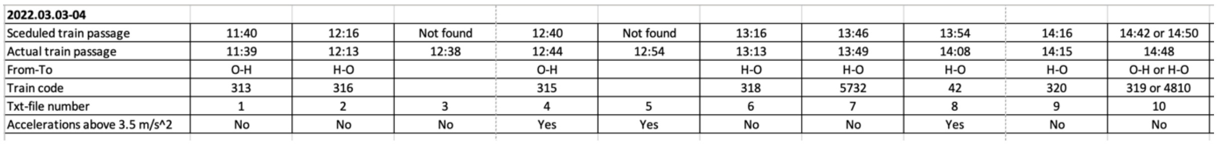

2022.03.03-04										
Sceduled train passage	11:40	12:16	Not found	12:40	Not found	13:16	13:46	13:54	14:16	14:42 or 14:50
Actual train passage	11:39	12:13	12:38	12:44	12:54	13:13	13:49	14:08	14:15	14:48
From-To	O-H	H-O		O-H		H-O	H-O	H-O	H-O	O-H or H-O
Train code	313	316		315		318	5732	42	320	319 or 4810
Txt-file number	1	2	3	4	5	6	7	8	9	10
Accelerations above 3.5 m/s^2	No	No	No	Yes	Yes	No	No	Yes	No	No

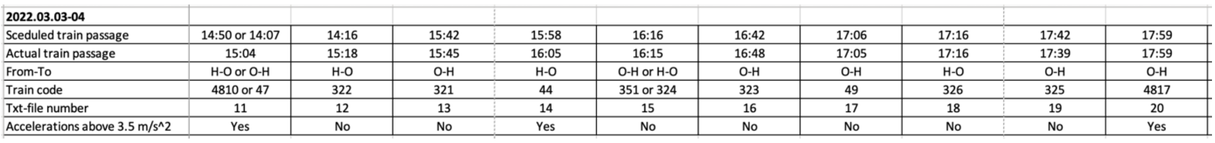

2022.03.03-04										
Sceduled train passage	14:50 or 14:07	14:16	15:42	15:58	16:16	16:42	17:06	17:16	17:42	17:59
Actual train passage	15:04	15:18	15:45	16:05	16:15	16:48	17:05	17:16	17:39	17:59
From-To	H-O or O-H	H-O	O-H	H-O	O-H or H-O	O-H	O-H	H-O	O-H	O-H
Train code	4810 or 47	322	321	44	351 or 324	323	49	326	325	4817
Txt-file number	11	12	13	14	15	16	17	18	19	20
Accelerations above 3.5 m/s^2	Yes	No	No	Yes	No	No	No	No	No	Yes

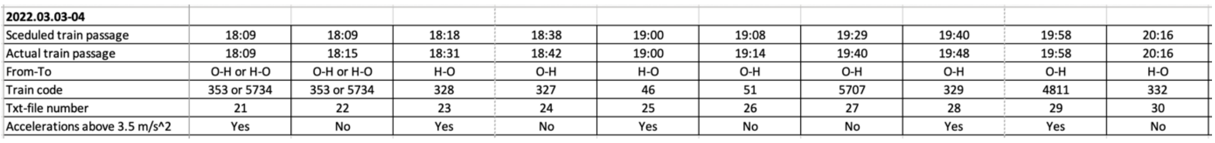

2022.03.03-04										
Sceduled train passage	18:09	18:09	18:18	18:38	19:00	19:08	19:29	19:40	19:58	20:16
Actual train passage	18:09	18:15	18:31	18:42	19:00	19:14	19:40	19:48	19:58	20:16
From-To	O-H or H-O	O-H or H-O	H-O	O-H	H-O	O-H	O-H	O-H	O-H	H-O
Train code	353 or 5734	353 or 5734	328	327	46	51	5707	329	4811	332
Txt-file number	21	22	23	24	25	26	27	28	29	30
Accelerations above 3.5 m/s^2	Yes	No	Yes	No	Yes	No	No	Yes	Yes	No

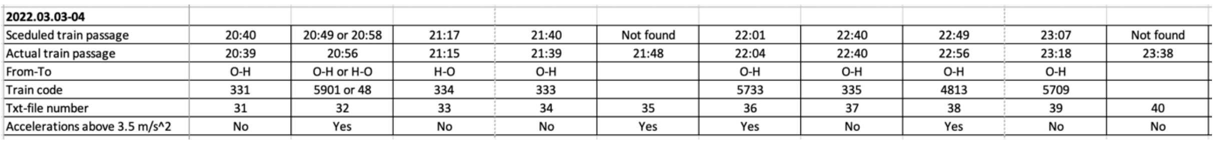

2022.03.03-04										
Sceduled train passage	20:40	20:49 or 20:58	21:17	21:40	Not found	22:01	22:40	22:49	23:07	Not found
Actual train passage	20:39	20:56	21:15	21:39	21:48	22:04	22:40	22:56	23:18	23:38
From-To	O-H	O-H or H-O	H-O	O-H		O-H	O-H	O-H	O-H	
Train code	331	5901 or 48	334	333		5733	335	4813	5709	
Txt-file number	31	32	33	34	35	36	37	38	39	40
Accelerations above 3.5 m/s^2	No	Yes	No	No	Yes	Yes	No	Yes	No	No

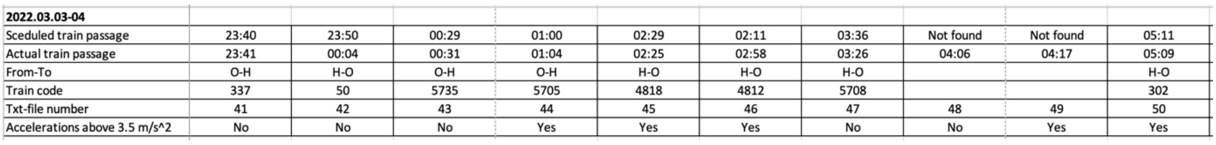

2022.03.03-04										
Sceduled train passage	23:40	23:50	00:29	01:00	02:29	02:11	03:36	Not found	Not found	05:11
Actual train passage	23:41	00:04	00:31	01:04	02:25	02:58	03:26	04:06	04:17	05:09
From-To	O-H	H-O	O-H	O-H	H-O	H-O	H-O			H-O
Train code	337	50	5735	5705	4818	4812	5708			302
Txt-file number	41	42	43	44	45	46	47	48	49	50
Accelerations above 3.5 m/s^2	No	No	No	Yes	Yes	Yes	No	No	Yes	Yes

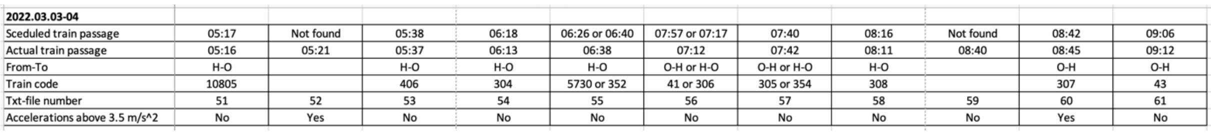

2022.03.03-04											
Sceduled train passage	05:17	Not found	05:38	06:18	06:26 or 06:40	07:57 or 07:17	07:40	08:16	Not found	08:42	09:06
Actual train passage	05:16	05:21	05:37	06:13	06:38	07:12	07:42	08:11	08:40	08:45	09:12
From-To	H-O		H-O	H-O	H-O	O-H or H-O	O-H or H-O	H-O		O-H	O-H
Train code	10805		406	304	5730 or 352	41 or 306	305 or 354	308		307	43
Txt-file number	51	52	53	54	55	56	57	58	59	60	61
Accelerations above 3.5 m/s^2	No	Yes	No	No	No	No	No	No	No	Yes	No